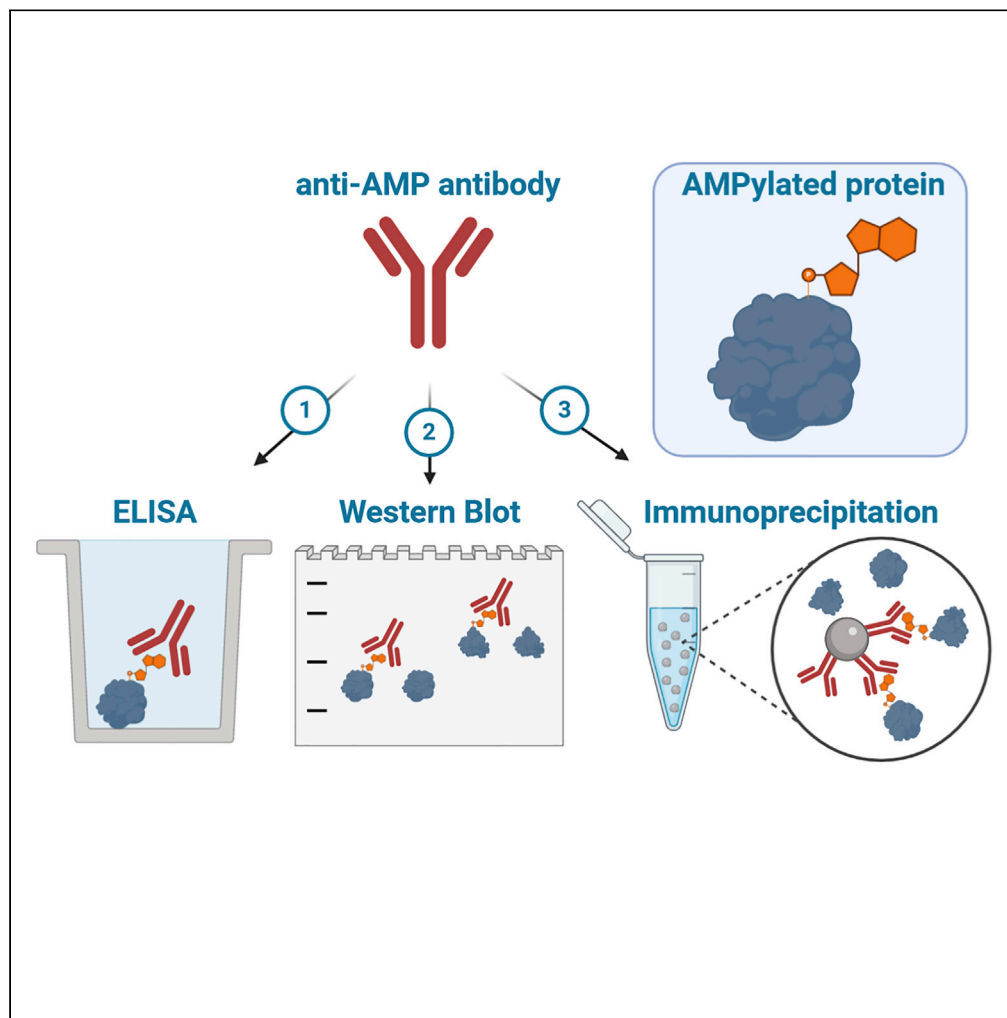


Article

Monoclonal Anti-AMP Antibodies Are Sensitive and Valuable Tools for Detecting Patterns of AMPylation



Dorothea Höpfner, Joel Fauser, Marietta S. Kaspers, Christian Pett, Christian Hedberg, Aymelt Itzen

christian.hedberg@umu.se (C.H.)
a.itzen@uke.de (A.I.)

HIGHLIGHTS

Generation of murine monoclonal anti-AMP antibodies via synthetic AMPylated peptide

Characterization in the applications western blot, ELISA, and immunoprecipitation

Sensitive and specific recognition of AMPylation independent of protein backbone

Expansion of toolbox for the detection and enrichment of AMPylation

Höpfner et al., iScience 23, 101800
December 18, 2020 © 2020 The Authors.
<https://doi.org/10.1016/j.isci.2020.101800>

Article

Monoclonal Anti-AMP Antibodies
Are Sensitive and Valuable Tools
for Detecting Patterns of AMPylationDorothea Höpfner,^{1,2} Joel Fauser,^{1,2} Marietta S. Kaspers,¹ Christian Pett,³ Christian Hedberg,^{3,*}
and Aymelt Itzen^{1,2,4,5,*}

SUMMARY

AMPylation is a post-translational modification that modifies amino acid side chains with adenosine monophosphate (AMP). Recently, a role of AMPylation as a universal regulatory mechanism in infection and cellular homeostasis has emerged, driving the demand for universal tools to study this modification. Here, we describe three monoclonal anti-AMP antibodies (mAbs) from mouse that are capable of protein backbone-independent recognition of AMPylation, in denatured (western blot) as well as native (ELISA, IP) applications, thereby outperforming previously reported tools. These antibodies are highly sensitive and specific for AMP modifications, highlighting their potential as tools for new target identification, as well as for validation of known targets. Interestingly, applying the anti-AMP mAbs to various cancer cell lines reveals a previously undescribed broad and diverse AMPylation pattern. In conclusion, these anti-AMP mAbs will further advance the current understanding of AMPylation and the spectrum of modified targets.

INTRODUCTION

Post-translational modifications (PTMs) are diverse covalent alterations that modulate the activity, localization, stability, and specificity of proteins. One such PTM is AMPylation (also referred to as adenylation) that occurs in both prokaryotes and eukaryotes. Enzymes utilize adenosine triphosphate (ATP) as donor substrate to transfer the adenosine monophosphate (AMP) to hydroxyl-bearing amino acid side chains (e.g., tyrosine, serine, threonine) of a target protein, with pyrophosphate being released as a side product. There are three different classes of AMPylators or protein adenylyl transferases known to date: DNA- β -Polymerase-like AMPylators with their most prominent member being glutamine synthetase adenylyltransferase from *Escherichia coli* (Kingdon et al., 1967); FIC (*Filamentation induced by cyclic AMP*) enzymes as represented by human FICD (Engel et al., 2012), IbpA from *Histophilus somni* (Worby et al., 2009), or VopS from *Vibrio parahaemolyticus* (Yarbrough et al., 2009); and, the most recently discovered, pseudokinases, specifically the highly conserved SelO (Sreelatha et al., 2018).

AMPylation has been studied over 50 years (Kingdon et al., 1967) and has gained recent attention with the identification of small GTPases as targets of AMPylating enzymes during various bacterial infections (Worby et al., 2009; Yarbrough et al., 2009). The discovery of FICD as the only metazoan FIC protein (Engel et al., 2012; Worby et al., 2009) and its modification of the endoplasmic reticulum (ER) chaperone BiP (Ham et al., 2014; Sanyal et al., 2015) illustrates a role of AMPylation in protein homeostasis (Preissler et al., 2015, 2016). Recent findings on AMPylation by pseudokinases (Sreelatha et al., 2018) hints at a broader occurrence of this modification as a general mechanism, and not just in the context of bacterial infections as previously thought.

However, despite a high prevalence of predicted FIC enzymes based on their conserved sequence, especially in pathogenic bacteria (Khater and Mohanty, 2015), only a limited amount of AMPylation targets are known. This discrepancy between the number of enzymes and identified targets highlights the challenge of detecting AMPylation. Available tools are both limited and are associated with disadvantages in terms of necessary resources and/or studying AMPylation in a physiologically relevant context. ATP analogs have reduced intracellular uptake (Plagemann and Wohlhueter, 1980) (although recent work established a cell-permeable pronucleotide probe, Kielkowski et al., 2020), are outcompeted by the high endogenous

¹Department of Biochemistry and Signaltransduction, University Medical Center Hamburg-Eppendorf (UKE), Martinistr. 52, 20246 Hamburg, Germany

²Center for Integrated Protein Science Munich (CIPSM), Department Chemistry, Technical University of Munich, Lichtenbergstrasse 4, 85747 Garching, Germany

³Chemical Biology Center (KBC), Department of Chemistry, Umeå University, Linnaeus väg 10, 90187 Umeå, Sweden

⁴Center for Structural Systems Biology (CSSB), University Medical Center Hamburg-Eppendorf (UKE), Notkestraße 85, Building 15, 22607 Hamburg, Germany

⁵Lead Contact

*Correspondence: christian.hedberg@umu.se (C.H.), a.itzen@uke.de (A.I.)
<https://doi.org/10.1016/j.isci.2020.101800>



concentrations of ATP, and are hampered by the potential inability of enzymes to use these analogs as substrates. When used in cell lysates, spatial and temporal regulation is abrogated.

Antibodies targeting AMPylation could overcome many of these challenges as well as offer further applications as an orthogonal approach. Ideally, such an antibody would be able to detect AMPylation with high sensitivity and specificity toward both native and denatured proteins, thus enabling western blot (WB) detection as well as enrichment by immunoprecipitation (IP). Previously generated polyclonal antibodies using AMPylated peptides do not fulfill these desired properties (Hao et al., 2011; Smit et al., 2011).

Here, we generate three new monoclonal antibodies from mice that recognize AMPylation independently of the protein backbone, under denatured as well as native conditions. In addition to target validation, they can serve as new tools for target identification. As new target identification hinges on proper positive controls, and false-negatives may not be detected, a thorough characterization of the antibodies' behavior in the specific application is crucial.

RESULTS

Previously published and commercially available antibodies claimed to recognize AMPylated threonine and tyrosine, respectively, independent of the peptide backbone and protein environment (see Sigma-Aldrich 09-890 and ABS184) (Hao et al., 2011). However, evaluation of their performance in WB on various recombinant proteins with different modified amino acid side chains (such as Rho GTPase Cdc42 AMPylated at threonine35 [VopS, Yarbrough et al., 2009] or tyrosine32 [IbpA, Worby et al., 2009], Rab GTPase Rab1b modified at tyrosine77 (DrrA from *Legionella pneumophila*, Müller et al., 2010), Histone H3.1 modified at threonine (FICD, Truttmann et al., 2016), the ER chaperone BiP/Grp-78 modified at threonine518 (FICD, Preissler et al., 2015), and the FIC enzyme FICD auto-modified at threonine80,183 + serine79 (Sanyal et al., 2015) showed that they do not recognize all AMPylations (Figure 1A): the commercially available anti-Thr-AMP antibody (Sigma-Aldrich 09-890) successfully recognized Cdc42-Thr-AMP and FICD-Thr-AMP, whereas the detection of H3.1-Thr-AMP and BiP-Thr-AMP was less sensitive and in the case of the latter no longer possible at 50 ng. The commercially available anti-Tyr-AMP antibody (ABS184, Merck) showed unsatisfactory performance by cross-reacting with unmodified Rab1b and FICD, respectively, as well as H3.1-Thr-AMP, in addition to exhibiting a generally weak detection signal. As both anti-AMP antibodies did not yield broad recognition of AMPylation, we considered whether available anti-ADP-ribosylation antibodies might also be able to detect AMPylation, because both modifications share the AMP moiety. We therefore tested the commercially available anti-pan-ADP-ribose-binding reagent (MABE1016, Merck) and, while detecting mono-ADP-ribosylated PARP3 (by autocatalysis, Vyas et al., 2014), found it unable to detect AMPylation with the exception of H3.1-Thr-AMP.

This number of false-positive and false-negative signals in commercially available anti-Tyr-AMP and anti-ADPR antibodies as well as the low sensitivity in the anti-Thr-AMP antibody led us to the development of new monoclonal anti-AMP antibodies in mice.

Design and Synthesis of the AMP-Bearing Peptide

Previously published antibodies worked mostly against denatured targets in WB and were only evaluated against small GTPases (dependent on the peptide used for immunization) (Hao et al., 2011; Smit et al., 2011). Our goal was to create a universal tool that can recognize AMPylation, not only on the rising number of known AMPylated proteins but also on unknown targets independent of backbone and protein environment, in denatured as well as native applications. This would allow for target enrichment from complex samples as well as target validation and characterization.

Instead of using an AMPylated peptide derived from a naturally occurring target protein as hapten, we chose a reductive approach that aimed to develop the antibody against the AMP side chain moiety alone, but not against the peptide sequence itself (Figure 1B). The strategy was therefore to reduce the peptide backbone (Figure 1C) to a non-immunogenic 8 amino acid sequence of glycine and alanine, long enough to not unintentionally cause an immune reaction to the termini, but short enough to diminish the immune response to the peptide itself. To lower the charge at the termini and simulate a natural protein peptide backbone, the peptide was N-terminally acetylated and C-terminally amidated. The AMPylated threonine was introduced in the middle of the synthesized peptide via the use of an AMPylated building block (Albers et al., 2011; Smit et al., 2011). An N-terminal cysteine was incorporated to enable fusion to carrier proteins for immunization (Figure 1D; for synthesis see Figures S1 and S2).

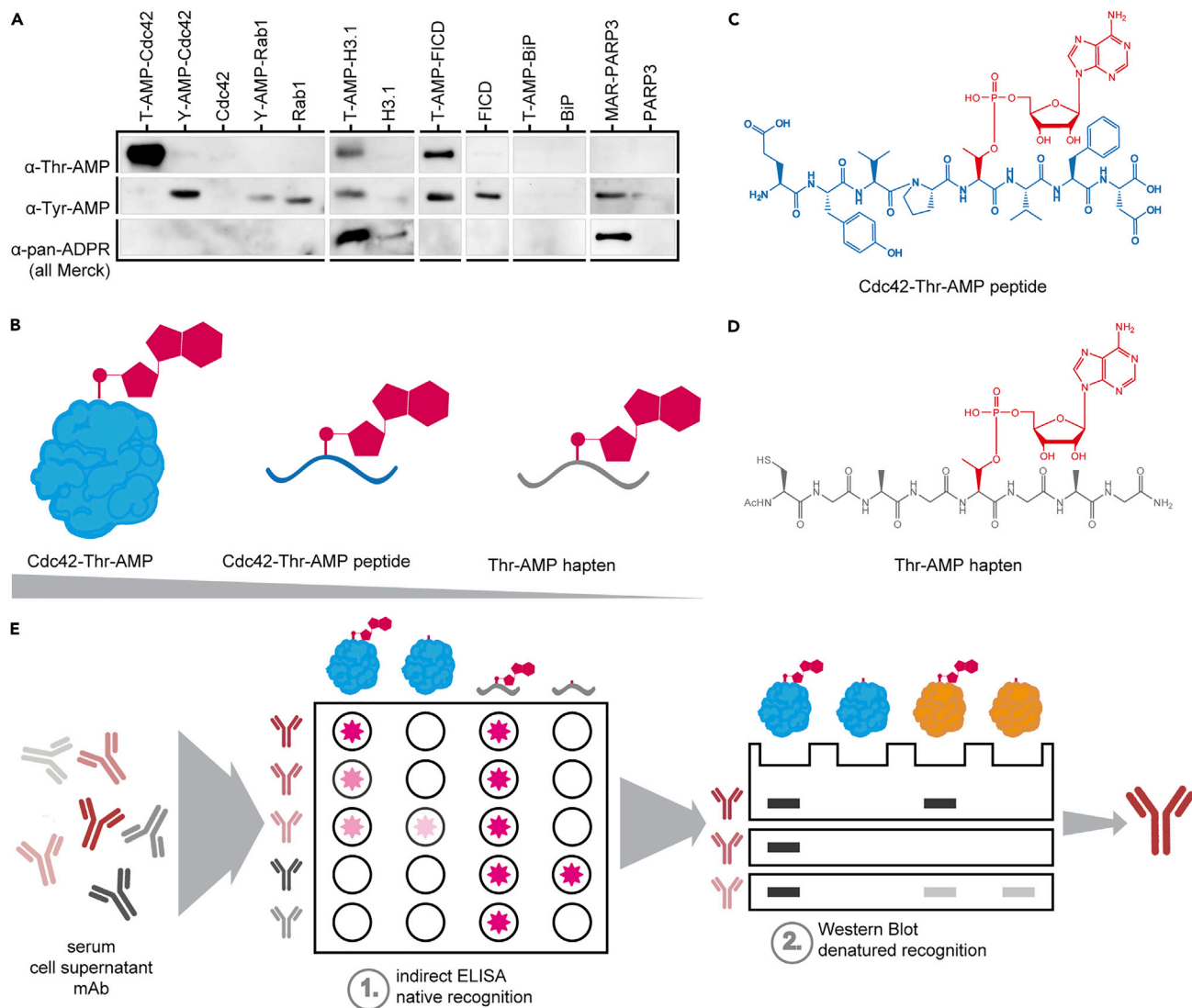


Figure 1. Motivation, Hapten Design, and Selection Strategy for the Generation of Monoclonal Anti-AMP Antibodies

(A) Performance of commercially available anti-AMP antibodies on AMPylated proteins. 50 ng of indicated recombinant protein was analyzed by WB using anti-threonine-AMP (Merck) and anti-tyrosine-AMP (Merck) antibodies as well as anti-ADPR binding probe (Merck) as indicated. Rows represent identical WBs.

(B) Reductive approach of hapten design. Instead of using intact AMPylated protein or AMPylated peptide (blue) from a naturally occurring target such as Cdc42, the peptide backbone's complexity was reduced (gray) to ensure development of antibodies against the AMP-moiety (red) alone.

(C) Representation of the peptide 31-38aa in naturally occurring Cdc42-Thr-AMP with its complex side chains (blue). The AMP-modified threonine is indicated in red.

(D) See also Figures S1 and S2. Representation of Thr-AMP hapten peptide with its reduced complexity of a glycine-alanine backbone, N-terminal acetylation, and C-terminal amidation. An N-terminal cysteine was included to enable fusion to carrier protein. The AMP-modified threonine is indicated in red.

(E) See also Figure S3. Illustration of the stepwise selection process of mice (sera), clones (supernatant), and subclones (supernatant) and confirmation of purified antibodies during antibody generation. Candidates were first subjected to ELISA against the AMPylated hapten peptide as well as AMPylated Cdc42-Thr and counterscreened against their unmodified counterparts; positive clones evaluated for their performance in WB on various AMPylated proteins and their unmodified counterparts.

As this reductive strategy of incorporating AMPylated threonine into a short glycine-alanine backbone has never been tested before and posed the risk of abolishing immunogenicity, we decided on a broad approach, choosing two different carrier proteins as hapten conjugates and two different mice breeds for immunization. In total, 10 mice were immunized with either BSA or keyhole limpet hemocyanin (KLH) conjugates, each of which were injected into three BALB/c and two C57BL/6 mice by GenScript.

To ensure backbone-independent recognition of AMPylation, antibody candidates were reversely selected by a stepwise screening procedure during all stages of development (Figure 1E). The screening process started with all candidates that were able to recognize the hapten with its reduced backbone complexity, proceeding to filter all candidates that were capable of recognition of native threonine-AMPyated Cdc42 as determined by ELISA (Figure 1E, first step), and subsequently testing recognition of multiple modified proteins in denatured state via WB (Figure 1E, second step). Only candidates positive for all these criteria and all target proteins were taken into consideration and used for further development (see Figure S3).

Our selection strategy, followed by rigorous characterization, aimed to overcome the aforementioned pitfalls of currently available antibodies and created three new antibodies against AMPylation: One promising clone, 17G6, with sensitive recognition of all AMPyated proteins in WB independent of their modified side chain, native recognition of Cdc42-Thr-AMP in ELISA, and low background was selected for subcloning and subsequent production and purification. Another candidate, 7C11, was selected for showing a bias in WB for threonine-modified protein. One further clone, 1G11, was selected due to its development of a Tyr-AMP-specific recognition, despite immunization with a threonine-modified peptide. All monoclonal antibodies were derived from C57 BL/6 mice. 17G6's immunogen was a BSA-fusion, whereas 7C11's and 1G11's immunogens were KLH-fusions (see Figure S3). For all three hybridoma cell lines, antibody variable domain sequencing was performed by GenScript as a service (for sequencing results see Supplemental Information).

Generated Anti-AMP Antibodies Are Highly Specific for AMPylation

The three new anti-AMP antibodies 17G6, 7C11, and 1G11 were subsequently produced by roller bottle cell culture, purified from the supernatant via Protein A affinity capture, and tested for their performance in the recognition of denatured protein targets via WB. Here, sensitivity and detection limits, specificity toward AMPylation as opposed to incorporation of other nucleotides, and cross-reactivity with other PTMs were evaluated. In addition, native binding as previously shown by ELISA was confirmed by protein complex formation between the antibodies and AMPyated antigens on size exclusion chromatography. To determine the detection limits of recognition (Figure 2A), we tested all three antibodies in WB against a dilution series of recombinant Cdc42-Tyr-AMP, -Thr-AMP, Rab1-Tyr-AMP, and BiP-Thr-AMP, which were enzymatically modified by IbpA, VopS, DrrA, and FICD, respectively, in the presence of ATP and Mg²⁺. All antibodies showed similar performance on all the targets and modified side chains: all three antibodies were able to recognize as little as 2 ng or even lower amounts of AMPyated protein, while showing no recognition of the unmodified controls (50 ng). Antibody 1G11 detected modified Cdc42 at the Thr side chain with less sensitivity than at the Tyr side chain, and 7C11 detected Tyr-modified GTPases with less sensitivity than Thr-modified protein. Antibody 17G6 did not show a preference for a specific AMPyated side chain.

Next, we aimed to confirm backbone-independent recognition of AMPylation by applying all three antibodies to a broad range of AMPyated targets (Figure 2B), and indeed, the recognition of AMPylation was not limited to small GTPases. AMPyated FICD, BiP, and H3 were also recognized, representing very different protein classes, sizes, and folds. It therefore seems likely that other proteins will be recognized as well, which is a crucial prerequisite for target identification. Native binding of the antibodies to their modified antigens was investigated by complex formation with different AMPyated proteins using size exclusion chromatography (Figures 2C and S4). The shift of retention time of the antibody peaks upon incubation with AMPyated proteins toward higher molecular weight but no shift for incubation with non-modified counterparts for all antibodies illustrates strong and specific binding of modified targets. The shifted antibody peaks were collected by fractionation and analyzed by SDS PAGE for their co-elution with the antigens. Indeed, in case of AMPyated antigens, the antibodies co-eluted with their antigens. In this experiment, the same preferences for side chains were observed as already shown from studies by WB (denaturing conditions): antibody 1G11 shows a preference for AMPyated tyrosine, exemplified by a striking peak shift upon Rab1-Tyr-AMP binding but little shift for Cdc42-Thr-AMP (see Figure S4). Antibody 17G6 shows broad recognition of all modified targets, including a very prominent peak shift upon incubation with AMPyated BiP (Figure 2C), whereas 7C11 prefers threonine AMPylation and does not show binding of Rab1-Tyr-AMP (Figure S4). Notably, Rab1-Tyr-AMP appears to be a difficult antigen for native as well as denatured recognition by the new antibodies: Already during selection, Rab1-Tyr-AMP recognition in WB was one of the main hurdles for most candidates, and there were only few candidates who showed a strong signal in WB.

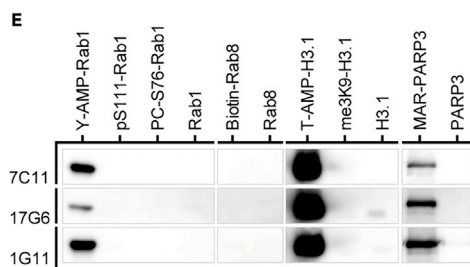
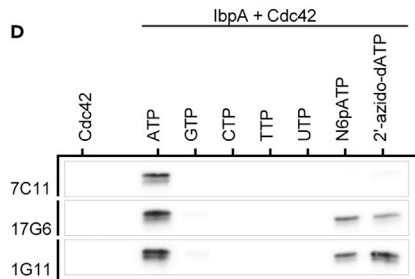
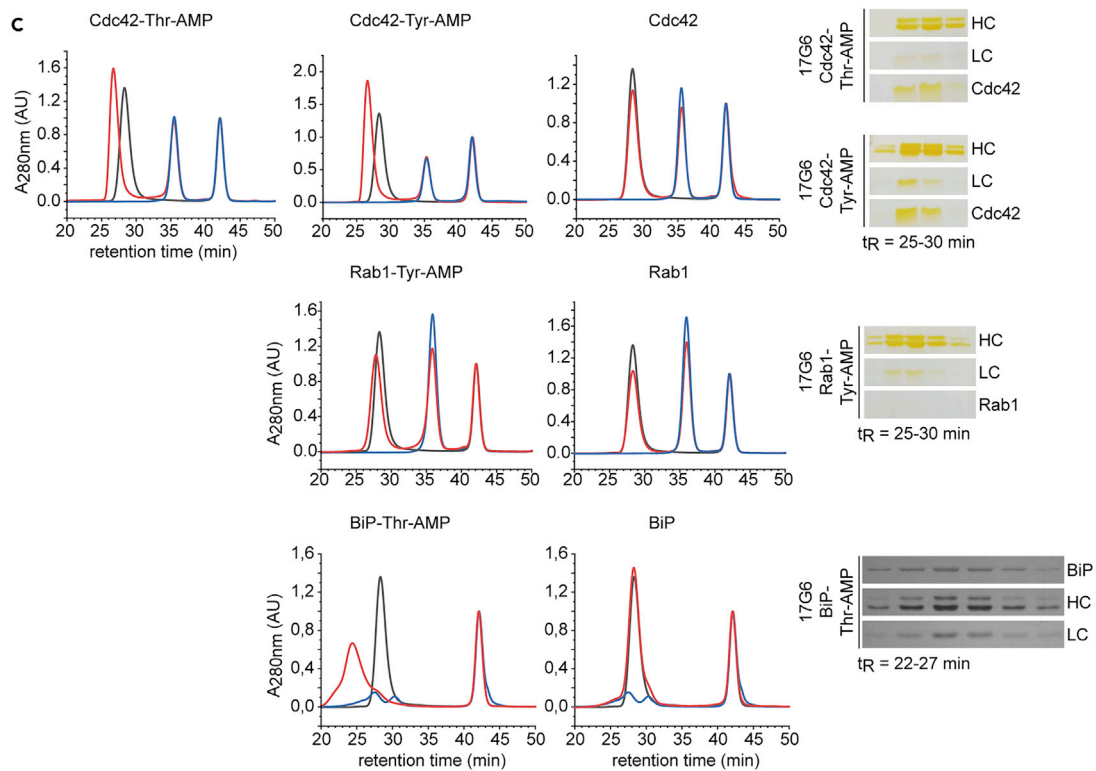
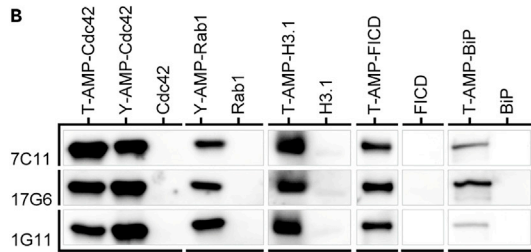
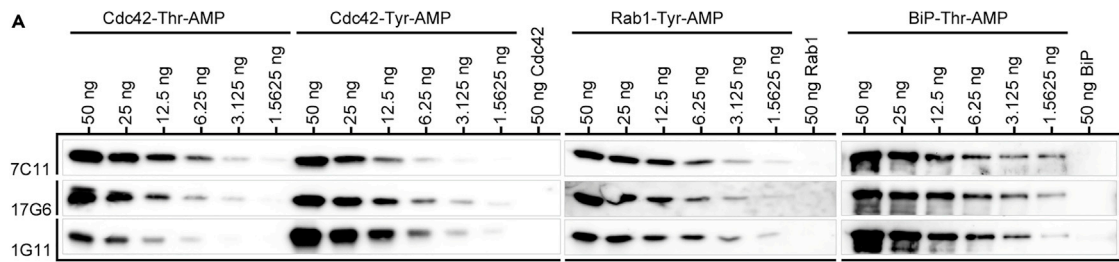


Figure 2. Evaluation of Specificity and Selectivity of Generated Anti-AMP Antibodies

(A) Detection limits of AMPylated recombinant protein by the monoclonal anti-AMP antibodies in WB. Dilution rows starting from 50 ng recombinant Cdc42-Thr-AMP, -Tyr-AMP, Rab1-Tyr-AMP, and BiP-Thr-AMP, respectively, were analyzed in WB using all three monoclonal anti-AMP antibodies as indicated. Unmodified controls were loaded at 50 ng on the same blots as their modified counterparts. Cdc42, Rab1, and BiP represent three separate WBs.

(B) Broadness of AMPylated target recognition by the monoclonal anti-AMP antibodies in WB. 50 ng recombinant protein was analyzed in WB using all three monoclonal anti-AMP antibodies as indicated. Rows represent identical WBs.

(C) See also [Figure S4](#). Native binding of AMPylated Cdc42, Rab1, and BiP by monoclonal anti-AMP antibody 17G6 analyzed by analytical size exclusion chromatography. 40 μ g antigen for Cdc42 and Rab1, or 20 μ g BiP was mixed with 60 μ g antibody, including 50 μ M vitamin B12 ($t_R = 42.5$ min) as internal standard. In black antibody 17G6 alone, in blue antigen alone as indicated, in red co-incubation of antibody 17G6 and antigen as indicated. Shifted antibody peaks (red) were fractionated and analyzed for co-elution of antibody (light chain, LC; heavy chain, HC) and antigen by silver-stained SDS PAGE (cropped rows represent identical gels).

(D) See also [Figure S5](#). Evaluation of specificity toward AMPylation by the monoclonal anti-AMP antibodies in WB. Cdc42 was NMPylated by IbpA using ATP, GTP, CTP, UTP, N6pATP, and 2'-azido-dATP. 50 ng recombinant Cdc42, unmodified or modified with nucleotides as indicated, was analyzed in WB using all three monoclonal anti-AMP antibodies as indicated. Rows represent identical WBs.

(E) Cross-reactivity with other PTMs by the monoclonal anti-AMP antibodies in WB. 50 ng of recombinant protein was analyzed in WB using all three monoclonal anti-AMP antibodies as indicated. Rows represent identical WBs.

To test the antibodies' specificity toward the transferred nucleotide and their ability to differentiate AMPylation from, e.g., GMPylation, recombinant IbpA was used to introduce UMPylation, GMPylation, CMPylation, and TMPylation onto Cdc42 ([Mattoo et al., 2011](#)) ([Figure 2D](#)). In addition, the recognition of two reactive ATP analogs that have been previously described in the context of AMPylation, N6-Propargyl-ATP (N6pATP) ([Grammel et al., 2011](#); [Yu et al., 2014](#)) and 2'-Azido-2'-dATP ([Wang and Silverman, 2016](#)), were tested (for mass spectrometric [MS] verification of incorporation see [Figure S5](#)). All antibodies successfully differentiated between the nucleotides and specifically recognized AMPylation in Cdc42. Using ATP analogs instead of ATP, we could confirm that the antibodies are also sensitive to base and ribose modifications, and only antibodies 17G6 and 1G11 showed slight recognition of modified ATP analogs ([Figure 2D](#)). This preference for AMPylation suggests a recognition of the adenine ring system by the antibodies.

After proving that the antibodies are sensitive and specific for AMPylation, we tested various other common PTMs for their ability to cross-react with the antibodies to rule out false-positive signals from competing modifications ([Figure 2E](#)). We tested phosphorylated (pS111) and phosphocholinated (PC-S76) Rab1b in direct comparison to its AMPylation, as well as biotinylated Rab8, trimethylated (me3K9) H3.1 in direct comparison to its AMPylation, and mono-ADP-ribosylated (MARylated) PARP3. To our satisfaction, the antibodies did not recognize phosphorylation, phosphocholination, biotinylation, or trimethylation on the chosen example proteins. However, the antibodies cross-reacted with MARYlation on PARP3, most likely recognizing the present adenosine moiety.

Anti-AMP Antibodies Can Shift Bias between AMPylation and MARYlation

Our findings show that the developed anti-AMP antibodies also detect mono-ADP-ribosylation as exemplified by auto-modified PARP3 ([Figure 2E](#)). We therefore screened different additives to the primary antibody incubation step during WB for their ability to abrogate reactivity with ADP-ribosylation, while still keeping the recognition of AMPylation intact ([Figure 3A](#)). Adenine, AMP, ADP, ATP, ADP-Ribose (ADPR), and nicotinamide adenine dinucleotide (NAD⁺) were selected for their similarity to both modifications and their potential ability to compete with binding of ADP-ribosylation or AMPylation and displace modified proteins. MnCl₂ and MgCl₂ were chosen as divalent cations for their potential to complex the negatively charged diphosphate present in ADP-ribosylation but not AMPylation, thereby shielding negative charge that could potentially be relevant for antibody binding. Hydroxylamine treatment of the membrane after blotting reportedly results in specific cleavage of ADP-ribosylation at aspartate and glutamate side chains ([Moss et al., 1983](#)), but has not been previously tested regarding the stability of AMPylation. None of the tested additives were able to selectively reduce reactivity toward neither AMPylation nor MARYlation, without significantly reducing overall sensitivity of the antibodies at the same time. Nevertheless, AMP, ADP, ATP, and NAD⁺ were able to reduce AMPylation signals to some extent, whereas the MARYlation signal remained largely unaffected. However, keeping in mind that PARP3 has 14 reported auto-MARYlation sites ([Vyas et al., 2014](#)), whereas Cdc42 is single AMPylated, this loss of signal in AMPylation but not MARYlation might be due to the multiple modifications on MAR-PARP3 and therefore not be easily translatable toward other single ADP-ribosylated proteins, where these additives might also result in signal loss. As expected, hydroxylamine treatment resulted in a strong loss of MARYlation signal due to cleavage of the ADP-ribosyl group. By contrast, the AMPylation signal remained entirely unaffected. The residual signal of

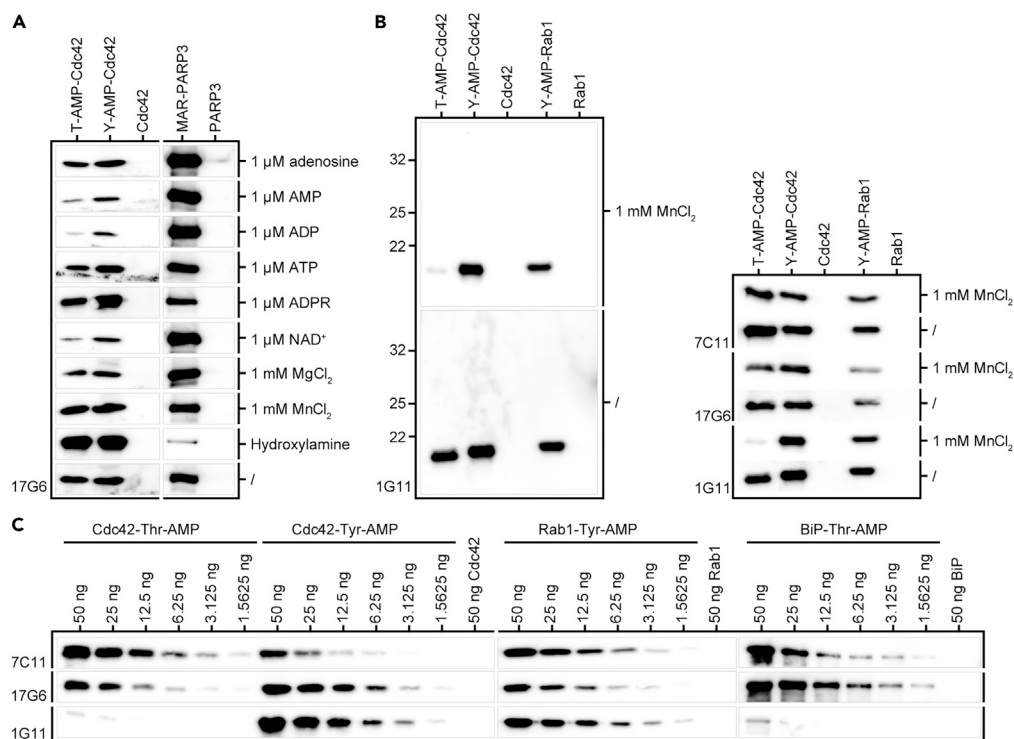


Figure 3. Detection of AMPylation and MARYlation in the Presence of Additives and the Influence of MnCl₂ on the Detection of AMPylation

(A) Recognition of AMPylation versus MARYlation by antibody 17G6 either in the presence of additives as indicated during primary antibody incubation or after hydroxylamine treatment. 50 ng recombinant Cdc42-Thr-AMP, -Tyr-AMP, as well as mono-ADP-ribosylated PARP3 and their unmodified counterparts as indicated were analyzed in WB using 17G6.

Additives as indicated, with the exception of hydroxylamine, were added during incubation with primary anti-AMP antibody overnight at 4°C. Hydroxylamine treatment to cleave off ADP-ribosylation at Asp and Glu residues took place for 8 h after blotting before primary antibody incubation. Rows represent identical WBs.

(B) Influence of 1 mM MnCl₂ on antibody background and side chain specificity. 50 ng recombinant protein as indicated were analyzed in WB using all three monoclonal anti-AMP antibodies in the presence or absence of 1 mM MnCl₂ during primary antibody incubation as indicated. Rows represent identical WBs. Left panel: exemplary full representation of the cropped rows of 1G11 (right) to illustrate change in background.

(C) Detection limits under the influence of 1 mM MnCl₂. Dilution rows starting from 50 ng recombinant Cdc42-Thr-AMP, -Tyr-AMP, Rab1-Tyr-AMP, and BiP-Thr-AMP, respectively, were analyzed in WB using all three monoclonal anti-AMP antibodies as indicated in the presence of 1 mM MnCl₂ during primary antibody incubation. Unmodified controls were loaded at 50 ng on the same blots as their modified counterparts. Cdc42, Rab1, and BiP represent three separate WBs.

auto-modified PARP3 is most likely resulting from the two reported auto-modification sites at lysine6 and lysine37 (Vyas et al., 2014) that will not be cleaved by hydroxylamine.

The addition of 1 mM MnCl₂ during the primary antibody incubation step, although not affecting signal intensity, resulted in a significantly reduced background. Strikingly, the addition of MnCl₂ also resulted in a sharply enhanced tyrosine specificity for antibody 1G11 in the presence of MnCl₂ (Figure 3B). The addition of MnCl₂ was therefore further evaluated in regard to the previously tested detection limits of the antibodies. We confirmed that the detection limits of antibodies 17G6 and 7C11 toward AMPylated antigens was not significantly changed by addition of MnCl₂, whereas 1G11's ability to detect Cdc42-Thr-AMP as well as BiP-Thr-AMP was greatly diminished (Figure 3C).

In summary, our newly developed antibodies are a combined tool for detection of AMPylation and mono-ADP-ribosylation. By addition of MnCl₂ to the primary antibody incubation steps in WB, the background of the antibodies can be significantly reduced and 1G11 shows pronounced tyrosine specificity. Treating membranes with hydroxylamine after blotting results in the cleavage of glutamate- and aspartate-linked ADP-ribosylation, whereas AMPylation remains unaffected. Therefore, the combination of all three

antibodies with addition of MnCl_2 and hydroxylamine treatment results in a tool kit that is able to sensitively detect ADP-ribosylation and AMPylation, to differentiate between the two, and, in the case of AMPylation, not only to recognize targets in general but also to give information on their modified side chains.

Generated Anti-AMP Antibodies Recognize Diverse Cellular AMPylation

After thorough characterization and evaluation of our produced antibodies on purified and MS-confirmed antigens, we next evaluated the antibody performance on cell lysates in known contexts under denatured as well as native conditions. The reproduction of previous results with these new tools is crucial for the trust in future findings and a smooth transition from previously used tools.

Previously, it was shown that BiP AMPylation by FICD is lost in cells upon stimulation of ER stress, e.g., by thapsigargin (TG) (Ham et al., 2014; Preissler et al., 2015). Cycloheximide (CHX), in contrast, will stall protein production, therefore relieving the ER of protein load, causing a significant increase in BiP AMPylation. To reproduce these findings, we first set out to confirm the detection levels of BiP-AMP in the environment of cell lysates (Figure 4A). Accordingly, we spiked 20 μg HEK293 lysate per lane, either untreated (ctrl) or treated for 2 h with TG to remove endogenously AMPylated BiP, with a titration of recombinant BiP-AMP. As controls, the lysates were either additionally spiked with 50 ng unmodified BiP or not. Probing the WB with antibody 17G6 in the presence of MnCl_2 we could confirm the same low detection limits of up to 1.5 ng for BiP-AMP in lysate as previously shown in Figure 3C on purified protein. To verify that the antibodies' previously confirmed ability to bind native AMPylated protein would translate into a successful IP, we applied antibody 17G6 in the context of BiP-AMPylation (Figure 4B). Using recombinant BiP and BiP-AMP showed that IP is dependent on the presence of antibody 17G6, as beads alone do not pull down either modified or unmodified BiP, and specific for AMPylation, as the non-modified BiP is not precipitated by antibody 17G6.

Having thus established that antibody 17G6 is capable of detecting BiP-AMP in cell lysates at low amounts in WB, as well as of binding BiP-AMP in IP, we applied both techniques to the aforementioned BiP-AMPylation in the context of ER stress. We reproduced these findings, representative for all our antibodies, with antibody 17G6 and MnCl_2 as an additive in HEK293 as well as CHO-K1 cells (Figure 4C) and could confirm these previously published results (Ham et al., 2014; Preissler et al., 2015). Although the initial endogenous amount of AMPylated BiP appears slightly higher in HEK293 than CHO-K1 cells, both cell lines similarly react to TG treatment for 2 h, with the complete removal of BiP-AMPylation, and to CHX treatment for 4 h with a strong increase in AMPylated BiP.

To verify that antibody 17G6's ability to immunoprecipitate recombinant BiP (Figure 4B) would successfully translate into an IP in the environment of cell lysate, we applied antibody 17G6 to the aforementioned (Figure 4C) TG as well as CHX-treated CHO-K1 cells (Figure 4D). The detection of a successful IP from cell lysates was hampered by the detection limit of the anti-BiP antibody, which did not recognize BiP at less than 50 ng per lane. With detection limits of the anti-AMP antibodies far lower, the difficulty to detect a band by the anti-AMP antibody 17G6 in untreated CHO-K1 whole-cell lysates (in WB, Figure 4C) hints at very low endogenous amounts of AMPylated BiP, whereas the less sensitive anti-BiP antibody leads to a more pronounced signal. Therefore, we had to assume that the percentage of AMPylated BiP in the untreated CHO-K1 cell lysates was very low. Consequently, AMPylation was stimulated by CHX treatment to create enough pull-down material for detection with anti-BiP antibody. Antibody 17G6 was able to immunoprecipitate AMPylated BiP from CHX-treated cell lysates, whereas the detection by anti-BiP antibody remains rather faint (Figure 4D). This effect may be explained by the high intracellular concentrations of nucleotides such as AMP, ADP, and ATP that will compete for binding with the anti-AMP antibodies. To overcome this challenge, we extracted the proteome from untreated (ctrl) as well as TG- and CHX-treated CHO-K1 cell lysates by methanol/chloroform precipitation to eliminate competing nucleotides. Denatured AMPylated BiP was immunoprecipitated from the resuspended protein pellets by antibody 17G6 (Figure 4E). Enriched BiP-AMP could be detected in the bound sample from CHX-treated CHO-K1 cells at much higher amounts in relation to the input than without methanol/chloroform precipitation (Figure 4D). The yield and efficiency of the IP of AMPylated BiP was thereby greatly improved.

After the thorough characterization of our antibodies' performance in WB, we asked the question whether these sensitive tools were able to detect new AMPylation bands in cell lysates. We therefore screened a number of available immortalized and cancer cell lines for occurrence of AMPylation bands using our newly

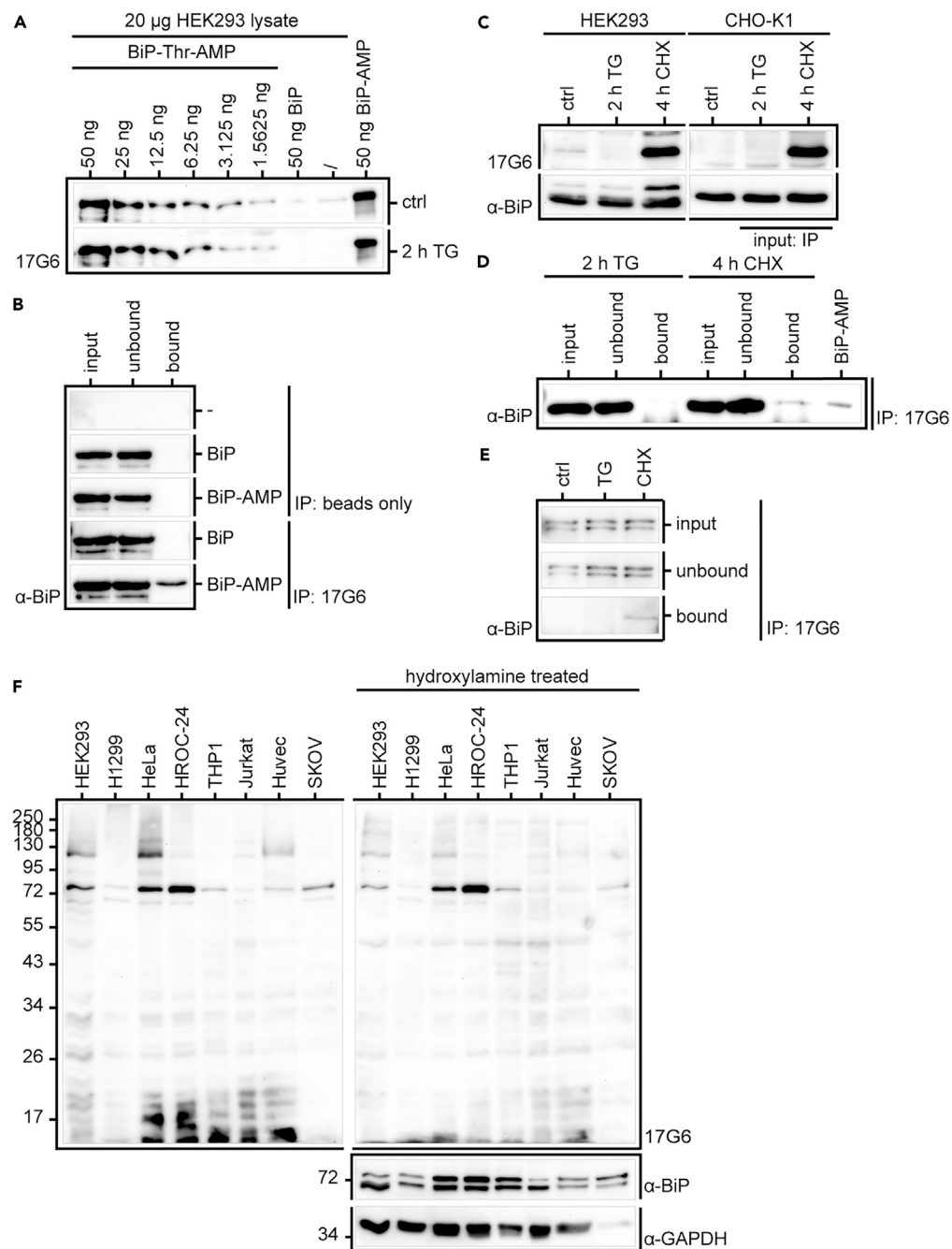


Figure 4. Evaluation of Generated Anti-AMP Antibodies in IP and Application to Whole-Cell Lysate

(A) Analysis of BiP-AMPylation detection levels in HEK293 lysate, either untreated (ctrl) or treated by TG, in WB by antibody 17G6 in the presence of $MnCl_2$. 20 μ g HEK293 lysate was spiked with a titration of recombinant BiP-AMP or 50 ng unmodified BiP as indicated. Unspiked lysate and 50 ng purified BiP-AMP alone served as negative and positive ctrl, respectively. Rows represent identical WBs.

(B) IP with antibody 17G6 on recombinant BiP or BiP-AMP in 500 μ L was precipitated by 10 μ g 17G6 and Protein A/G Magnetic Beads or beads alone. Bound protein was eluted with 100 μ L 1 \times Laemmli. Samples with and without addition of 17G6 were treated identically. 7.5 μ L each of input and unbound samples supplemented with 5 \times Laemmli buffer and 2.5 μ L elution were analyzed in WB using an anti-BiP antibody. Rows of IP: beads only and IP: 17G6 represent the same WB.

(C) Analysis of BiP-AMPylation upon ER stress by TG or CHX in WB. 20 μ g total protein lysate of HEK293 and CHO-K1 cells, untreated or treated with either TG for 2 h or CHX for 4 h was analyzed in WB using antibody 17G6 in the presence of

Figure 4. Continued

MnCl₂, before the blot was stripped and reprobed with an anti-BiP antibody. 10 ng recombinant Cdc42-Tyr-AMP as well as unmodified Cdc42 was blotted as control (see [Supplemental Information](#)). The indicated CHO-K1 samples served as input for the IP in [Figure 4D](#). All samples represent one WB.

(D) IP of endogenous BiP-AMP with antibody 17G6 from TG- and CHX-treated (as indicated) CHO-K1 cell lysates. 1 mg (in 500 μL) total protein lysate of CHO-K1 cells treated with either TG for 2 h or CHX for 4 h was precipitated by 10 μg 17G6 and Protein A/G Magnetic Beads. Bound proteins were eluted with 100 μL 1× Laemmli and concentrated to 20 μL. 5 μL each of input and unbound sample supplemented with 6× Laemmli buffer and 20 μL concentrated elution were analyzed in WB using an anti-BiP antibody. 50 ng recombinant BiP-AMP was blotted as control.

(E) IP of endogenous BiP-AMP with antibody 17G6 from untreated (ctrl) and TG- and CHX-treated (as indicated) CHO-K1 cell lysates after methanol/chloroform precipitation. 250 μg total protein lysate of CHO-K1 cells, untreated or treated with either TG for 2 h or CHX for 4 h, was precipitated by methanol/chloroform precipitation. Denatured protein from the resuspended protein pellet was immunoprecipitated by 5 μg 17G6 in 125 μL Protein A/G Magnetic Beads. Bound proteins were eluted with 50 μL 1× Laemmli. 5 μL each of input and unbound sample supplemented with 6× Laemmli buffer and 20 μL of elution were analyzed in WB using an anti-BiP antibody. All rows represent the same WB. 50 ng recombinant BiP-AMP and BiP were blotted as control.

(F) See also [Figures S6](#) and [S7](#). Analysis of AMPylation patterns in various immortalized and cancer cell lines in WB by antibody 17G6 in the presence of MnCl₂. 20 μg total protein lysate per lane of cell lines as indicated was probed with antibody 17G6 using 1 mM MnCl₂ as additive during primary antibody incubation. Afterward the blot was treated with 1 M hydroxylamine to cleave ADP-ribosylation at aspartate and glutamate residues, and reprobed with antibody 17G6 in the presence of 1 mM MnCl₂. The identical blot was stripped and reprobed with antibodies against BiP and GAPDH as loading control.

developed monoclonal antibodies ([Figures 4F](#) and [S6](#)). Indeed, our anti-AMP antibodies were able to detect a multitude of bands in the range of 58–245 kDa and 11–22 kDa. Strikingly, some bands differed among cell lysates, whereas others were distinctive and reoccurring. Some cell lines, such as THP-1, show very little to no AMPylation signals, whereas other cell lines such as HeLa, HEK293, and HROC-24 cells show strong AMPylation signals. Treatment of membranes with hydroxylamine to cleave off ADP-ribosylation at aspartate and glutamate residues does remove bands at 11–22 kDa but does not significantly diminish the bands at 70–80 kDa. Furthermore, these bands are not detected by the anti-pan-ADPR-binding reagent (Merck) ([Figure S7](#)), or tyrosine-specific anti-AMP antibody 1G11 ([Figure S6](#)), but both anti-AMP antibodies 7C11 ([Figure S6](#)) and 17G6 ([Figure 4F](#)), strongly suggesting AMPylation at threonine residues. As antibody 1G11 switches between a general recognition of all AMPylated side chains ([Figures 2A](#) and [2B](#)) and a tyrosine-specific recognition in the presence of MnCl₂ ([Figures 3B](#) and [3C](#)), we reprobed the blot previously incubated with antibody 1G11 in the presence of MnCl₂ with antibody 1G11 alone ([Figure S6](#)), both before and after hydroxylamine treatment. In both cases, a band pattern very similar to the blots of 7C11 and 17G6 arose, further supporting a predominance of threonine AMPylation in human cells. The reoccurring band at 70 kDa, most likely representing BiP-AMP, strongly differs in intensity among cell lysates: whereas H1299, THP-1, Jurkat, and Huvec cells do not show this band at all, it is strongly represented in HeLa, HROC-24, and HEK293 cells. Probing the same cell lysates with both commercial anti-AMP antibodies (Merck) resulted in no significant bands for the anti-Thr-AMP antibody ([Figure S7](#)) as expected based on its performance on recombinant AMPylated protein ([Figure 1A](#)). Although the anti-Tyr-AMP did detect a band at around 30 kDa in THP-1 as well as Jurkat cell lysates ([Figure S7](#)), it did not recognize the positive control of Cdc42-Tyr-AMP, thus the significance of the band remains doubtful.

DISCUSSION

Here, we report and characterize three new monoclonal anti-AMP antibodies that recognize AMPylation independent of the protein backbone. To reduce the inherent batch-to-batch variability of the previously published polyclonal antibodies, as well as generate defined specificities, we created monoclonal antibodies in mice. The reproducibility crisis of antibodies in recent years ([Baker, 2015](#)), as well as the limitations of commercially available anti-AMPylation-antibodies ([Hao et al., 2011](#)) (Sigma-Aldrich ABS184 and 09-890) let us to perform a thorough evaluation of the new monoclonal antibodies' performance in two different applications. For denatured recognition, we tested sensitivity, specificity, and cross-reactivity of our antibodies in WBs. For native recognition, we studied complex formation of the antibody with different modified targets by size exclusion chromatography, as well as confirmed native binding in IP experiments. In WB, the antibodies show cross-reactivity toward MARYlation. Although hydroxylamine treatment of membranes proves helpful in cleaving off MARYlation at aspartate and glutamate residues, it might not always completely remove the MARYlation signal, either due to the abundance of the modified protein or due to modification on residues other than aspartate and glutamate, such as lysine. Therefore, a careful

evaluation of findings with orthogonal methods such as MS is crucial. In IP, low abundance of AMPylation might hinder efficient enrichment, especially if high amounts of competing nucleotides or mono-ADP-ribosylation are present. A proteome extraction by methanol/chloroform protein precipitation might help to get rid of competing nucleotides and enrich AMPylated protein in a denatured state.

The antibodies were generated with the help of an AMPylated synthetic peptide with reduced backbone complexity. A major bottleneck in antibody generation based on synthesized peptides, which is also reported for the generation of other anti-PTM antibodies such as anti-phospho antibodies (Archuleta et al., 2011), is the phenomenon of predominantly positive peptide ELISA readings against modified haptens that do not translate to a positive WB performance. Common procedure is to only select via ELISA against the modified hapten. According to Archuleta et al. (2011), this method selects antibodies whose performance fails in other applications in 25%–50% cases. However, in our selection process we observed a high correlation between positive ELISA readings against modified protein, which we performed in addition to peptide ELISA, and good WB performance. The inclusion of a native AMPylated protein in the form of Cdc42-Thr-AMP in the ELISA screening process allowed us to generate monoclonal antibodies combined with efficient preselection of candidates before WB evaluation. We therefore recommend including native modified protein in the ELISA screening process for all anti-PTM antibodies.

First efforts in the creation of anti-AMP antibodies were undertaken in 1984 by fusing AMP directly to the carrier protein BSA (Chung and Rhee, 1984), thus generating murine monoclonal antibodies that were purified from ascitic fluid and employed in the purification of AMPylated glutamine synthetase. Later on, other antibodies were accidentally produced by aiming for ADP-ribose antibodies, where the hapten was degraded to contain AMP, resulting in antibodies recognizing free 5'-AMP (Bredehorst et al., 1978; Meyer and Hilz, 1986). Hao et al. (2011) achieved polyclonal antibodies by immunization of rabbits with a synthetic seven-amino-acid-long Rac1-peptide containing a threonine AMPylation (now commercially available as Anti-pan-AMPylated Threonine Antibody 09-890, Sigma-Aldrich Merck). After depletion with tyrosine-AMPylated protein the serum was reported to detect threonine AMPylation independently of protein backbone and structure, in WB as well as in IP. The most recent antibody was produced by an AMPylated Rab1b peptide of 13 amino acids coupled to KLH in rabbit, resulting in polyclonal serum, aided again by efficient synthesis of AMPylated peptides (Smit et al., 2011). However, both published rabbit antibodies are hampered by low sensitivity and little characterization, especially concerning cross-reactivity with other PTMs and recognition of targets outside the protein class of small GTPases or BiP. In addition, all recently developed antibodies are polyclonal with the accompanying challenges of batch-to-batch reproducibility and reliability of tool development on the basis of that antibody. Considering the special challenges connected with the generation of antibodies that target PTMs (Hattori and Koide, 2018), and their necessity for extensive characterization, polyclonal antibodies are not an ideal choice. A stringent retesting of every new batch regarding proper AMP recognition and lack of cross-reactivity would have to be performed before application to cell lysates. Previous antibodies therefore represent no general recognition tool of AMPylation, especially if searching for new targets and effects where the number of potential false-negative or false-positive findings would render them unreliable. Our experiments show that all commercially available anti-AMP antibodies offer no broad recognition of targets, despite claiming to recognize AMPylation backbone independently, and are exhibiting a significant amount of false-positive and negative reactions in our in-house testing. The limitations in performance and cross-reactivity of both anti-ADPR reagents and anti-AMPylation antibodies in combination causes the danger of false-positives for ADP-ribosylation as well as false-negatives in AMPylated proteins, and a bias in AMPylation research toward small GTPases and threonine modifications (Figure 1A). As many researchers lack suitable positive and negative controls of protein of interest, these performance failures might never be detected.

Little is known about AMPylation in eukaryotic cells outside the modification of BiP in the context of ER stress. In accordance with recent publications (Kielkowski et al., 2020; Sreelatha et al., 2018), the application of our new monoclonal antibodies to cell lysates of immortalized and cancer cell lines hints at a much stronger prevalence of AMPylation than ever perceived. The limited number of tools, especially in medium to high throughput, has hampered reliable detection of AMPylation in cellular systems. Our antibodies expand the available toolbox by offering sensitive detection and enrichment of AMPylation, while at the same time requiring little resources that might hamper applicability in a standard laboratory. These antibodies therefore open new opportunities in an expanding research field. The recent antibody “reproducibility crisis,” especially in regard to antibodies targeting PTMs (Baker, 2015; Egelhofer et al., 2011),

suggested a thorough characterization of the AMPylation specificity and sensitivity of our new monoclonal antibodies in the applications WB, ELISA, and IP. With their high sensitivity and broad target recognition, they overcome the limitations of previously published anti-AMP antibodies and create opportunities for new target identification and study of cellular AMPylation. Our data suggest that they can successfully be used for enrichment of AMPylated proteins and peptides for MS to overcome the limitation of low occurrence of AMPylation in proteomic studies. As all three monoclonal antibodies are sequenced (see [Supplemental Information](#)), thereby enabling recombinant antibody production, they form a good basis for long-term reproducibility in AMPylation research.

Limitations of the Study

The present study generated and characterizes three new monoclonal anti-AMP antibodies in the applications WB, ELISA, and IP. In WB, the antibodies show cross-reactivity toward MARYlation: although hydroxylamine treatment of membranes proves helpful in cleaving off MARYlation at aspartate and glutamate residues, it might not always completely remove MARYlation signal, either due to a high abundance of the modified protein or modification on residues other than aspartate and glutamate, such as lysine. Therefore, a careful evaluation of findings with orthogonal methods such as MS, etc., is crucial. In IP, low abundance of AMPylation might hinder efficient enrichment, especially if high amounts of competing nucleotides or mono-ADP-ribosylation are present. Other applications such as immunofluorescence and immunohistochemistry remain uncharacterized.

Resource Availability

Lead Contact

Further information and requests for resources and reagents should be directed to and will be fulfilled by the Lead Contact, Aymelt Itzen (a.itzen@uke.de).

Materials Availability

Plasmids generated in this study are available upon request. Reasonable requests for the generated monoclonal anti-AMP antibodies will be fulfilled by the Lead Contact, Aymelt Itzen.

Data and Code Availability

This study did not generate or analyze datasets or code. All uncropped WB and gel images along with their dynamic range are depicted in the [Supplemental Information \(Data S1\)](#). The antibody sequencing results of all three monoclonal anti-AMP antibodies are included in the [Supplemental Information](#).

METHODS

All methods can be found in the accompanying [Transparent Methods supplemental file](#).

SUPPLEMENTAL INFORMATION

Supplemental Information can be found online at <https://doi.org/10.1016/j.isci.2020.101800>.

ACKNOWLEDGMENTS

SKOV3 cells were a kind gift of Leticia Oliveira-Ferrer, Department of Gynecology, University Medical Centre Hamburg-Eppendorf. HROC24 cells were a kind gift of Yuan-Na Lin, Department of General, Visceral and Thoracic Surgery, University Medical Centre Hamburg-Eppendorf. Jurkat cells, subclone JMP (DMSZ verified), and CHO-K1-FlpIn cells were a kind gift of Ralf Fliegert, Institute of Biochemistry and Molecular Cell Biology, University Medical Centre Hamburg-Eppendorf. HUVEC cells isolated from umbilical cords were a kind gift of Volker Huck, Centre for Internal Medicine/Diagnostics, University Medical Centre Hamburg-Eppendorf in cooperation with Kurt Hecher, Department of Obstetrics and Fetal Medicine, University Medical Center Hamburg-Eppendorf. Schemes were created with [BioRender.com](#). D.H. was supported by a PhD scholarship of the Konrad-Adenauer-Stiftung. This work was performed within the framework of SFB 1035 (German Research Foundation DFG, Sonderforschungsbereich 1035, Projektnummer 201302640, project B05). We are grateful to the Knut and Alice Wallenberg Foundation, Sweden (KAW 2013.0187 to C.H.), and the Swedish Research Council (VR) for generous support.

AUTHORS CONTRIBUTION

D.H., C.H., and A.I. designed peptides and strategy for antibody generation; D.H. and A.I. designed antibody characterization; D.H. performed evaluation of antibody generation; D.H., J.F., and M.S.K. performed antibody characterization; C.P. performed peptide synthesis; D.H. and A.I. wrote the paper; C.H. and A.I. provided oversight over the project.

DECLARATION OF INTERESTS

The authors declare that they have no competing interests.

Received: August 7, 2020

Revised: October 16, 2020

Accepted: November 10, 2020

Published: December 18, 2020

REFERENCES

- Albers, M.F., Van Vliet, B., and Hedberg, C. (2011). Amino acid building blocks for efficient Fmoc solid-phase synthesis of peptides adenylated at serine or threonine. *Org. Lett.* **13**, 6014–6017.
- Archuleta, A.J., Stutzke, C.A., Nixon, K.M., and Browning, M.D. (2011). Optimized protocol to make phospho-specific antibodies that work. In *Signal transduction immunohistochemistry: methods and protocols, methods in molecular biology*, A.E. Kalyuzhny, ed. (Springer Science+Business Media), pp. 69–88.
- Baker, M. (2015). Blame it on the antibodies. *Nature* **521**, 274–276, <https://doi.org/10.1038/521274a>.
- Bredehorst, R., Ferro, A.M., and Hilz, H. (1978). Production of antibodies against ADP-ribose and 5'-AMP with the aid of N⁶-carboxymethylated ADP-ribose conjugates. *Eur. J. Biochem.* **82**, 105–113.
- Chung, H.K., and Rhee, S.G. (1984). Separation of glutamine synthetase species with different states of adenylation by chromatography on monoclonal anti-AMP antibody affinity columns. *Proc. Natl. Acad. Sci. U S A* **81**, 4677–4681.
- Egelhofer, T.A., Minoda, A., Klugman, S., Lee, K., Kolasinska-Zwierz, P., Alekseyenko, A.A., Cheung, M.S., Day, D.S., Gadel, S., Gorchakov, A.A., et al. (2011). An assessment of histone-modification antibody quality. *Nat. Struct. Mol. Biol.* **18**, 91–94.
- Engel, P., Goepfert, A., Stanger, F.V., Harms, A., Schmidt, A., Schirmer, T., and Dehio, C. (2012). Adenylation control by intra- or intermolecular active-site obstruction in Fic proteins. *Nature* **482**, 107–110.
- Grammel, M., Luong, P., Orth, K., and Hang, H.C. (2011). A chemical reporter for protein AMPylation. *J. Am. Chem. Soc.* **133**, 17103–17105.
- Ham, H., Woolery, A.R., Tracy, C., Stenesen, D., Krämer, H., and Orth, K. (2014). Unfolded protein response-regulated Drosophila Fic (dFic) protein reversibly AMPylates BiP chaperone during endoplasmic reticulum homeostasis. *J. Biol. Chem.* **289**, 36059–36069.
- Hao, Y.H., Chuang, T., Ball, H.L., Luong, P., Li, Y., Flores-Saaib, R.D., and Orth, K. (2011). Characterization of a rabbit polyclonal antibody against threonine-AMPylation. *J. Biotechnol.* **151**, 251–254.
- Hattori, T., and Koide, S. (2018). Next-generation antibodies for post-translational modifications. *Curr. Opin. Struct. Biol.* <https://doi.org/10.1016/j.sbi.2018.04.006>.
- Khater, S., and Mohanty, D. (2015). In silico identification of AMPylating enzymes and study of their divergent evolution. *Sci. Rep.* **5**, 10804.
- Kielkowski, P., Buchsbaum, I.Y., Kirsch, V.C., Bach, N.C., Drukker, M., Cappello, S., and Sieber, S.A. (2020). FICD activity and AMPylation remodelling modulate human neurogenesis. *Nat. Commun.* **11**, 1–13.
- Kingdon, H.S., Shapiro, B.M., and Stadtman, E.R. (1967). Regulation of glutamine synthetase. VIII. ATP: glutamine synthetase adenylyltransferase, an enzyme that catalyzes alterations in the regulatory properties of glutamine synthetase. *Proc. Natl. Acad. Sci. U S A* **58**, 1703–1710.
- Mattoo, S., Durrant, E., Chen, M.J., Xiao, J., Lazar, C.S., Manning, G., Dixon, J.E., and Worby, C.A. (2011). Comparative analysis of Histophilus somni immunoglobulin-binding protein A (IbpA) with other Fic domain-containing enzymes reveals differences in substrate and nucleotide specificities. *J. Biol. Chem.* <https://doi.org/10.1074/jbc.M111.227603>.
- Meyer, T., and Hilz, H. (1986). Production of anti-(ADP-ribose) antibodies with the aid of a dinucleotide-pyrophosphatase-resistant hapten and their application for the detection of mono(ADP-ribosyl)ated polypeptides. *Eur. J. Biochem.* **155**, 157–165.
- Moss, J., Yost, D.A., and Stanley, S.J. (1983). Amino acid-specific ADP-ribosylation. *J. Biol. Chem.* **258**, 6466–6470.
- Müller, M.P., Peters, H., Blümer, J., Blankenfeldt, W., Goody, R.S., and Itzen, A. (2010). The Legionella effector protein DrrA AMPylates the membrane traffic regulator Rab1b. *Science* **329**, 946–949.
- Plagemann, P.G.W., and Wohlhueter, R.M. (1980). Permeation of nucleosides, nucleic acid bases, and nucleotides in Animal cells. *Curr. Top. Membr. Transp.* **14**, 225–330.
- Preissler, S., Rato, C., Chen, R., Antrobus, R., Ding, S., Fearnley, I.M., and Ron, D. (2015). AMPylation matches BiP activity to client protein load in the endoplasmic reticulum. *Elife* **4**, e12621.
- Preissler, S., Rato, C., Perera, L.A., Saudek, V., and Ron, D. (2016). FICD acts bifunctionally to AMPylate and de-AMPylate the endoplasmic reticulum chaperone BiP. *Nat. Struct. Mol. Biol.* **24**, 23–29.
- Sanyal, A., Chen, A.J., Nakayasu, E.S., Lazar, C.S., Zbornik, E.A., Worby, C.A., Koller, A., and Mattoo, S. (2015). A novel link between fic (filamentation induced by cAMP)-mediated adenylation/AMPylation and the unfolded protein response. *J. Biol. Chem.* **290**, 8482–8499.
- Smit, C., Blümer, J., Eerland, M.F., Albers, M.F., Müller, M.P., Goody, R.S., Itzen, A., and Hedberg, C. (2011). Efficient synthesis and applications of peptides containing adenylylated tyrosine residues. *Angew. Chem. Int. Ed.* **50**, 9200–9204.
- Sreelatha, A., Yee, S.S., Lopez, V.A., Park, B.C., Kinch, L.N., Pilch, S., Servage, K.A., Zhang, J., Jiou, J., Karasiewicz-Urbańska, M., et al. (2018). Protein AMPylation by an evolutionarily conserved pseudokinase. *Cell* **175**, 809–821.e19.
- Truttmann, M.C., Cruz, V.E., Guo, X., Engert, C., Schwartz, T.U., and Ploegh, H.L. (2016). The Caenorhabditis elegans protein FIC-1 is an AMPylase that covalently modifies heat-shock 70 family proteins, translation elongation factors and histones. *PLoS Genet.* **12**, 1–26.
- Vyas, S., Matic, I., Uchima, L., Rood, J., Zaja, R., Hay, R.T., Ahel, I., and Chang, P. (2014). Family-wide analysis of poly(ADP-ribose) polymerase activity. *Nat. Commun.* **5**, 4426.
- Wang, P., and Silverman, S.K. (2016). DNA-catalyzed introduction of azide at tyrosine for peptide modification. *Angew. Chem. Int. Ed.* **55**, 10052–10056.
- Worby, C.A., Mattoo, S., Kruger, R.P., Corbeil, L.B., Koller, A., Mendez, J.C., Zekarias, B., Lazar, C., and Dixon, J.E. (2009). The fic domain: regulation of cell signaling by adenylation. *Mol. Cell* **34**, 93–103.

Yarborough, M.L., Li, Y., Kinch, L.N., Grishin, N.V., Ball, H.L., and Orth, K. (2009). AMPylation of Rho GTPases by *Vibrio* VopS disrupts effector binding and downstream signaling. *Science* 323, 269–272.

Yu, X., Woolery, A.R., Luong, P., Hao, Y.H., Grammel, M., Westcott, N., Park, J., Wang, J., Bian, X., Demirkan, G., et al. (2014). Copper-catalyzed azide-alkyne cycloaddition (click

chemistry)-based detection of global pathogen-host AMPylation on self-assembled human protein microarrays. *Mol. Cell. Proteomics* 13, 3164–3176.

iScience, Volume 23

Supplemental Information

Monoclonal Anti-AMP Antibodies Are Sensitive and Valuable Tools for Detecting Patterns of AMPylation

Dorothea Höpfner, Joel Fauser, Marietta S. Kaspers, Christian Pett, Christian Hedberg, and Aymelt Itzen

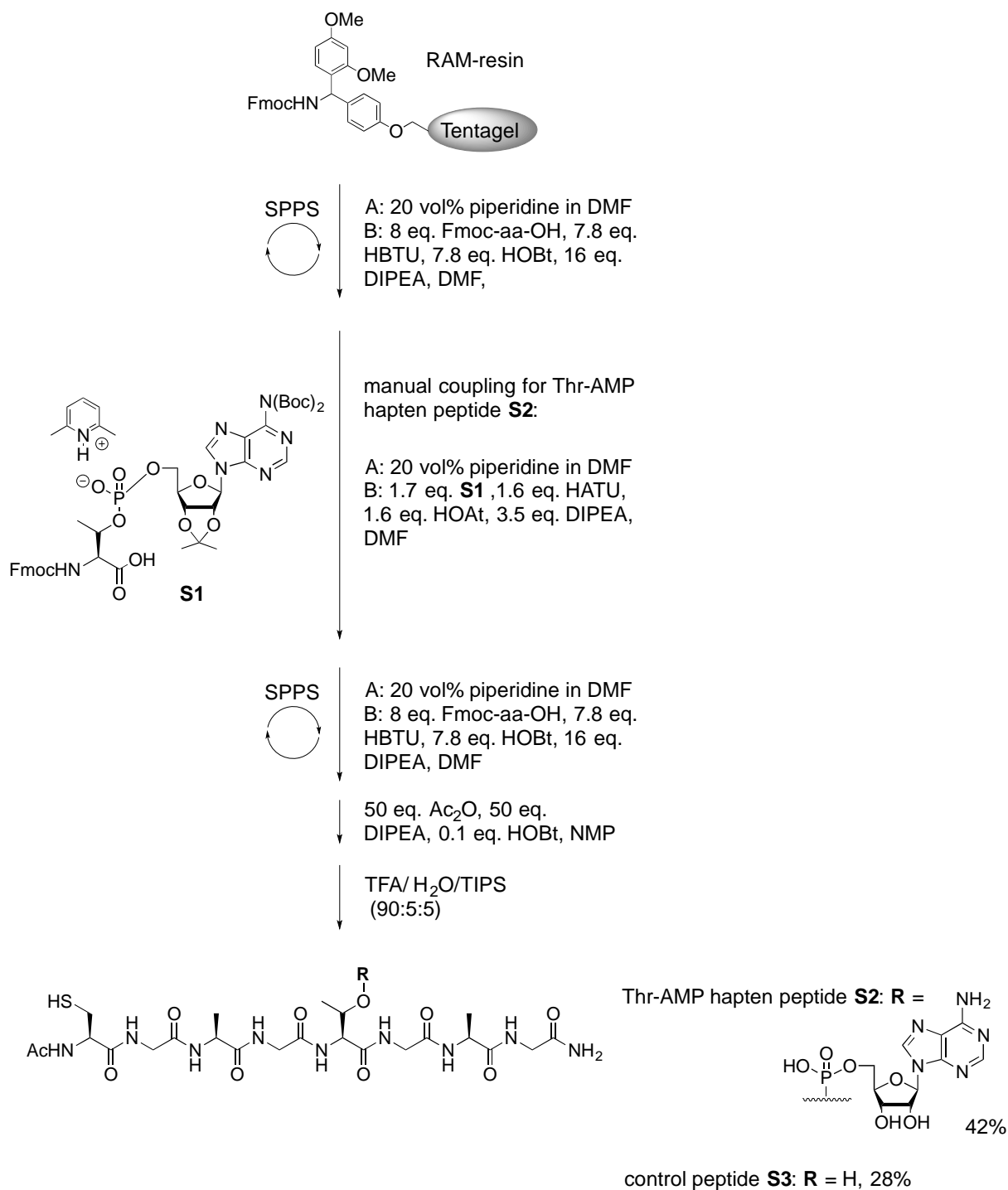


Figure S1: Solid phase peptide synthesis scheme of peptides S2 and S3. Related to Figure 1D.

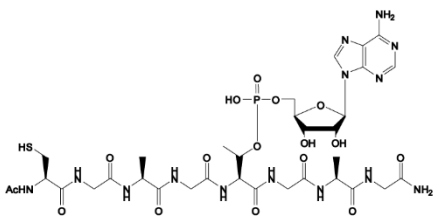
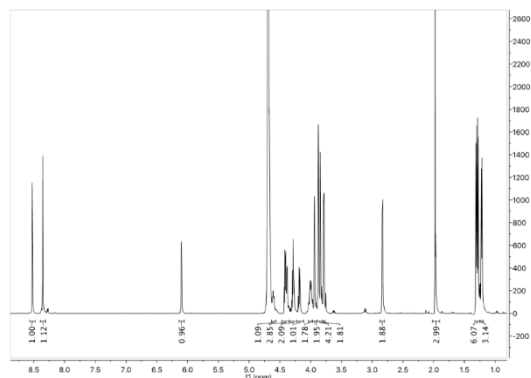
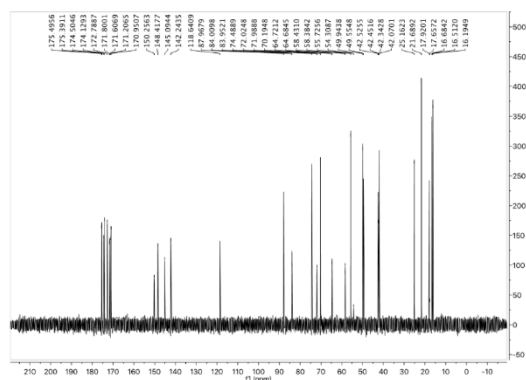
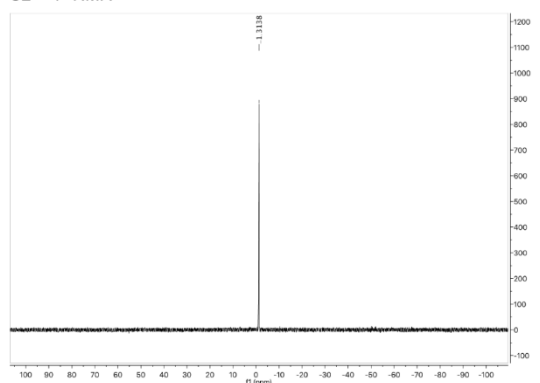
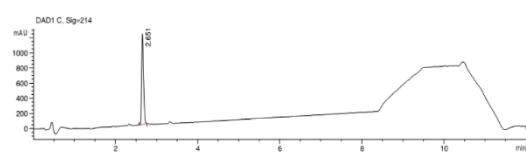
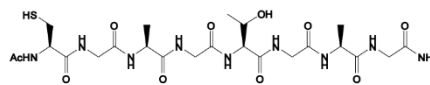
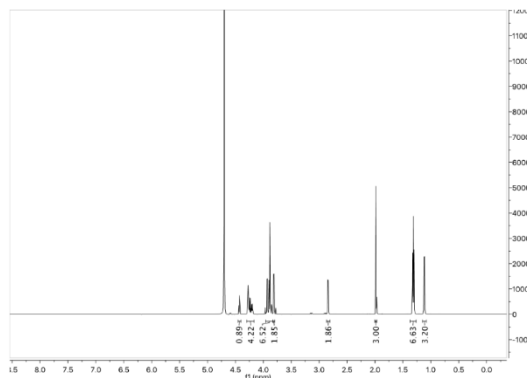
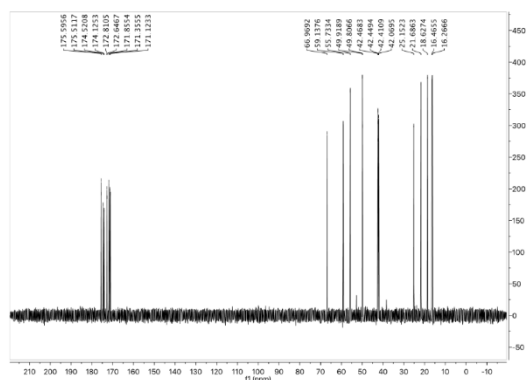
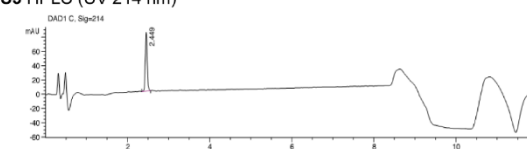
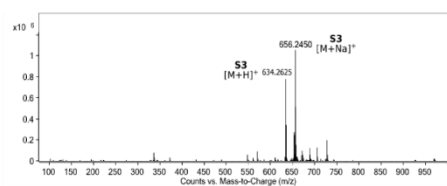
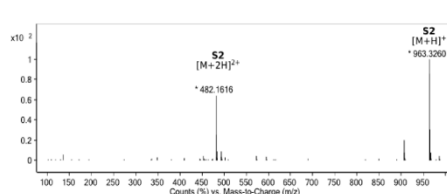
S2**S2** ¹H-NMR**S2** ¹³C-NMR**S2** ³¹P-NMR**S2** HPLC (UV 214 nm)**S3****S3** ¹H-NMR**S3** ¹³C-NMR**S3** HPLC (UV 214 nm)**S3** HR-ESI-MS**S2** HR-ESI-MS

Figure S2: Quality control of synthesized peptides S2 and S3. Related to Figure 1D. Thr-AMP hapten peptide Ac-CGAGT(AMP)GAG-NH₂ (**S2**) was synthesized on 100 mg (25 μmol) of Tentagel-S-RAM resin. Yield: 42% (10.0 mg, 10.4 μmol). Analytical HPLC R_t = 2.651 min (A/B, (98 : 2) → (75 : 25), 500 μL/min, 7 min); Preparative HPLC R_t = 8.945 min (A/B, (97.5 : 2.5) → (50 : 50), 20 mL/min,

10 min). **HR-ESI-MS**, m/z: 482.1616 ($[M+2H]^{2+}$, calc. 482.1606), 963.3260 ($[M+H]^+$, calc. 963.3139). **¹H NMR** (600 MHz, D₂O) δ : 8.52 (s, 1H), 8.35 (s, 1H), 4.62-4.59 (m, 1H), 4.43-4.39 (m, 3H), 4.31-4.27 (m, 2H), 4.18 (q, J = 7.3 Hz, 1H), 4.04-3.97 (m, 2H), 3.94 (s_{br}, 2H), 3.87 (s, 2H), 3.84 (s, 2H), 3.79 (d, J = 5.2 Hz, 2H), 2.83 (d, J = 6.0 Hz, 2H), 1.98 (s, 3H), 1.31 (d, J = 7.3 Hz, 3H), 1.28 (d, J = 7.3 Hz, 3H), 1.22 (d, J = 6.4 Hz, 3H). **³¹P NMR** (242.9 MHz, D₂O) δ : -1.31 (s). **¹³C NMR** (125.9 MHz, D₂O) δ : 175.50, 175.39, 174.50, 174.13, 172.79, 171.80, 171.61, 171.21, 170.95, 150.25, 148.09, 142.24, 118.64, 118.64, 87.97, 84.01, 83.95, 74.49, 72.02, 71.99, 70.19, 64.72, 64.68, 58.43, 58.38, 55.73, 49.94, 49.55, 42.52, 42.45, 42.34, 42.07, 25.16, 21.69, 17.92, 16.68, 16.19.

The threonine peptide Ac-CGAGTGAG-NH₂ (**S3**) was synthesized on 100 mg (25 μ mol) of Tentagel-S-RAM resin. Yield: 28% (4.4 mg, 6.9 μ mol). Analytical **HPLC** R_t = 2.449 min (A/B, (98 : 2) \rightarrow (75 : 25), 500 μ L/min, 7 min); Preparative HPLC R_t = 7.148 min (A/B, (97.5 : 2.5) \rightarrow (50 : 50), 20 mL/min, 10 min). **HR-ESI-MS**, m/z: 634.2625 ($[M+H]^+$, calc. 634.2613), 656.2450 ($[M+Na]^+$, calc. 656.2433). **¹H NMR** (600 MHz, D₂O) δ : 4.43 (t, J = 6.1 Hz, 1H), 4.29-4.18 (m, 4H), 3.94-3.88 (m, 6H), 3.81 (d, J = 5.7 Hz, 2H), 2.85 (d, J = 6.2 Hz, 2H), 1.98 (s, 3H), 1.33-1.30 (m, 6H), 1.12 (d, J = 6.4 Hz, 3H). **¹³C NMR** (125.9 MHz, D₂O) δ : 175.60, 175.51, 174.52, 174.13, 172.81, 172.65, 171.86, 171.36, 171.12, 66.97, 59.14, 58.38, 55.73, 49.92, 49.80, 42.47, 42.45, 42.41, 42.07, 25.15, 21.69, 18.63, 16.47, 16.27.

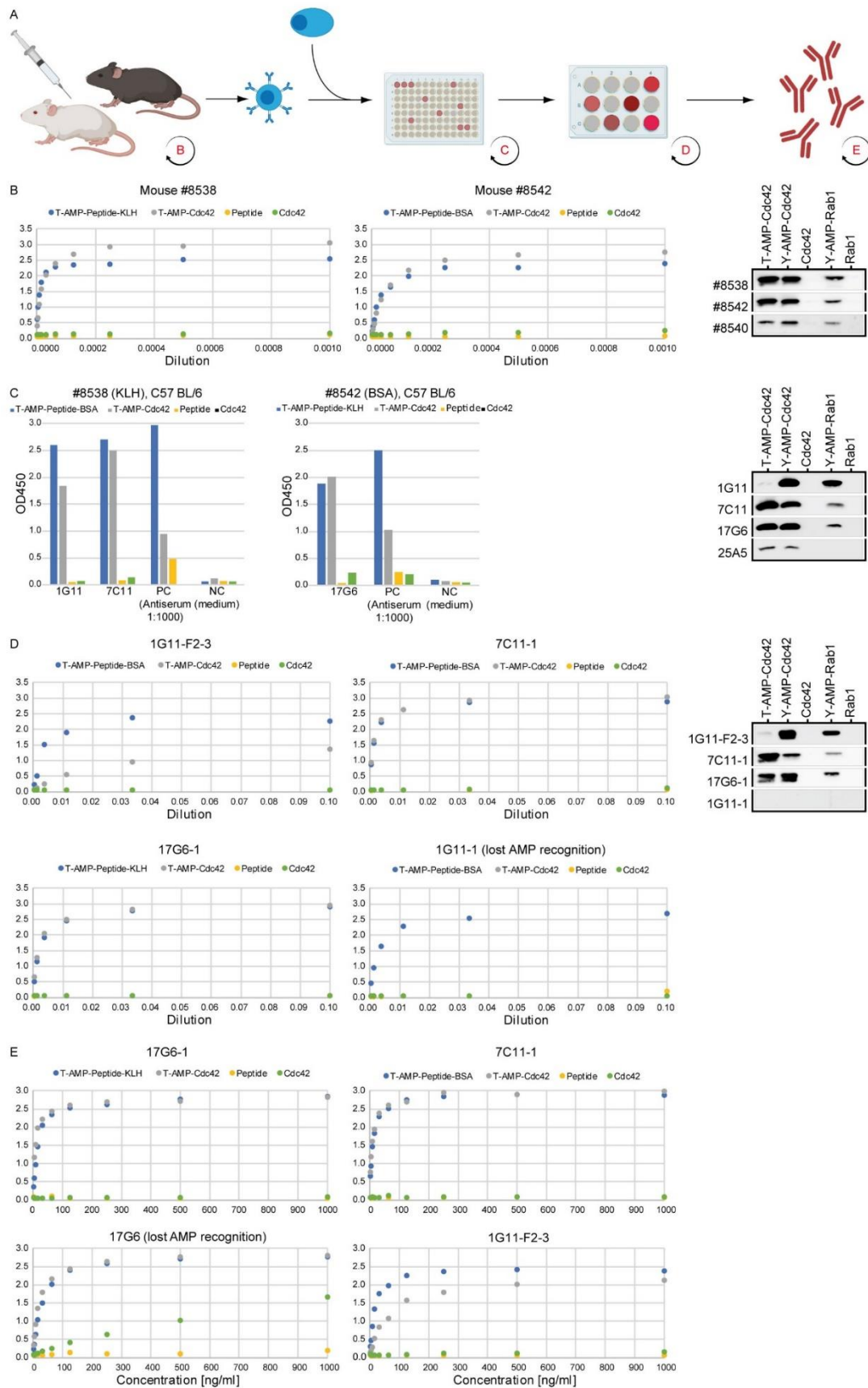


Figure S3: Antibody generation and selection of antibodies binding to native epitopes. Related to Figure 1E. **(A)** Immunization protocol of mice. Evaluation time points are indicated by circular arrows. **(B-D)** Evaluation regarding recognition of AMPylation in WB and ELISA of **(B)** mice sera **(C)** parental hybridoma clones **(D)** subclones and **(E)** produced and purified antibodies.

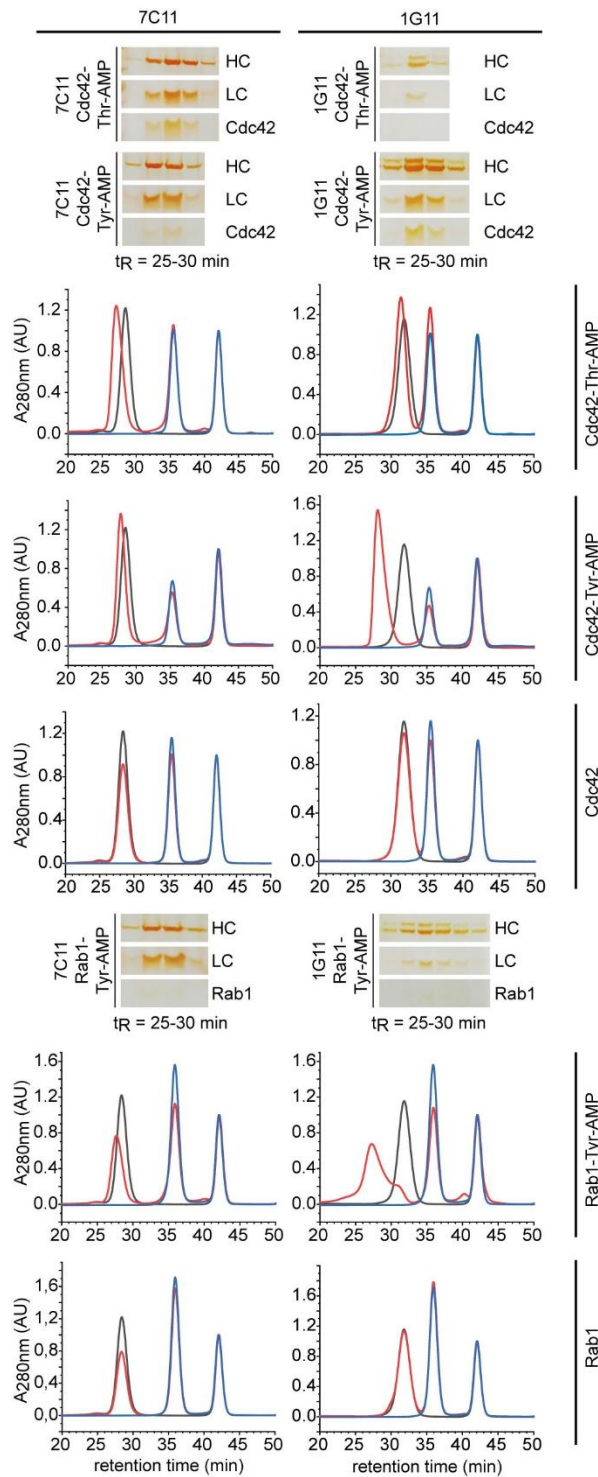


Figure S4: Native binding of AMPylated antigens by monoclonal antibodies 7C11 and 1G11 as determined by analytical size exclusion chromatography. Related to Figure 2C. In black antibody alone, in blue antigen alone as indicated, in red co-incubation of antibody and antigen as indicated. Shifted antibody peaks (red) upon co-incubation with AMPylated antigens were fractionated and analyzed for co-elution of antibody (light chain, LC; heavy chain, HC) and antigen by silver stained SDS PAGE (cropped rows represent identical gels).

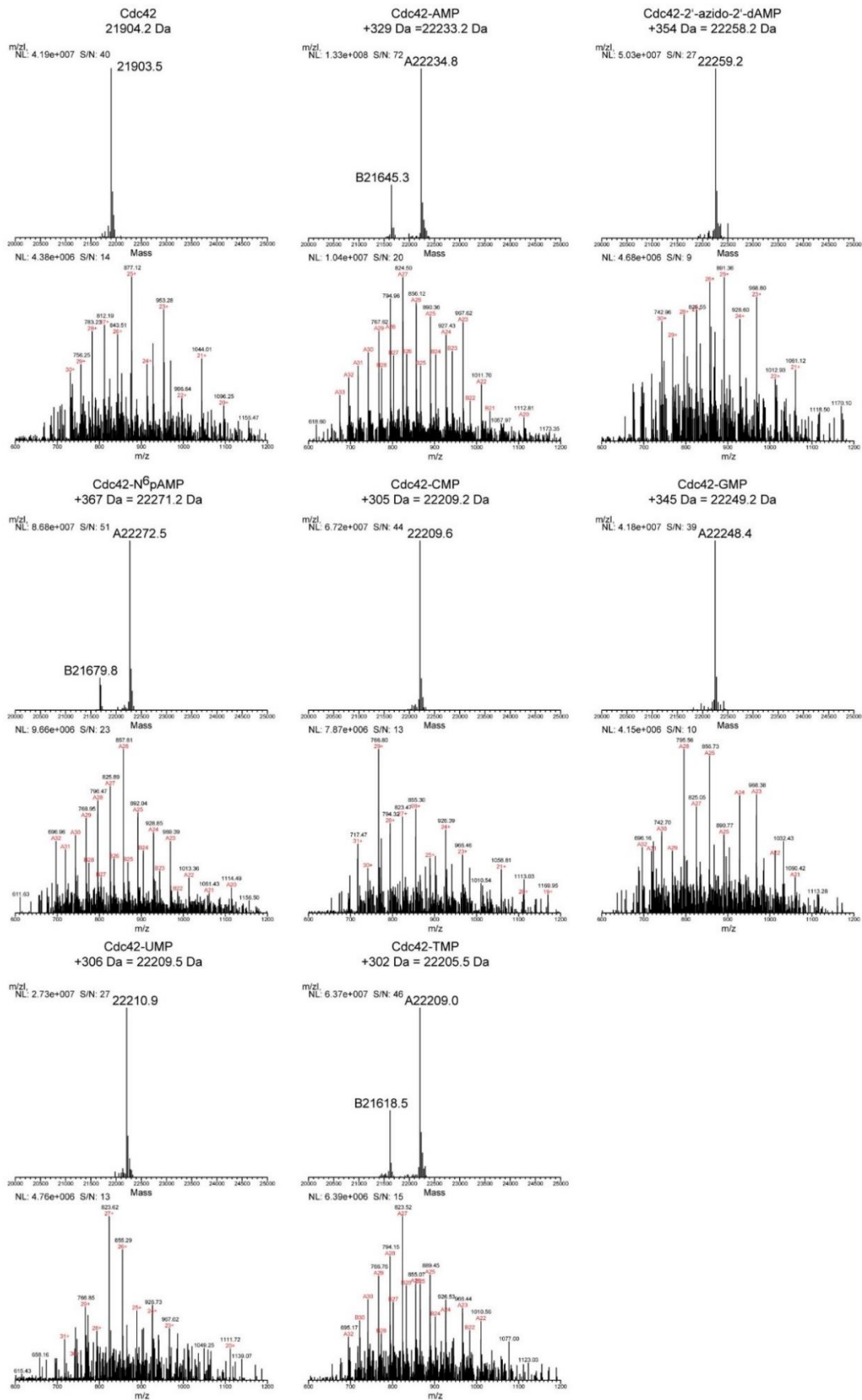


Figure S5: Mass spectrometry confirmation of NMP incorporation by IbpA into Cdc42. Related to Figure 2D. Expected molecular weights are indicated above spectra.

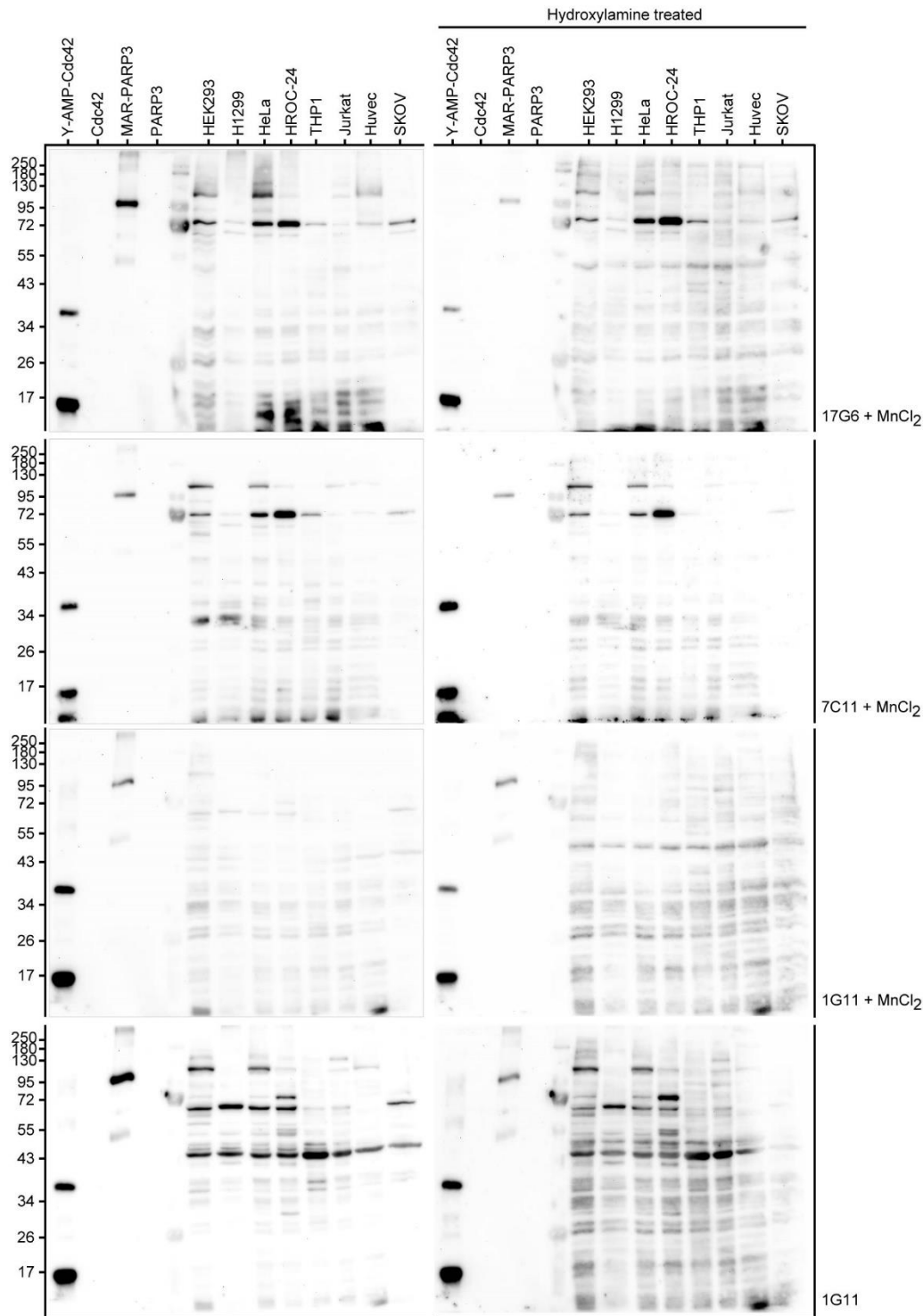


Figure S6: Analysis of AMPylation patterns in various immortalized and cancer cell lines in WB. Related to Figure 4F. 20 μ g total protein cell lysate per lane of cell lines as indicated were blotted and probed with monoclonal anti-AMP antibodies as indicated using 1 mM MnCl_2 as additive during primary antibody incubation. Afterwards the identical blot was treated with 1 M hydroxylamine to cleave ADP-ribosylation at aspartate and glutamate residues and reprobbed with monoclonal anti-AMP antibodies in the presence of 1 mM MnCl_2 . In case of antibody 1G11, the identical blot was reprobbed with 1G11 in the absence of MnCl_2 before and after hydroxylamine treatment. 10 ng recombinant Cdc42-Tyr-AMP serve as positive ctrl for AMPylation, 10 ng recombinant MAR-PARP3 as positive ctrl for ADP-ribosylation and successful hydroxylamine treatment. 10 ng unmodified counterparts are included as negative ctrl.

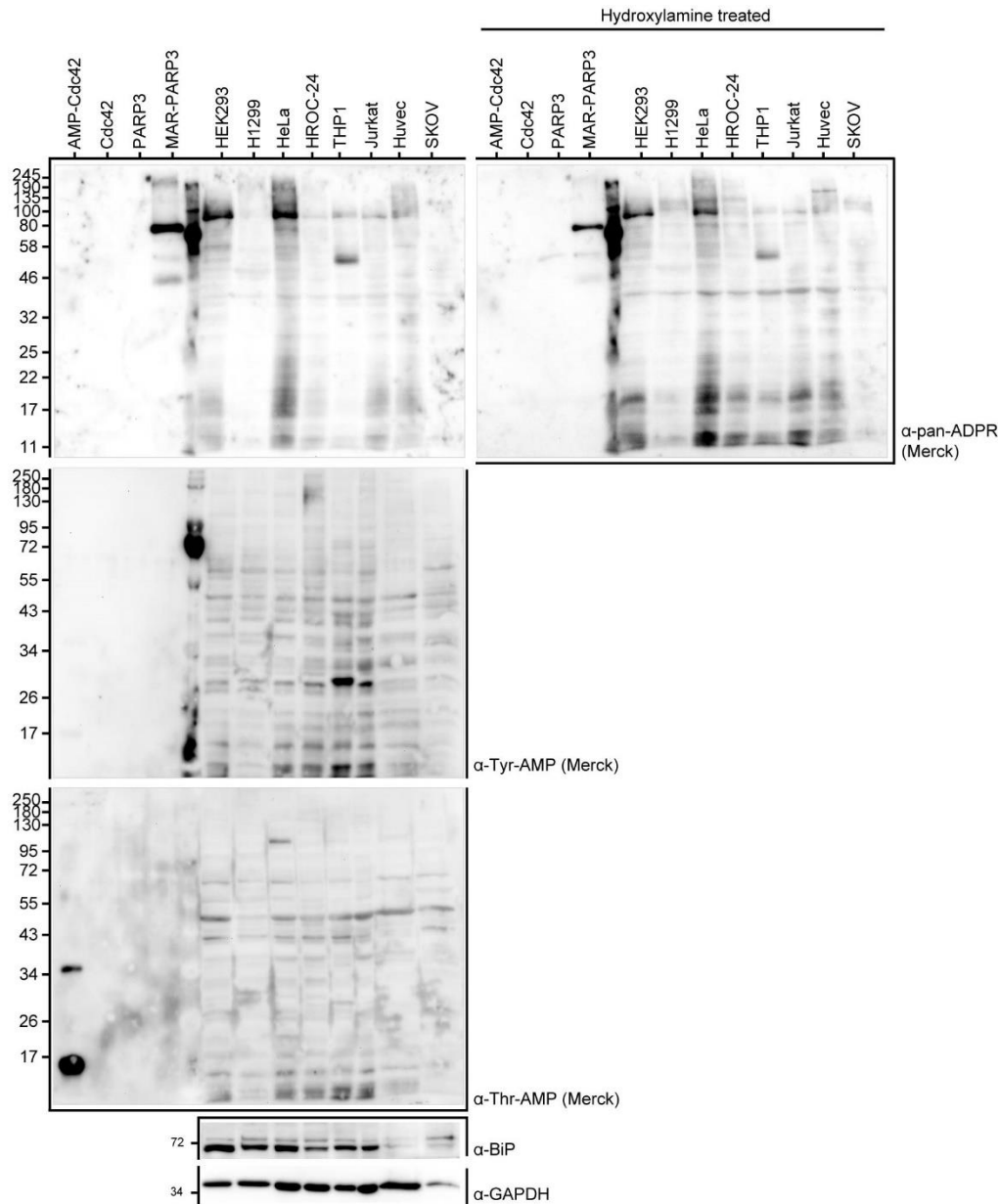


Figure S7: Analysis of AMPylation patterns in various immortalized and cancer cell lines in WB.

Related to Figure 4F. 20 µg total protein RIPA cell lysate per lane of cell lines as indicated were blotted and probed with commercial anti-AMP antibodies as indicated as well as commercial anti-ADPR probe. For the anti-ADPR probe, the identical blot was afterwards treated with 1 M hydroxylamine to cleave ADP-ribosylation at aspartate and glutamate residues and reprobbed with the anti-ADPR probe. The blot previously probed with commercial anti-Thr-AMP was stripped and reprobbed with antibodies against BiP and GAPDH as loading control. 10 ng recombinant Cdc42-Tyr-AMP, or 10 ng recombinant Cdc42-Thr-AMP in case of anti-Thr-AMP antibody, serve as positive ctrl for AMPylation, 10 ng recombinant MAR-PARP3 as positive ctrl for ADP-ribosylation and successful hydroxylamine treatment. 10 ng unmodified counterparts are included as negative ctrl.

Transparent Methods

Table S1: Strategy for monoclonal anti-AMP antibody generation in mice. Related to Figures 1 and S3. Experiments were conducted as indicated as a service by GenScript, Piscataway Township, New Jersey.

Stage	Description	Shipment
Immunogen preparation	Peptide conjugation with KLH and BSA.	-
Phase I: Immunization	Group A: 3 BALB/c +2 C57 mice, immunization with KLH conjugates, Group B: 3 BALB/c +2 C57 mice, immunization with BSA conjugates, Immunization with conventional protocol, indirect ELISA primary screening with target peptide (AcNH-CGAGT(AMP)GAG-NH ₂), and confirmatory screening by indirect ELISA by target protein (Cdc42-AMP)	15µl sera of 10 animals
Phase II: Cell fusion	2 cell fusions, indirect ELISA primary screening with target peptide (AcNH-CGAGT(AMP)GAG-NH ₂), and confirmatory screening by indirect ELISA by target protein (Cdc42-AMP)	Supernatants of 10 clones, 2ml per clone
Phase III: Subcloning, Screening and Expansion	3 cell lines subcloning, indirect ELISA primary screening with target peptide (AcNH-CGAGT(AMP)GAG-NH ₂), and confirmatory screening by indirect ELISA by target protein (Cdc42-AMP)	2 vials and 5ml supernatant per subclone
Antibody production	1 L roller bottle cell culture and protein A purification, indirect ELISA primary screening with target peptide (AcNH-CGAGT(AMP)GAG-NH ₂), and confirmatory screening by indirect ELISA by target protein (Cdc42-AMP)	>15mg purified antibody per subclone

Solid phase peptide synthesis (SPPS)

The peptides S2 and S3 (Supplemental Figure S1 and S2) were synthesized on a MultiSyntech Syro I automated peptide synthesizer, using Tentagel Rink-amide resin as solid phase employing 8 equivalents of amino acid and 7.8 equivalents HBTU, 7.8 equivalents HOBt and 16 equivalents DIPEA in DMF. Threonine-AMP building block S1 (Smit et al., 2011) was manually coupled according to below. The resin was pre-swollen by treatment with DCM (15 min). Removal of Fmoc protecting group was performed by treatment with 2 times 3 minutes followed by 1 time 9 minutes 20 vol% piperidine in DMF. The resin was washed with DMF three times. The building block S1 (1.7 equivalents) was coupled using 1.6 equivalents HATU, 1.6 equivalents HOAt and 3.5 equivalents DIPEA in DMF. The coupling reaction was allowed to proceed for 4 h at room temperature. N-terminal acetyl-capping was achieved by adding 50 equivalents acetic anhydride and 50 equivalents DIPEA in NMP to the resin (1 h), followed by washing with DMF. Before cleavage, the resin was washed thoroughly with DCM (5 times), isopropanol (5 times) and diethyl ether (5 times). The peptides were cleaved with 5% TIPS and 5% water in TFA (1 x 2 h + 2 x 10 min). An additional 10% water was added to the combined TFA-fractions and allowed to age for one hour, in order to ensure complete hydrolysis of the acetonide moiety. The cleavage mixture was evaporated to dryness *in vacuo*. The resulting solid was dissolved in a minimum TFA and precipitated by the addition of 10 ml ice cold diethyl ether. The precipitate was dissolved in water/acetonitrile and subsequently lyophilized overnight. Pure peptides were obtained after purification by preparative HPLC. Preparative HPLC purifications of the peptides were performed with an Agilent 1260 Infinity series instrument equipped with a Phenomenex Luna (5 µm, C18(2) 100 Å, 250 x 21.2 mm) column. Used mobile phases were water with 0.1% TFA (eluent A) and acetonitrile with 0.1% TFA (eluent B). Analytical HRMS-HPLC was performed on an Agilent 1290 Infinity II series instrument equipped with an Agilent Extend (1.8 µm, C18, 100 Å, 50 x 2.1 mm) column and connected to an Agilent 6230 TOF LC/MS instrument. Used mobile phases were water with 0.1% FA (eluent A) and acetonitrile with 0.1% FA (eluent B). For complete description see supplemental data.

Immunogen preparation

Immunogen peptide S2 (ACNH-CGAGT(AMP)GAG-NH₂) was conjugated with KLH and BSA as immunogen via its N-terminal cysteine (GenScript).

Immunization

3 BALB/c and 2 C57 BL/6 mice were immunized with either S2 conjugated to KLH (group A, BALB/c mice #8534 - #8536 and C57 BL/6 mice #8537 - #8538) or BSA (group B, BALB/c mice #8539 - #8541 and C57 BL/6 mice #8542 - #8543), respectively, according to the conventional protocol of GenScript (Table 2), resulting in 10 immunized mice in total.

Table S2: Immunization schedule. Related to Figures 1 and S3.

Procedure	Schedule	Dosage and route	Adjuvant
Pre-Immune Bleed	T= - 4 days		
Primary Immunization	T= 0 days	50 µg /animal, i.p.	CFA
Boost 1	T= 14 days	25 µg /animal, i.p.	IFA
Test Bleed 1	T= 21 days		
Boost 2	T= 28 days	25 µg /animal, i.p.	IFA
Test Bleed 2	T= 35 days		
Final Boost	T= 50±7 days	25 µg /animal, i.p.	IFA
Cell Fusion	4 days after final boost		

Test bleed: 7 days after each boost immunization, immunized animal sera were tested by indirect ELISA and competitive ELISA for immune response by GenScript. Western blot evaluation of pre-sera and sera after 3rd immunization against 200 ng of purified protein/lane using a 1:1000 dilution was performed in-house as described. Animals #8538 (group A) and #8542 (group B), both C57 BL/6 mice, were selected for phase II.

After three boosts, the sera of immunized mice were evaluated for their ability to recognize the peptide hapten conjugate and native Cdc42-Thr-AMP in ELISA. Only positive hits were evaluated for their WB performance on various AMPylated proteins to check for backbone independent recognition and potential side chain bias. Of ten immunized mice, five of these were able to recognize native Cdc42-Thr-AMP in ELISA as good as the AMPylated hapten without showing binding of Cdc42 alone. All of them were positive against all tested proteins in WB, although no preference for AMPylation at threonine side chains was observable and all sera reacted with tyrosine as well as threonine modifications. After the final bleed, the two positive animals #8538 and #8542, both C57 BL/6 mice, with superior recognition of native and denatured targets in WB and ELISA and no discernible background against unmodified proteins and peptides were selected to perform cell fusion to hybridoma cells.

Phase II: cell fusion and screening

For cell fusion and clone plating, two fusions were performed by electro-fusion. The average fusion efficiency at GenScript is around 1 hybridoma/2,000 splenocytes, thus the anticipated hybridoma clones would be ~ 2×10^4 . All fused cells from each cell fusion were plated into 96-well plates. Up to 15 plates were used for each fusion. For the primary binder screening, the conditioned medium was screened by ELISA with the target peptide. In the confirmatory screening, the conditioned medium of primary binder screening positive clones were screened against the positive screening material (Cdc42-Thr-AMP) and counter screening material (Cdc42). The expected clones should be positive against target peptides, positive screening material while negative against the negative peptide and counter screening material. For clone expansion and freezing, 10 positive clones were expanded into 24-well plates. 2 ml of supernatant (conditioned media) were collected for each clone and cells were frozen down to avoid clone loss (GenScript). The conditioned media of all 10 positive clones were analyzed in-house by WB against 200 ng of purified protein/lane using a 1:10 dilution as described. Clones 17G6 (#8542), 1G11 and 7C11 (#8538) were selected for phase III.

Evaluation using ELISA resulted in 10 clones that were able to recognize native Cdc42-Thr-AMP and were subsequently chosen for WB testing as described above. The variation of performance among the clones proved to be a lot higher than between mice sera samples, with many clones showing a lack of universal recognition of all targets, high background or strong differences in strength of recognition depending on the AMPylated protein. Two promising clones, 7C11 and 17G6, with similar very good recognition of all AMPylated proteins in WB independent of their modified side chain, native recognition of Cdc42-Thr-AMP in ELISA and low background were selected for subcloning and

subsequent production and purification. One further clone, 1G11, was selected for its unexpected development of a tyrosine-specific recognition, despite immunization with a threonine-modified peptide.

Phase III: subcloning, screening, expansion.

For subcloning, 3 positive primary clones were sub-cloned by limiting dilution to ensure that the sub-clones were derived from a single parental cell. The clones were carried for a maximum of 3 generations. Subcloning was screened by ELISA as before. For monoclonal cryopreservation, two stable sub-clonal cell lines of each parental clone were chosen for cryopreservation based on the result of ELISA (GenScript). Positive cell supernatants were evaluated by WB against 200 ng of purified protein/lane using a 1:10 dilution in-house as described. The stable sub-clonal cell lines 17G6-1 (isotype IgG2b, k), 1G11-F3-3 (isotype IgG2b, k) and 7C11-1 (isotype IgG2a, k) were chosen for production and isotyped, and the cell lines stored with 2 vials at GenScript and 2 vials in-house. They were negatively tested for mycoplasma, detected by the PCR Mycoplasma Detection Set (TAKARA BIO INC, Kusatsu, Japan).

In our experience, subcloning and upscaling for antibody production poses the risk of losing binding abilities. One clone, 1G11-1, lost its AMPylation recognition abilities during subcloning and had to be recloned (1G11-F2-3) (Switch in isotypes from IgG1 to IgG2b). Another clone, 17G6-1, lost its performance during upscaling for antibody production and had to be redone. Therefore, rigorous retesting after each step is crucial. Interestingly, clone 1G11 lost its clear preference for tyrosine AMPylation after upscaling for production (Figure 2A). However, tyrosine-specific recognition of antibody 1G11 could be sharply enhanced in the presence of 1 mM MnCl₂ (Figure 3B).

For all three final hybridoma cell lines 17G6-1, 7C11-1 and 1G11-F2-3, antibody variable domain sequencing was done by GenScript as a service.

Antibody variable domain sequencing of hybridoma cell lines

Total RNA was isolated from frozen hybridoma cell lysates following the technical manual of TRIzol® Reagent (Ambion, Thermo Fisher Scientific Inc.). Total RNA was then reverse transcribed into cDNA using isotype-specific anti-sense primers or universal primers following the technical manual of PrimeScript™ 1st Strand cDNA Synthesis Kit (Takara, Kusatsu, Japan). The antibody fragments of V_H and V_L were amplified according to the standard operating procedure (SOP) of rapid amplification of cDNA ends (RACE) of GenScript. Amplified antibody fragments were cloned into a standard cloning vector separately. Colony PCR was performed to screen for clones with inserts of correct sizes. No less than five colonies with inserts of correct sizes were sequenced for each fragment. The sequences of different clones were aligned and the consensus sequences of these clones were provided (GenScript).

17G6-1 antibody variable domain sequencing

Heavy chain: DNA sequence (411 bp)

Leader sequence-FR1-CDR1-FR2-CDR2-FR3-CDR3-FR4

ATGGGATGGAGCTGGATCTTTCTCTTTCTCCTGTCAGGAAGTGCAGGTGTCCTCTCTGAGGTCCA
GCTGCAACAATCTGGACCTGAGCTGGTGAAGCCTGGGGCTTCAGTGAAGATATCCTGTAAGGCT
TCTGGATACACGTTCACTGACTACTATCTGAACTGGGTGAAGCAGAGCCATGGAAGAGCCTTGA
GTGGATTGGAGATATTCATCCTAACAAAGGTATTAATAAGTACAACCAGAAGTTCAAGGGCAAGG
CCACATTGACTGTAGACAAGTCTCCAGTACAGCCTACATGGAGCTCCGCAGCCTGACATCTGAG
GACTCTGCAGTCTATTACTGTGCAAGATACTACGGTAAGAGGTACTTCGATGTCTGGGGCACAGG
GACCATGGTCACCGTCTCCTCA

Heavy chain: Amino acid sequence (137 aa)

Leader sequence-FR1-CDR1-FR2-CDR2-FR3-CDR3-FR4

MGWSWIFLFLLSGTAGVLS^EVQLQQSGPELVKPGASVKISCKASGYFTD^YYLN^WVVKQSHGKSLEWI
GDIHPNKGINKYNQKFKGKATLTVDKSSSTAYMELRSLTSEDSAVYYCARY^YGKRYFDVWGTGTMVT
VSS

Light chain: DNA sequence (396 bp)

Leader sequence-FR1-CDR1-FR2-CDR2-FR3-CDR3-FR4

ATGATGAGTCCTGCCAGTTCCTGTTTCTGTTAGTGCTCTGGATTCGGGAAACCAACGGT^GATGT
^TG^TG^AT^GA^CC^CA^GA^CT^CC^AC^TC^AC^TT^TG^TC^GG^TA^CC^TT^TG^AC^AA^CC^AG^CC^TC^CA^TC^TC^TT^GC^A
^AG^TC^AC^GT^CA^GA^GC^CT^TA^GA^TA^GT^GA^TG^GA^AA^GA^CA^TA^TT^TG^AA^TT^TG^GT^TG^TT^AC^AG^AG^GC^CA
^GG^CC^AG^TC^TC^CA^AG^CG^CT^AA^TC^TA^TC^TG^GT^GT^CT^AA^AT^TG^GA^CT^CT^GG^AG^TC^CC^TG^AC^AG^GT^T

CACTGGCAGTGGATCAGGGACAGATTTCACTGAAAATCAGCAGAGTGGAGGCTGAGGATTTG
GGAGTTTACTATTGCTGGCAAGGTACACATTTCCGTACACGTTCCGGAGGGGGGACCAAGCTGG
AAATAAAA

Light chain: Amino acid sequence (132 aa)

Leader sequence-FR1-CDR1-FR2-CDR2-FR3-CDR3-FR4

MMSPAQFLFLLVLWIRETNGDVVMTQTPLTSLVTLGQPASISCKSRQSLDSDGKTYLNWLLQRPQG
SPKRLIYLVSKLDSGVPDRFTGSGSGTDFTLKISRVEAEDLGVYYCWQGFHFPYTFGGGTKLEIK

7C11-1 antibody variable domain sequencing

Heavy chain: DNA sequence (417 bp)

Leader sequence-FR1-CDR1-FR2-CDR2-FR3-CDR3-FR4

ATGGGATGGAGCTGGATCTTTCTCTTTCTCCTGTCAGGAAGTGCACGTGTCCTCTCTGAGGTCCA
GCTGCAACAATCTGGACCTGAGCTGGTGAAGCCTGGGGCTTCAGTGAAGATATCCTGTAAGGCT
TCTGGATACACGTTCACTGACTACTACATTAAGTGGGTGAAGCAGAGCCATGGAAAGAGCCTTGA
GTGGATTGGAGATATTAATCCTAACCATGGTAGTGCTGGCTCCAACCAGAATTTCCAGGGCAAGG
CCACATTGACTGTAGACAAGTCTCCAGCACAGCCTACATGGAGCTCCGCAGCCTGACATCTGA
GGACTCTGCAGTCTATTACTGTACAAAGTACTACGGTACTGGCTACAGGTACTTCGATGTCTGGG
GCACAGGGACCACGGTCACCGTCTCCTCA

Heavy chain: Amino acid sequence (139 aa)

Leader sequence-FR1-CDR1-FR2-CDR2-FR3-CDR3-FR4

MGWSWIFLFLLSGTARVLSVQLQQSGPELVKPGASVKISCKASGYTFTDYYINWVKQSHGKSLEWI
GDINPNHGSAGSNQNFQ GKATLTVDKSSSTAYMELRSLTSEDSAVYYCTKY YGTGYRYFDVWGTGT
TVT VSS

Light chain: DNA sequence (396 bp)

Leader sequence-FR1-CDR1-FR2-CDR2-FR3-CDR3-FR4

ATGATGAGTCCTGCCAGTTCCTGTTTCTGTTAGTGTCTGGATTCCGGAAACCAACGGT GATGT
TGTGATGACCCAGACTCCACTCACTTTGTCGGTTACCATTGGACAACCAGCCTCCATCTCTTGCA
AGTCAAGGCTGAGCCTCTTAGAAAGTGATGGAAAGACATATTTGAATTGGTTGTTACAGAGACCA
GGCCAGTCTCCAAAGCGCCTAATCTATCAGGTGTCTAAGCTGGACTCTGGAGTCCCTGACAGGT
CACTGGCAGTGGATCAGGGACAGATTTACACTGAAATCAGCAGAGTGGAGGCTGAGGATTTG
GGAGTTTATTATTGCTGGCAAGGTACACATTTTCCGTACACGTTCCGGAGGGGGGACCAAGCTGG
AAATAAAA

Light chain: Amino acid sequence (132 aa)

Leader sequence-FR1-CDR1-FR2-CDR2-FR3-CDR3-FR4

MMSPAQFLFLLVLWIRETNGDVVMTQTPLTSLVTIGQPASISCKSRLSLLSDGKTYLNWLLQRPQGS
PKRLIYQVSKLDSGVPDRFTGSGSGTDFTLKISRVEAEDLGVYYC WQGFHPYTFGGGKLEIK

1G11-F2-3 antibody variable domain sequencing

Heavy chain: DNA sequence (423 bp)

Signal sequence-FR1-CDR1-FR2-CDR2-FR3-CDR3-FR4

ATGGGTTGGCTGTGGACCTTGCTATTCCTGATGACAGCTGCCCAAAGTGCCCAAGCACAGATCC
AGTTGGTACAGTCTGGACCTGAACTGAAGAAGCCTGGAGAGACAGTCAAGATCTCCTGCAAGGC
TGCTGGGTATACCTTCAACCTATGGAATGAGCTGGGTGAAACAGGCTCCAGGAAAGGGTTTAA
AGTGGCTGGCTGGATAAACACCTACTCTGGAGTGCCAACATATGCTGATGACTTCAAGGGACG
GTTTGCCTTCTCTTTGGATATCTCTGCCAGCACTGCCTATTTGCAGATCAACAACCTCATAAATGA
GGACACGGTGCATATTTCTGTACAAGGAGGGACCGTACTATCCTAACTACGACTACTTTGACT
ACTGGGGCCAAGGCACCACTCTCACAGTCTCCTCA

Heavy chain: Amino acid sequence (141 aa)

Signal peptide-FR1-CDR1-FR2-CDR2-FR3-CDR3-FR4

MGWLWTLFLMATAAQAQSAQAQIQLVQSGPELKKPGETVKISCKAAGYFTTYGMSWVKQAPGKGLKW
LGWINTYSGVPTYADDFKGRFAFSLDISASTAYLQINNLINEDTAAFYCTRDRDRYPNYDYFDYWGGQ
TTLTVSS

Light chain: DNA sequence (393 bp)

Signal sequence-FR1-CDR1-FR2-CDR2-FR3-CDR3-FR4

ATGAAGTTGCCTGTTAGGCTGTTGGTGTCTGATGTTCTGGATTCCCTGCTTCCACCAGT GATGTTTTG
TTGACCCAAACTCCACTCTCCCTGCCTGTCAGTCTTGGAGATCAAGCCTCCATCTCTTGCAGATC
TAGTCAGAGCCTTGACATAGTACTGGAAACACCTATTTAGAATGGTACCTGCAGAAACCAGGCC
AGTCTCCAAACTCCTGATCTACAAGTTTTCCACCCGATTTTCTGGGGTCCAGACAGGTTTCAGT
GGTAGTGGATCAGGGACAGATTTCACTCAAGATCAGCAGAGTGGAGGCTGAGGATCTGGGAG
TTTATTACTGCTTCAAGGTTACATGGACCGCTCAGTTCCGGTGTCTGGGACCAAGCTGGAGCTG
AAA

Light chain: Amino acid sequence (131 aa)

Signal peptide-FR1-CDR1-FR2-CDR2-FR3-CDR3-FR4

MKLPVRLVLMFWIPASTSDVLLTQTPLSLPVSLGDQASISCRSSQSLVHSTGNTYLEWYLQKPGQSP
KLLIYKVSTRFSGVDFRFSGSGTDFILKISRVEAEDLGVYYCFQGSHPITFGAGTKLELK

Antibody production

Three stable sub-clonal cell lines were each cultured in 1 l roller bottle cell culture using SFM + 2% low IgG FBS culture medium. Monoclonal antibody was Protein A purified from the supernatant and stored in phosphate buffered saline (PBS, pH 7.4) with 0.02% sodium azide as preservative. Purity was measured by SDS-PAGE and concentration by NanoDrop Spectrophotometer A280nm (Thermo Fisher Scientific Inc., Waltham, Massachusetts) (GenScript). This way 36.38 mg of 7C11 with 95% purity, 17.10 mg 17G6 with 91% purity and 30.99 mg 1G11 with 92% purity were produced.

Molecular biology

Unless otherwise indicated, all genes were codon optimized for expression in *E. coli* by omitting rare amino acid codons, and all cloning was done by sequence and ligation independent cloning (SLIC) using T4 DNA polymerase (New England Biolabs, Ipswich, Massachusetts).

The human Cdc42 1-179aa Q61L (referred to as Cdc42)-encoding DNA was cloned into a modified pGEX-4T-1 vector (GE Healthcare, Chicago, Illinois) as previously described (Barthelmes et al., 2020), resulting in a construct with a N-terminal glutathione S-transferase (GST) tag followed by the Tobacco Etch Virus (TEV) protease cleavage site. As previously described (Schoebel et al., 2009), the human Rab1b 3-174aa (referred to as Rab1b)-encoding DNA was cloned into a modified pMAL vector (New England Biolabs), resulting in a construct with a N-terminal hexahistidine (6xHis) tag, followed by maltose-binding protein (MBP) and the TEV protease cleavage site. The human BiP 19-654aa (referred to as BiP)-encoding DNA was cloned into a modified pProEx™-HTb vector (Thermo Fisher Scientific Inc.), resulting in a construct with a N-terminal 6xHis tag, followed by the TEV protease cleavage site. The human FICD 102-458aa E234G (referred to as FICD)-encoding DNA was cloned into a modified pMAL vector (New England Biolabs), resulting in a construct with a N-terminal 6xHis tag, followed by the HaloTag®, the TEV protease cleavage site and a Strep-tag® II. The *Vibrio parahaemolyticus* VopS 31-387aa (referred to as VopS)-encoding DNA was cloned into a modified pMAL vector (New England Biolabs) as previously described (Barthelmes et al., 2020), resulting in a construct with a N-terminal 6xHis tag, followed by MBP and the TEV protease cleavage site. The *Histophilus somni* lbpA 3483-3797aa I3455C (referred to as lbpA)-encoding DNA was cloned into a modified pSF vector (Oxford Genetics Ltd, Oxford, UK), resulting in a construct with a N-terminal decahistidine (10xHis) tag, followed by MBP, the TEV protease cleavage site and a 3xFLAG® tag. The *Legionella pneumophila* DrrA 8-533aa (referred to as DrrA)-encoding DNA was cloned into a modified pET19 vector (Merck Millipore, Burlington, Massachusetts) as previously described (Müller et al., 2010), resulting in a construct with a N-terminal 6xHis tag and the TEV protease cleavage site. The *Legionella pneumophila* AnkX 1-800aa (referred to as AnkX)-encoding DNA, which previously had been amplified from *Legionella pneumophila* genomic DNA (Goody et al., 2012), was cloned into a modified pSF vector (Oxford Genetics) as previously described (Ernst et al., 2020), resulting in a construct with a N-terminal 10xHis tag, followed by enhanced green fluorescent protein (eGFP) and the TEV protease cleavage site. Human Rab8a 6-176aa (referred to as Rab8a)-encoding DNA was cloned into a pet51b(+) vector (Merck Millipore), resulting in a construct with a N-terminal Strep® II tag and enterokinase cleavage site and a C-terminal 10xHis tag. All site-specific mutagenesis was performed with the Q5 Site-Directed Mutagenesis Kit (New England Biolabs).

Recombinant expression and purification of proteins

Recombinant human histone H3.1 was purchased from New England Biolabs (M2503S), and active human PARP3 from Sigma-Aldrich, St. Louis, Missouri (SRP0194-10UG, Lot #8050330111). Human pSer111 Rab1b was a kind gift of Dr. Sophie Vieweg and was produced as published before (Vieweg et al., 2020).

Cdc42, VopS, Rab1b, DrrA and AnkX were expressed and purified as previously described (Barthelmes et al., 2020; Ernst et al., 2020; Müller et al., 2010; Schoebel et al., 2009). In brief, plasmids were transformed into chemically competent BL21 (DE3) cells (Cdc42, Rab1b, lbpA) or Lemo21 cells (VopS) or BL21-CodonPlus (DE3)-RIL cells (DrrA, Rab8a, AnkX) or Rosetta 2 cells (BiP, FICD) and protein was expressed in LB medium after induction with 0.5 mM isopropyl- β -dithiogalactopyranoside (IPTG) for 20 h at 25 °C (Cdc42, Rab1b) or 20 °C (VopS, DrrA, Rab8a, AnkX, lbpA) or 23 °C (FICD) or 3 h at 37 °C (BiP). Cells were harvested, washed with PBS and lysed in 50 mM 4-(2-hydroxyethyl)-1-piperazineethanesulfonic acid (Hepes) pH 7.5, 500 mM sodium chloride (NaCl), 1 mM MgCl₂, 2 mM β -mercaptoethanol (β Me), 10 μ M guanosine diphosphate (GDP), 1 mM PMSF (Cdc42, Rab1b, Rab8a) or 50 mM Tris pH 8.0, 500 mM NaCl, 5% (v/v) glycerol, 2 mM β -Me, 1 mM PMSF (AnkX) or 50mM Hepes pH 7.5, 500 mM NaCl, 1 mM MgCl₂, 2mM β Me, 1 mM PMSF (VopS, FICD) or 50 mM Hepes pH 8.0, 500 mM lithium chloride (LiCl), 2 mM β -Me, 1 mM PMSF (DrrA, lbpA) or 50 mM Hepes pH 7.4, 400 mM NaCl, 20 mM imidazole, 1 mM PMSF (BiP) after addition of DNase I by French press at 1.8 kbar. The lysates were cleared by centrifugation. For GST-tagged proteins (Cdc42), the lysate was loaded onto a pre-equilibrated GST-Trap column (GE) and eluted with 3-5 column volumes (CV) of the same buffer supplemented with 10 mM glutathione. For His-tagged proteins (VopS, Rab1b, DrrA, BiP, FICD, Rab8a, lbpA), the lysate was loaded onto a pre-equilibrated Ni²⁺-charged Bio-Scale Mini Nuvia IMAC Cartridge (Bio-Rad Laboratories, Hercules, California), washed with 30 mM imidazole and eluted with a fractionated gradient from 30 mM – 350 mM imidazole over 20 CV.

The protein containing eluate was digested with 6x-His tagged TEV during dialysis against 50 mM Hepes pH 7.5, 100 mM NaCl, 2 mM β -Me, 10 μ M GDP (Cdc42, Rab1b) or 20 mM Hepes pH 8.0, 100 mM NaCl, 2 mM β -Me (DrrA, IbpA) or 20 mM Tris pH 8.0, 300 mM NaCl, 5% (v/v) glycerol, 2 mM β -Me (AnkX) 20 mM Hepes pH 7.4, 100 mM NaCl (BiP) or 20 mM Hepes pH 7.4, 100 mM NaCl, 1 mM $MgCl_2$, 1 mM β -Me (FICD) with a cut off of MW 6000-8000 (Serva) for 16h at 4°C. Digested, formerly His-tagged proteins (Rab1b, DrrA, BiP, FICD, AnkX, IbpA) were reapplied to the Ni^{2+} -charged column pre-equilibrated with dialysis buffer in order to remove the His-tag, uncleaved protein and TEV protease. The flow through was collected, concentrated and applied to a HiLoad™ 16/600 Superdex™ 75pg column (GE Healthcare) in 20 mM Hepes pH 7.5, 50 mM NaCl, 1 mM $MgCl_2$, 1 mM dithioerythritol (DTE), 10 μ M GDP (Rab1b) or 20 mM Hepes pH 8.0, 100 mM NaCl, 2 mM DTE (DrrA) or 20 mM Tris pH 8.0, 300 mM NaCl, 5% (v/v) glycerol, 1 mM β -Me (AnkX) or 20 mM Hepes pH 7.4, 150 mM potassium chloride (KCl), 1 mM $MgCl_2$, 1 mM tris(2-carboxyethyl)phosphine (TCEP), 5% glycerol (FICD) or 20 mM Hepes pH 8.0, 100 mM NaCl, 1 mM $MgCl_2$, 2 mM DTE (IbpA) or applied to a HiLoad™ 16/600 Superdex™ 200pg column (GE Healthcare) in 20 mM Hepes pH 7.4, 150 mM KCl, 10 mM $MgCl_2$ (BiP). For VopS and Rab8a, protein containing eluate was concentrated and applied to a HiLoad™ 16/600 Superdex™ 75pg column (GE Healthcare) in 20 mM Hepes pH 7.5, 100 mM NaCl, 1 mM $MgCl_2$, 1 mM DTT (VopS) or 20 mM Hepes pH 7.5, 50 mM NaCl, 1 mM $MgCl_2$, 1 mM DTE, 10 μ M GDP (Rab8a) without TEV digestion. For digested, formerly GST-tagged proteins (Cdc42), protein digestion was concentrated and applied to a HiLoad™ 16/600 Superdex™ 75pg column (GE Healthcare) in 20 mM Hepes pH 7.5, 50 mM NaCl, 1 mM $MgCl_2$, 1 mM DTE, 10 μ M GDP (Cdc42). During all steps of protein purification, fractions were collected and analyzed by Coomassie blue stained sodium dodecyl sulfate (SDS) polyacrylamide gel electrophoresis (PAGE). Fractions containing pure protein of interest were pooled, concentrated to around 10 mg/ml, snap-frozen in liquid nitrogen and stored in multiple aliquots at -80 °C.

***In vitro* AMPylation of recombinant proteins**

For Cdc42-Thr-AMP, 200 μ M Cdc42 were incubated with 10 μ M VopS in the presence of 800 μ M ATP in 20 mM Hepes pH 7.5, 100 mM NaCl, 1 mM $MgCl_2$, 1 mM DTE at 20 °C overnight. For Cdc42-Tyr-AMP, 10 μ M Cdc42 were incubated with 0.1 μ M IbpA in the presence of 1 mM ATP in 20 mM HEPES pH 7.4, 100 mM NaCl, 1 mM $MgCl_2$, 1 mM TCEP, 10 μ M GDP at 20 °C overnight. For Rab1-Tyr-AMP, 10 μ M Rab1b were incubated in the presence of 50 μ M ATP and 0.1 μ M DrrA at 25°C as previously described (Müller et al., 2010). AMPylated Cdc42 and Rab1b were purified by size exclusion chromatography on a HiLoad™ 16/600 Superdex™ 75pg column (GE Healthcare) in 20 mM Hepes pH 7.5, 50 mM NaCl, 1 mM $MgCl_2$, 1 mM DTE, 10 μ M GDP and full AMPylation was confirmed by MS. For H3-Thr-AMP and auto-AMPylated FICD, 30 μ M H3.1 were incubated with 25 μ M FICD in the presence of 10 mM ATP in 20 mM HEPES pH 7.5, 150 mM NaCl, 1 mM $MgCl_2$, 2 mM DTT at 20 °C overnight. For BiP-Thr-AMP, 50 μ M BiP were incubated with 2.5 μ M FICD in the presence of 1.5 mM ATP in 25 mM Hepes pH 7.4, 100 mM KCl, 4 mM $MgCl_2$, 1 mM calcium chloride ($CaCl_2$) for 2 h at 30 °C. BiP-AMP was purified with Protino™ Ni-NTA Agarose (Macherey-Nagel, Düren, Germany) in previously listed buffers according to the manufacturer's instructions.

***In vitro* NMPylation of recombinant Cdc42 by IbpA**

10 μ M Cdc42 were incubated with 0.1 μ M IbpA in the presence of 0.5 mM of either CTP, UTP, TTP, GTP, N6pATP (Jena Bioscience, Jena, Germany) and 2'-Azido-2'-dATP (TriLink BioTechnologies, San Diego, California) in 20 mM Tris-HCl pH 7.4, 100 mM NaCl, 1 mM $MgCl_2$, 1 mM TCEP, 10 μ M GDP at 20 °C overnight. Successful NMPylation was confirmed by MS.

***In vitro* auto-mono-ADP-ribosylation of PARP3**

500 ng PARP-3 (Sigma-Aldrich) were incubated at 25°C in a 100 μ L reaction volume in 20 mM HEPES pH 8.0, 5 mM $MgCl_2$, 5 mM $CaCl_2$, 0.01% NP-40, 25 mM KCl, 1 mM DTT, 0.1 mg/mL salmon sperm DNA (Thermo Fisher Scientific), 0.1 mg/mL BSA (New England Biolabs) in the presence of 250 μ M NAD^+ for 30 minutes as published before (Gibson et al., 2017). The reaction was stopped by the addition of 5x SDS-PAGE Loading Buffer, followed by heating to 95°C for 5 min.

***In vitro* phosphocholination or Rab1b by AnkX**

10 μ M Rab1b was incubated with 0.1 μ M AnkX in the presence of 1 mM CDP-choline (Enzo Life Sciences, Farmingdale, New York) for 2 h at 23 °C as published before (Goody et al., 2012).

***In vitro* biotinylation of Rab8a**

200 mM EZ-Link® Maleimide-PEG2-Biotin (Thermo Fisher Scientific) stock solution in DMSO was diluted 1:10 in 1x PBS to a final concentration of 20 mM Maleimide-PEG2-Biotin label. 200 μ M Maleimide-PEG2-Biotin label were added to 100 μ M of Rab8a in PBS for 2 h on ice, before Rab8a was washed 3 times with PBS in an Amicon filter (Merck Millipore, 10 kDa NMWL). Incorporation of label was confirmed by MS.

Analytical size exclusion chromatography (aSEC)

In 100 μ l, 40 μ g antigen were mixed with 60 μ g antibody, including 50 μ M Vitamin B12 as internal standard. 90 μ l sample were injected onto a Superdeep 10/300 200pg column (GE Healthcare) coupled to a Prominence HPLC system (Shimadzu, Kyōto, Japan) and run at 0.5 ml/min for 60 min in 20 mM HEPES pH 7.5, 150 mM NaCl. Protein retention times were detected at 280 nm (A280nm), and intensities were normed to Vitamin B12. Peaks containing antigen:antibody complexes were collected in 500 μ l fractions. Fractions were supplemented with 6x Laemmli and concentrated in a SpeedVac alpha RVC (Martin Christ Gefriertrocknungsanlagen GmbH, Osterode am Harz, Germany) without heat to 200 μ l. 10 μ l concentrated fractions were analyzed by 15% SDS PAGE and silver stained.

Mass spectrometry

To verify the degree of modification, samples containing 100 ng recombinant protein were run over a 5 μ m Jupiter C4 300Å LC column (Phenomenex, Torrance, California) using the 1260 Infinity LC system (Agilent Technologies, Santa Clara, California) and then subjected to mass spectrometry with the 6100 Quadrupole LC/MS System (Agilent Technologies). The resulting ion spectra were deconvoluted using the Magic Transformer (MagTran) software (Zhang and Marshall, 1998).

Cell culture

CHO-K1 FlpIn cells (Thermo Fisher Scientific) were cultured in RPMI-1640 medium (Sigma-Aldrich) supplemented with 10% FBS (Thermo Fisher Scientific). HEK293 cells were cultured as described below. 90% confluent cells were stimulated by either 0.5 μ M thapsigargin (Biosynth Carbosynth) for 2 h or 100 μ g/ml cycloheximide (Sigma-Aldrich) for 4 h. Cells were washed twice with Dulbecco's Phosphate Buffered Saline (DPBS) (Sigma-Aldrich) and lysed in MPER buffer (Thermo Fisher Scientific) supplemented with cOmplete EDTA free protease inhibitor (Roche, Basel, Switzerland). Protein concentration was determined using the Bradford assay (Thermo Fisher Scientific).

For analysis of cell lysates, SKOV3-cells were cultured in McCoy's 5A Medium supplemented with 10% FCS (Thermo Fisher Scientific). HROC24-cells were cultured in DMEM/Ham's F12 (Thermo Fisher Scientific) supplemented with 10% FCS and 3 mM glutamine (Thermo Fisher Scientific). Jurkat subclone JMP cells were cultured in RPMI (Thermo Fisher Scientific) supplemented with 10% NCS (Thermo Fisher Scientific). Huvec cells were cultured in Medium 199 without phenol red (Thermo Fisher Scientific) supplemented with 6.6% FCS and 33% EBM™-2 Endothelial Cell Growth Basal Medium-2 (Lonza, Basel, Switzerland). HELA cells (DSMZ ACC-57) and HEK293 cells (DSMZ ACC-305) were cultured in DMEM (Thermo Fisher Scientific) supplemented with 10% FCS. THP-1 cells (ATCC TIB-202) were cultured in RPMI supplemented with 10% FCS. Cells were washed in DPBS (Sigma-Aldrich), before being lysed in M-PER buffer (Thermo Fisher Scientific) supplemented with protease inhibitor cOmplete EDTA-free (Roche) and Phosphatase Stop (Roche). Protein concentration was determined using the Bradford assay (Thermo Fisher Scientific).

Immunoprecipitation

AMPylated proteins were precipitated from purified recombinant BiP and BiP-AMP or CHO-K1 lysates stressed with either thapsigargin or cycloheximide with antibody 17G6 using Pierce ChIP-grade Protein A/G Magnetic Beads (Thermo Fisher Scientific) according to the manufacturer's protocol. In short, in a total volume of 500 μ l 20 μ g recombinant protein or 1 mg total protein lysate were incubated with 10 μ g 17G6 antibody in 25 mM Tris pH 7.4, 150 mM NaCl, 1 mM EDTA, 5% glycerol, 1% NP40 overnight at 4°C, before being precipitated with 25 μ l equilibrated beads for 1 h at room temperature. Beads were washed twice with the binding buffer, before AMPylated proteins were eluted with 100 μ l 1x Laemmli for 15 min at 30 °C. Lysate elutions were concentrated to 20 μ l in a SpeedVac alpha RVC (Christ) without heat. For recombinant protein samples 7.5 μ l each of input and unbound sample supplemented with 5x Laemmli buffer and 2.5 μ l elution, for lysate samples 5 μ l each of input and unbound sample supplemented with 6x Laemmli buffer and 20 μ l of concentrated elution were analyzed by 12% SDS PAGE and WB as described.

For immunoprecipitation after methanol/chloroform precipitation, 250 μ g CHO-K1 lysates untreated or stressed with either thapsigargin or cycloheximide were diluted with 3 volumes of methanol and vortexed, before 1 volume of chloroform (Sigma-Aldrich) was added and samples were vortexed. 3 volumes of water were added, samples vortexed, before centrifugation at 15 000 rpm for 2 min at 4°C. The aqueous upper phase was carefully aspirated, 3 volumes of methanol were added, samples vortexed, before centrifugation at 15 000 rpm for 5 min at 4°C. Afterwards the supernatant was removed and protein pellets left to dry. Protein pellets were resuspended in 25 μ l 1 M NaOH, before 80 μ l binding buffer (25 mM Tris pH 7.4, 150 mM NaCl, 5% glycerol) were added and pH adjusted to 7.5 with 10% HCl. 2.5 μ g 17G6 antibody were added and incubated overnight at 4°C, before being precipitated with 25 μ l equilibrated beads for 1 h at room temperature. Beads were washed twice with the binding buffer, before AMPylated proteins were eluted with 50 μ l 1x Laemmli for 15 min at 30 °C.

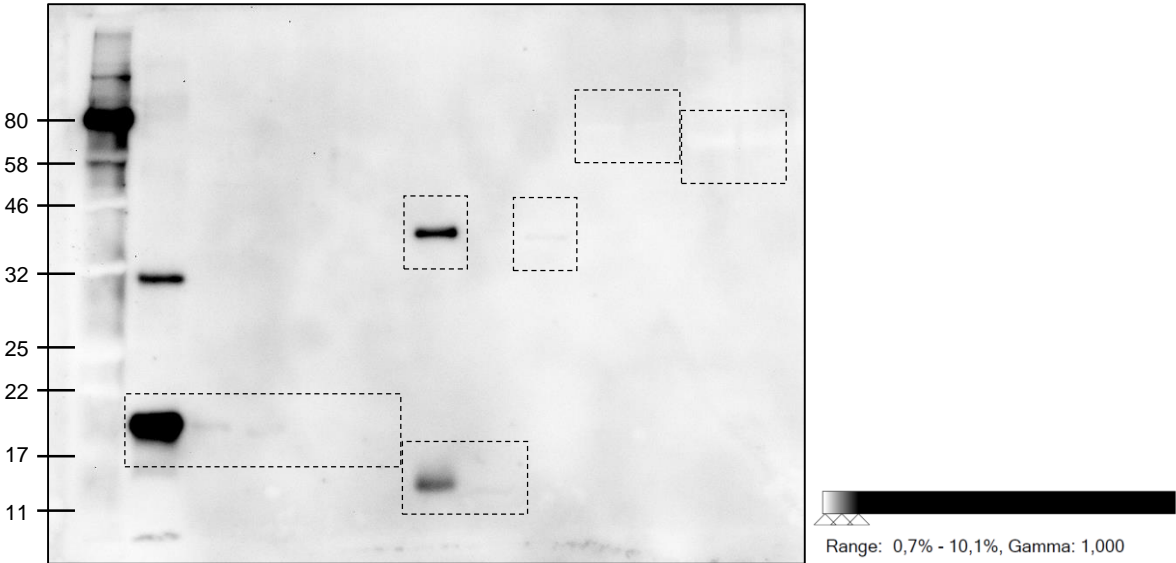
5 μ l each of input and unbound sample supplemented with 6x Laemmli buffer and 20 μ l of elution were analyzed by 12% SDS PAGE and WB as described.

Western blotting

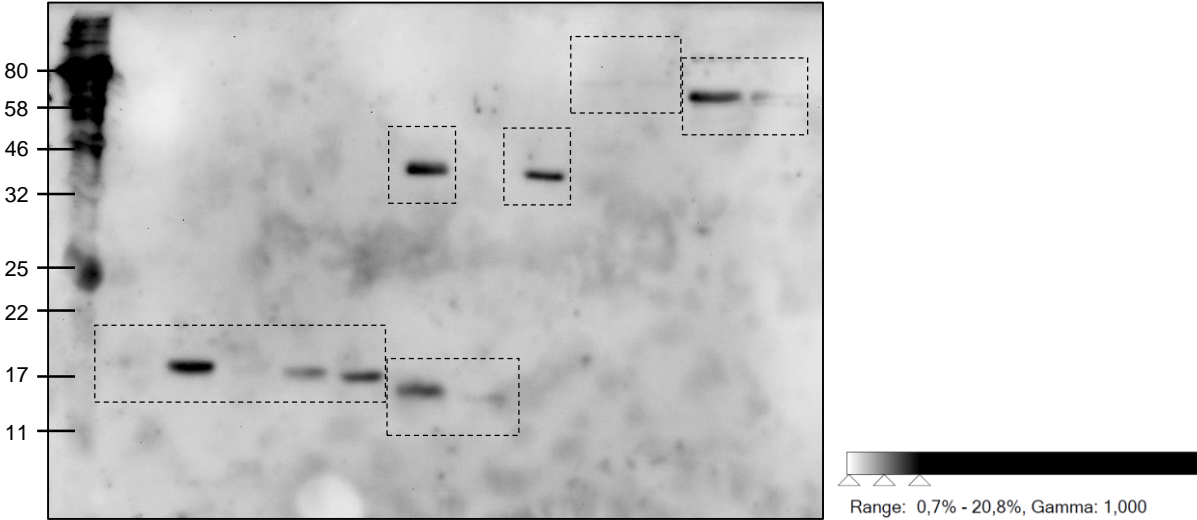
200 ng or 50 ng recombinant protein as indicated or 20 μ g cell lysate, respectively, were separated by 15% or 12% SDS-PAGE and protein was transferred to MeOH-activated Immobilon®-P membrane (Merck Millipore) using Whatman paper and a transfer buffer of 48 mM Tris, 39 mM glycine, 1.3 mM SDS, 20% methanol. For the blotting procedure, a constant current of 0.7 mA/cm² was applied to the V20-SDP semi-dry blotter (SCIE-PLAS, Cambourne, UK) for 2 h. After blotting, the PVDF membrane was blocked with Roti®-Block (Carl Roth, Karlsruhe, Germany) in Tris-buffered saline containing 0.1% Tween20 (TBS-T) for 1 h. Subsequently, the primary antibody was added to the blocking solution and incubated overnight at 4°C. Afterwards, the membrane was washed three times with TBS-T for 10 minutes and then incubated with a secondary antibody-peroxidase conjugate in TBS-T for 1 h. Again, the membrane was washed in TBS-T three times for 10 min, before the peroxidase signal was developed with the SuperSignal™ West Dura (Thermo Fisher Scientific) and chemoluminescence was detected using the Intas ECL Chemocam (Intas Science Imaging Instruments, Göttingen, Germany). Antibodies: Mouse pre-immune serum and antiserum after 3rd immunization (GenScript) was used 1:1000. Cell supernatant from hybridoma clones and subclones (GenScript) was used 1:10. Purified monoclonal mouse anti-AMP antibodies 17G6, 1G11, 7C11 (GenScript) were used 1:1000 at 0.5 μ g/ml. Monoclonal mouse anti-GAPDH sc-47724 (Santa Cruz Biotechnology, Dallas, Texas) was used 1:1000. Polyclonal rabbit anti-histone H3 antibody ab1791 (Abcam, Cambridge, UK) was used 1:5000. Polyclonal rabbit anti-AMPylated Tyrosine Antibody ABS184 (Merck Millipore) was used 1:1000. Polyclonal rabbit anti-pan-AMPylated Threonine Antibody 09-890 (Sigma-Aldrich) was used 1:2000. Recombinant rabbit anti-pan-ADP-ribose binding reagent MABE1016 (Merck Millipore) was used 1:1000. Polyclonal rabbit anti-GRP78/BiP antibody PA5-34941 (Thermo Fisher Scientific) was used 1:5000. Secondary goat anti-mouse IgG (H + L) HRP conjugate (Thermo Fisher Scientific) was used 1:20000. Secondary goat anti-rabbit IgG HRP (Sigma-Aldrich) was used 1:40000. Additives as indicated were added during the primary antibody incubation step at a final concentration of 1 μ M for adenosine (Jena Bioscience), AMP (Sigma-Aldrich), ADP (Biosynth Carbosynth, Staad, Switzerland), ATP (Biosynth Carbosynth), ADPR (Sigma-Aldrich), NAD⁺ (Biosynth Carbosynth) or 1 mM for MnCl₂, MgCl₂ (VWR International, Radnor, Pennsylvania), respectively. Hydroxylamine treatment was performed as previously described (Gibson et al., 2017). In short, after development of membrane with anti-AMP antibodies, the membrane was incubated with 1 M hydroxylamine (Sigma-Aldrich) in blocking solution for 8 h at room temperature, washed three times in TBS-T, blocked again for 1 h at room temperature, and proceeded with a second round of anti-AMP antibody probing. All western blots on recombinant proteins were performed as technical duplicates. Analysis of cell lysate samples was performed as biological duplicate. Representative blots are shown; unless otherwise indicated, rows represent same exposure times from identical blots. All changes in brightness and contrast were applied equally across the entire image. Cropping, e.g. due to different molecular weights, is indicated by a break in the frame. All blots are depicted in full along with their dynamic range in the supplemental information (Data S1).

Data S1: Uncropped gel and WB images with dynamic range. Related to Figure 1, Figure 2, Figure 3, Figure 4, Figure S4, Figure S6 and Figure S7.

Figure 1A
 α -Thr-AMP (Merck)



α -Tyr-AMP (Merck)



A-pan-ADPR (Merck)

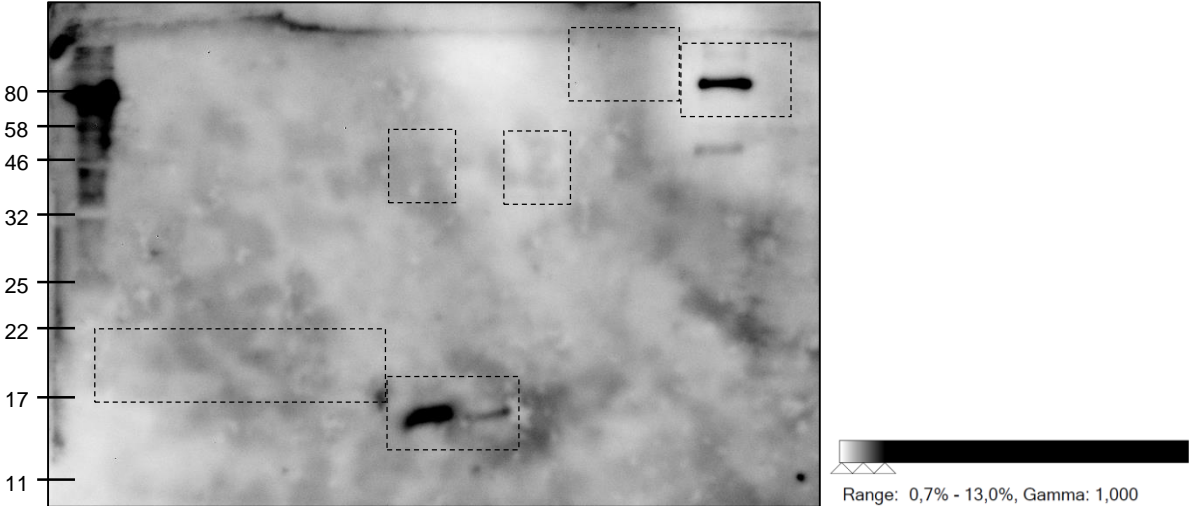
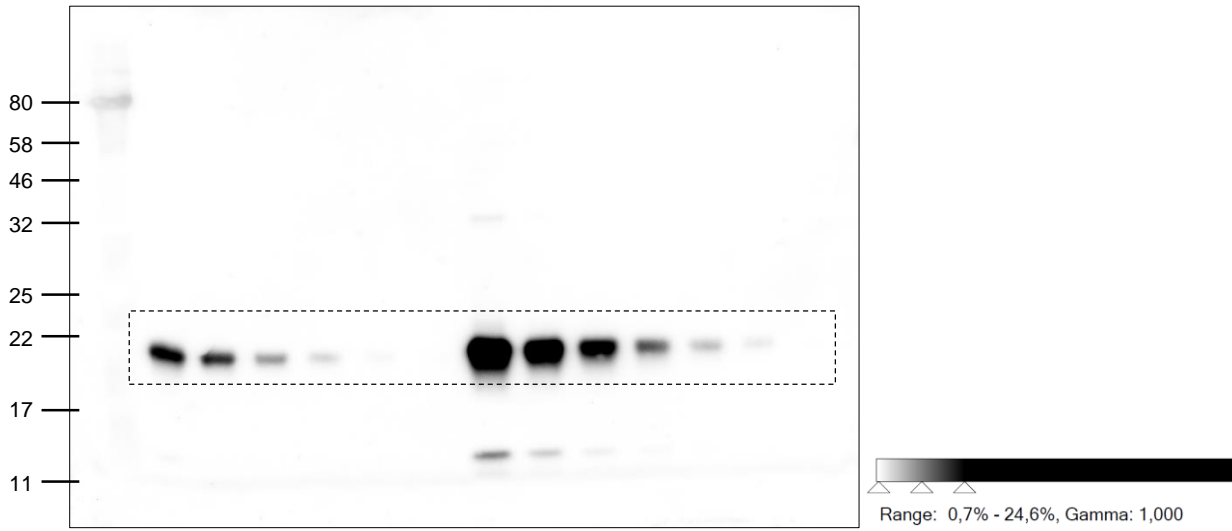
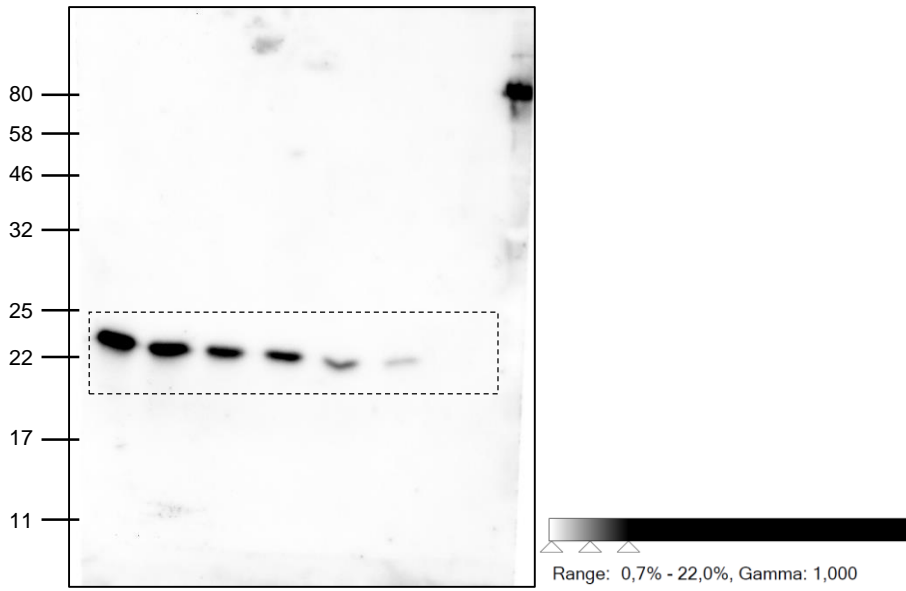


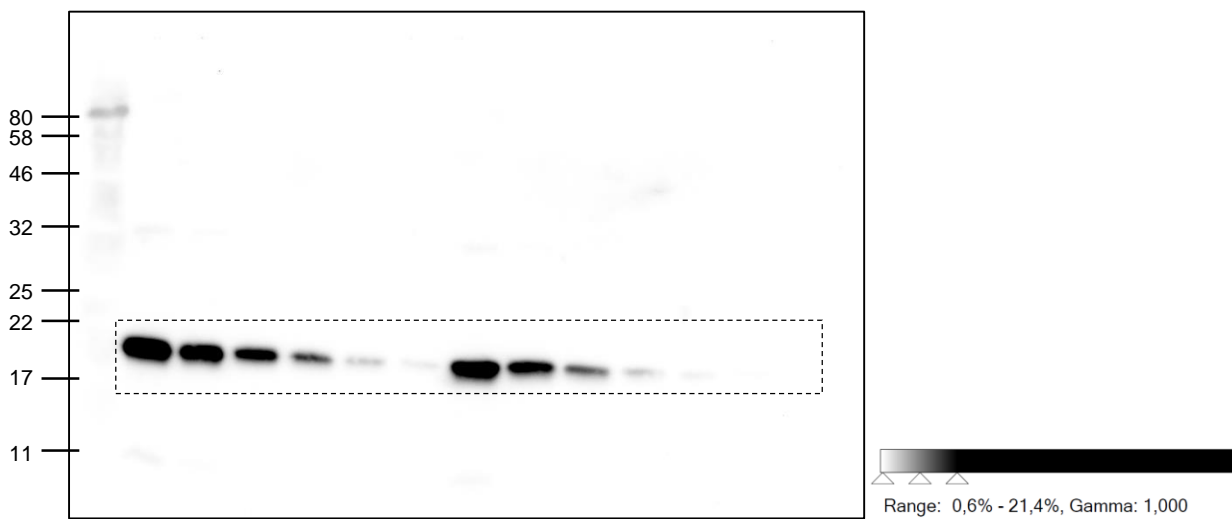
Figure 2A
1G11_Cdc42



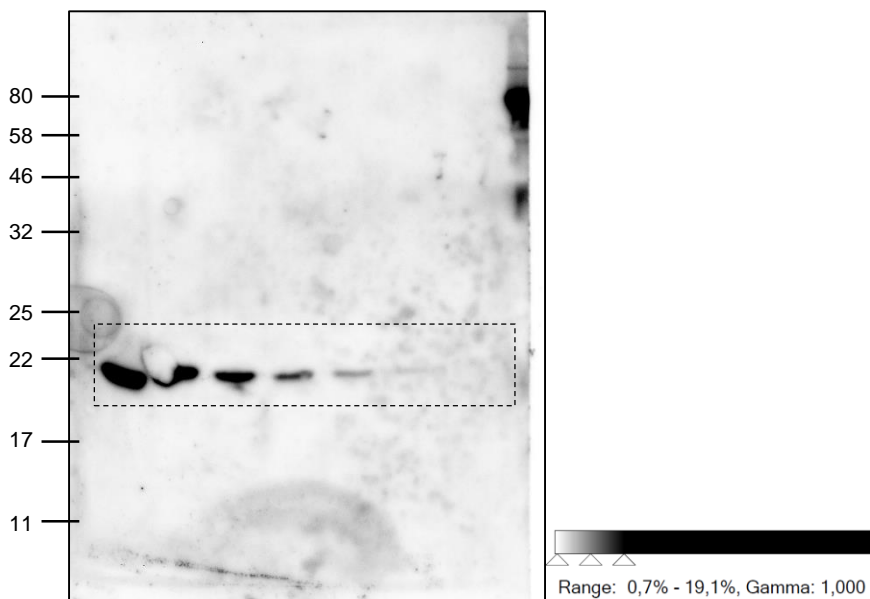
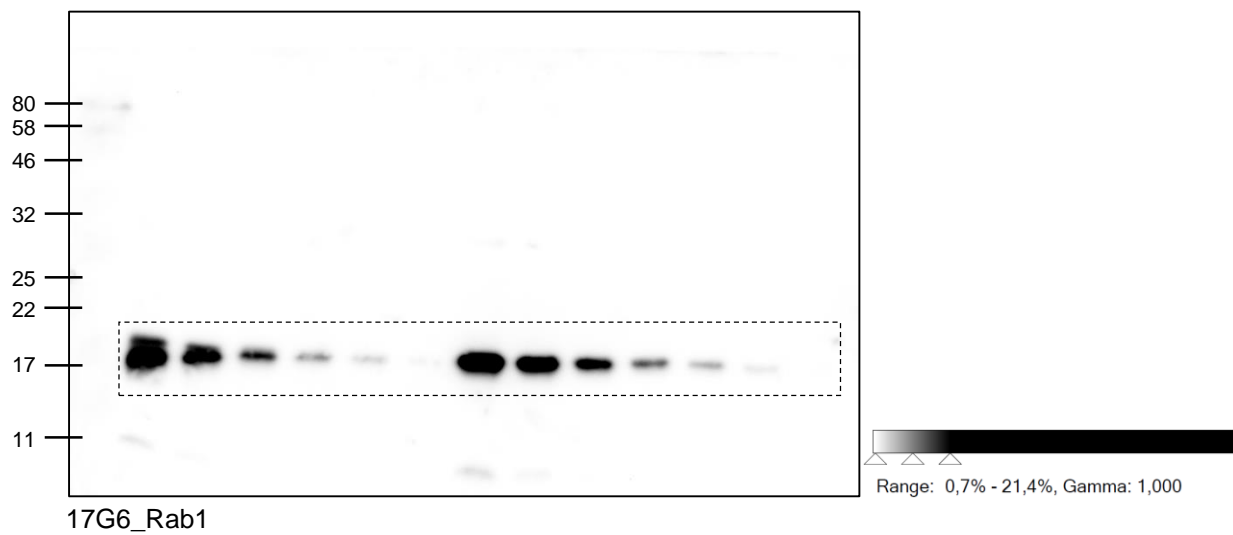
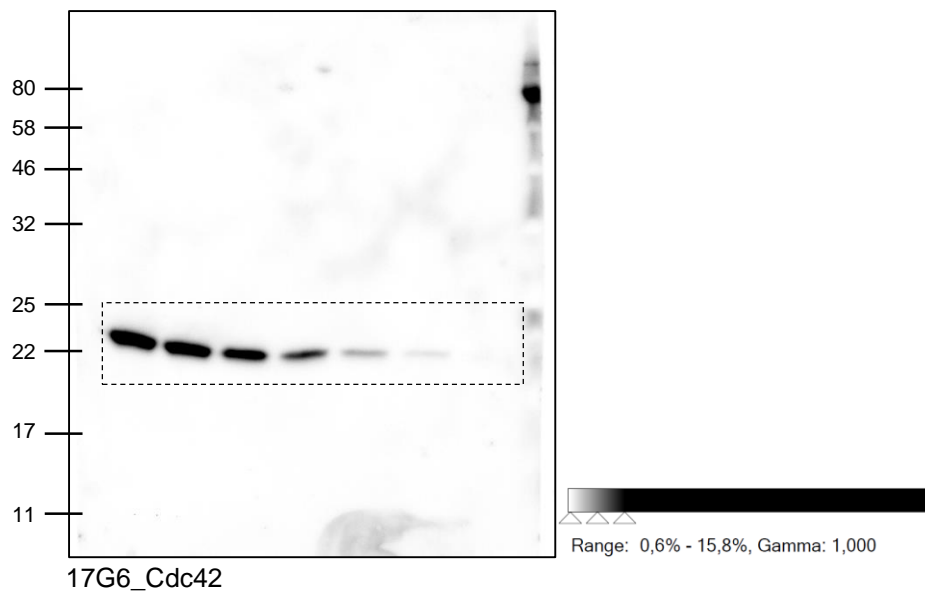
1G11_Rab1



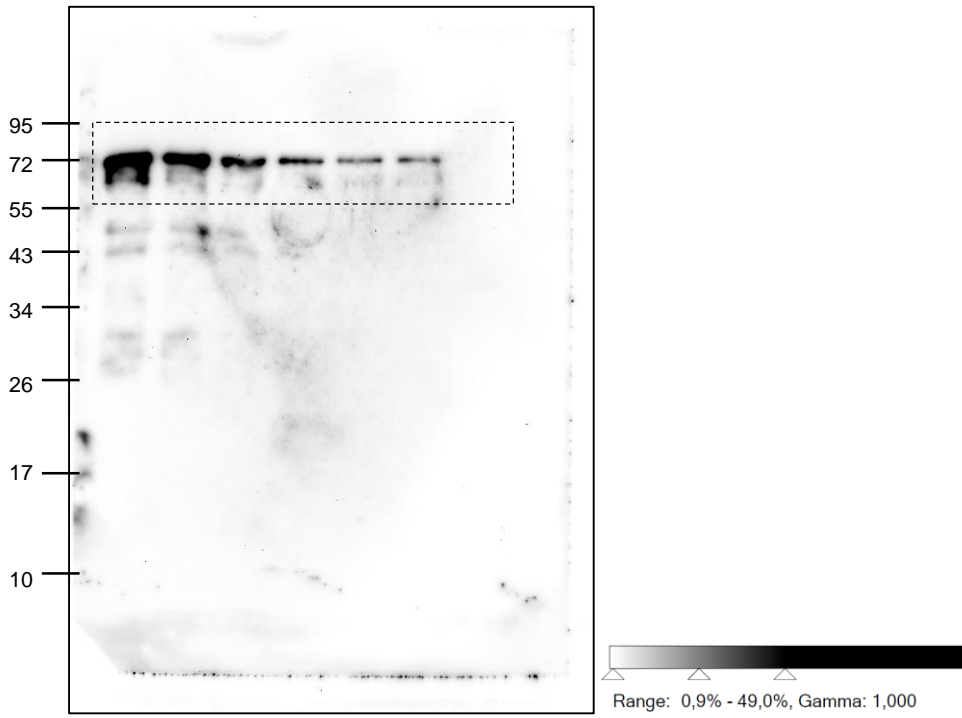
7C11_Cdc42



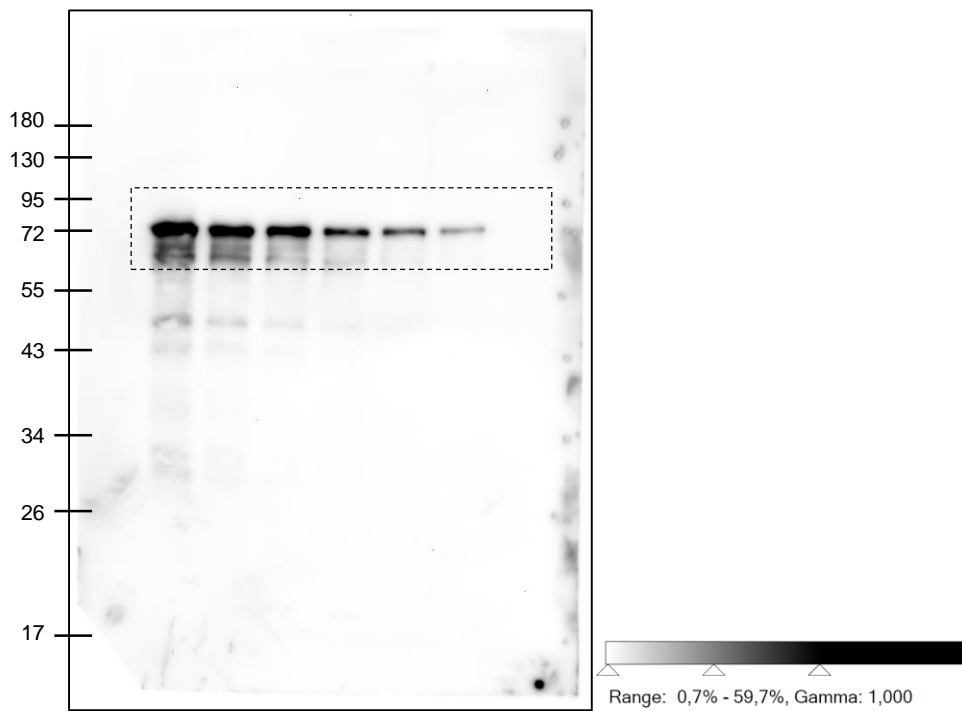
7C11_Rab1



7C11_BiP



17G6_BiP



1G11_BiP

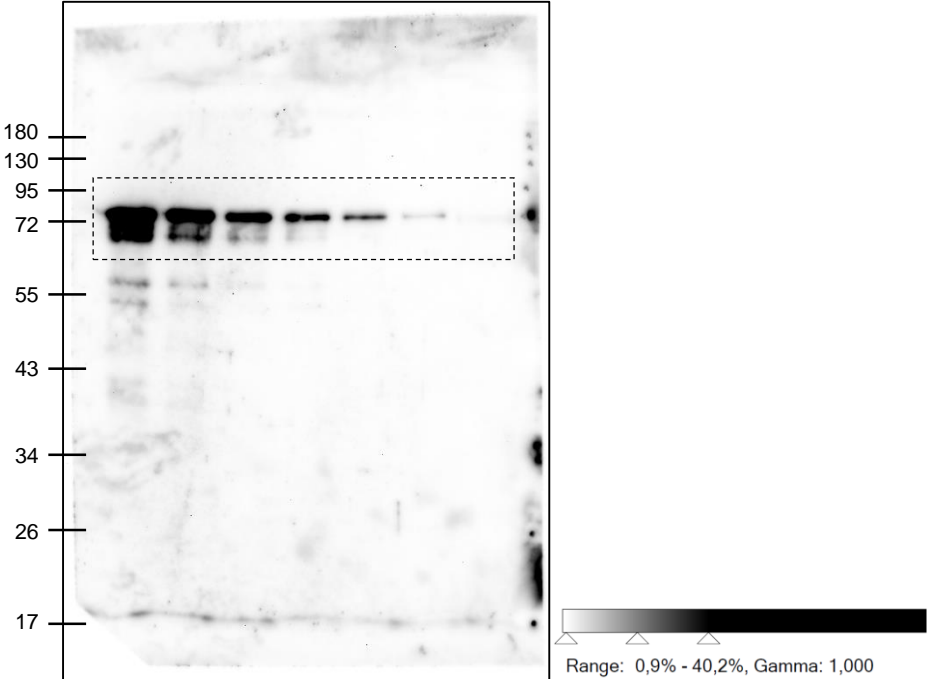
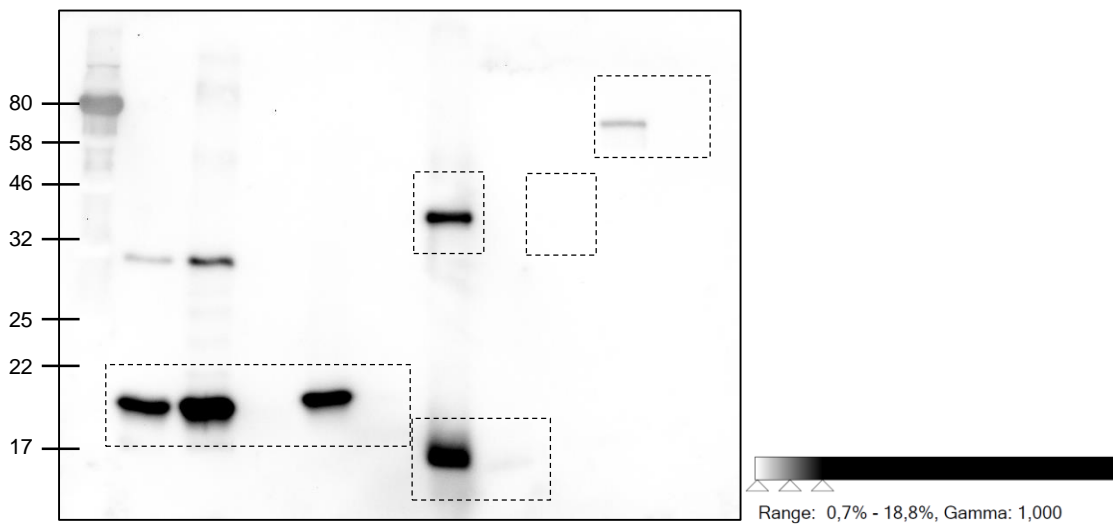
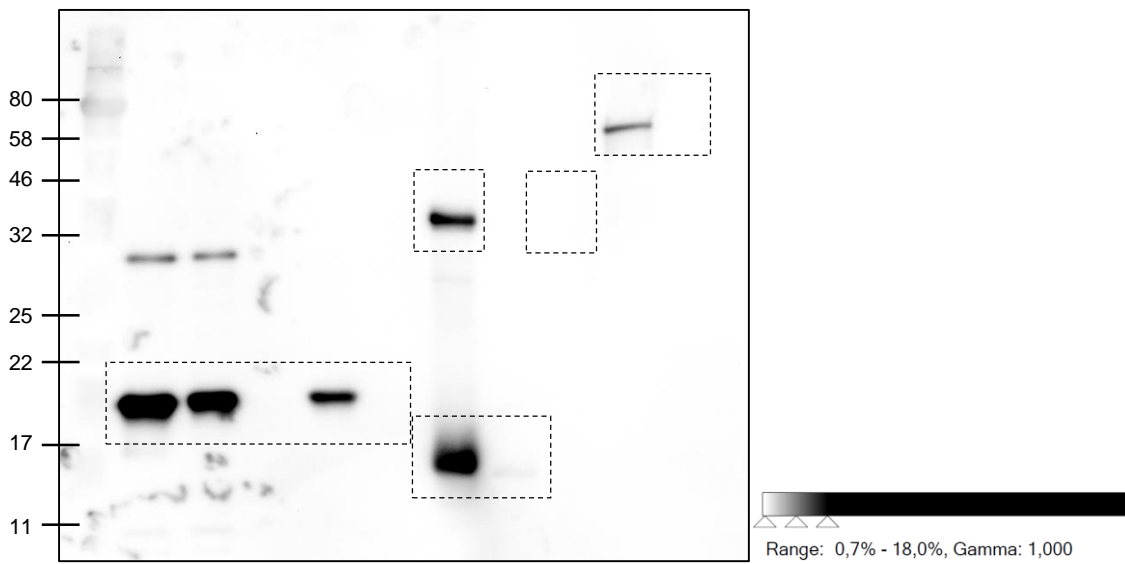


Figure 2B
1G11



7C11



17G6

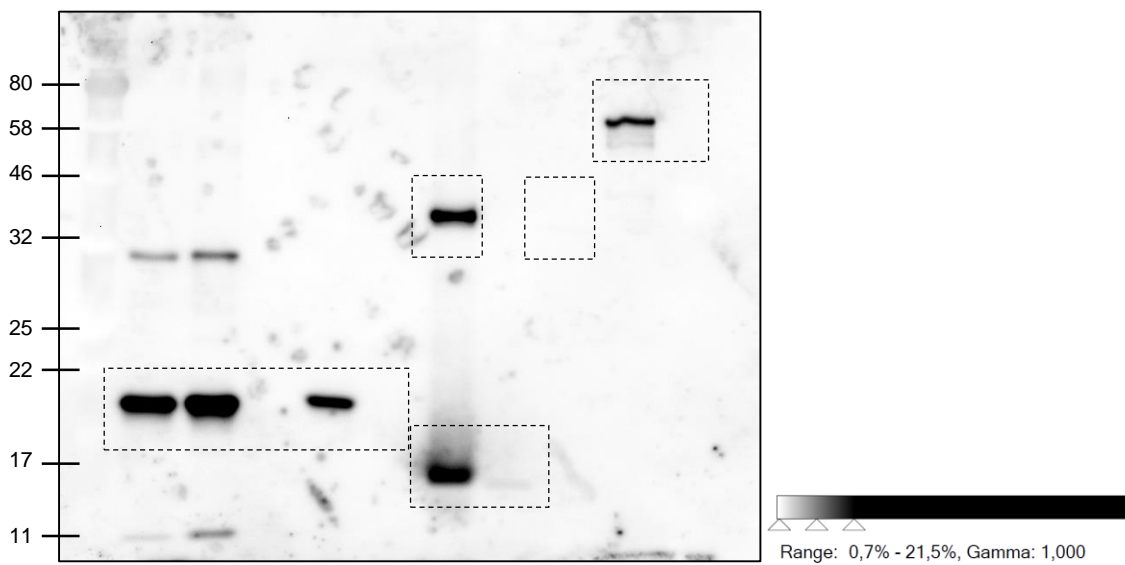
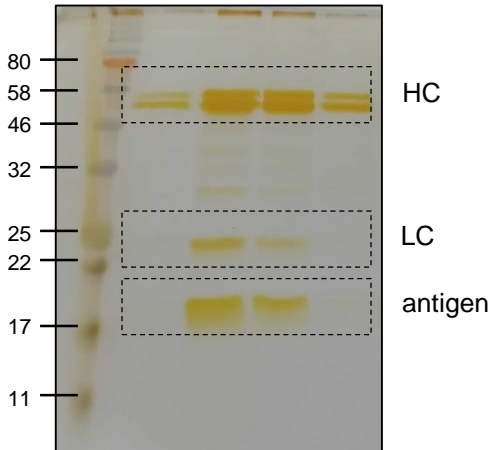
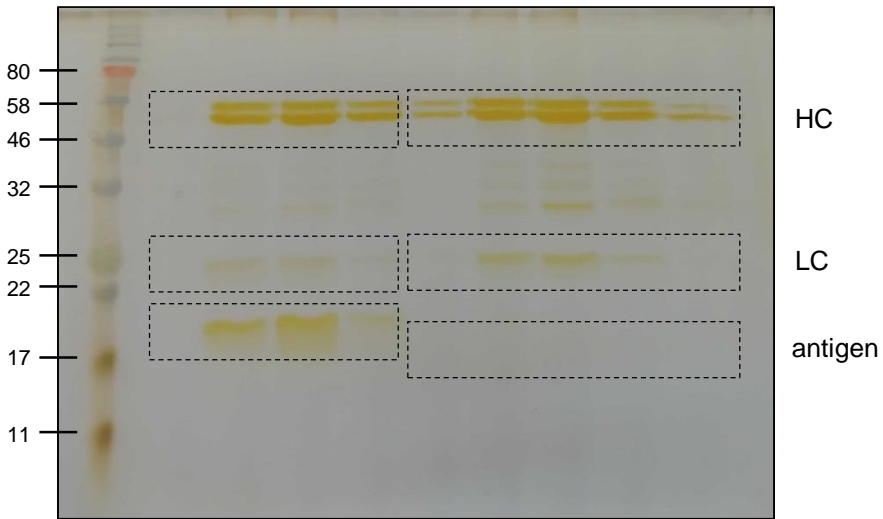


Figure 2C

17G6_Cdc42-Tyr-AMP



17G6_Cdc42-Thr-AMP (left), _Rab1-AMP (right)



17G6_BiP-AMP

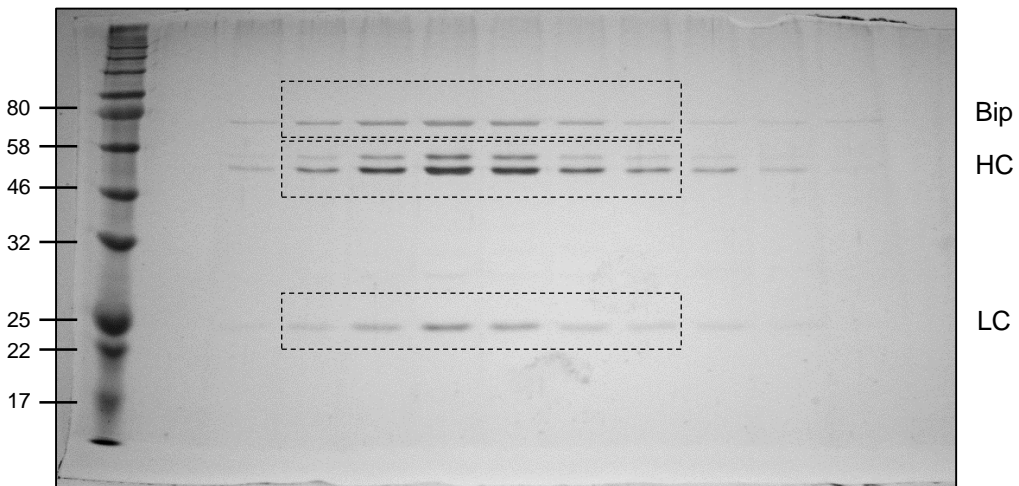
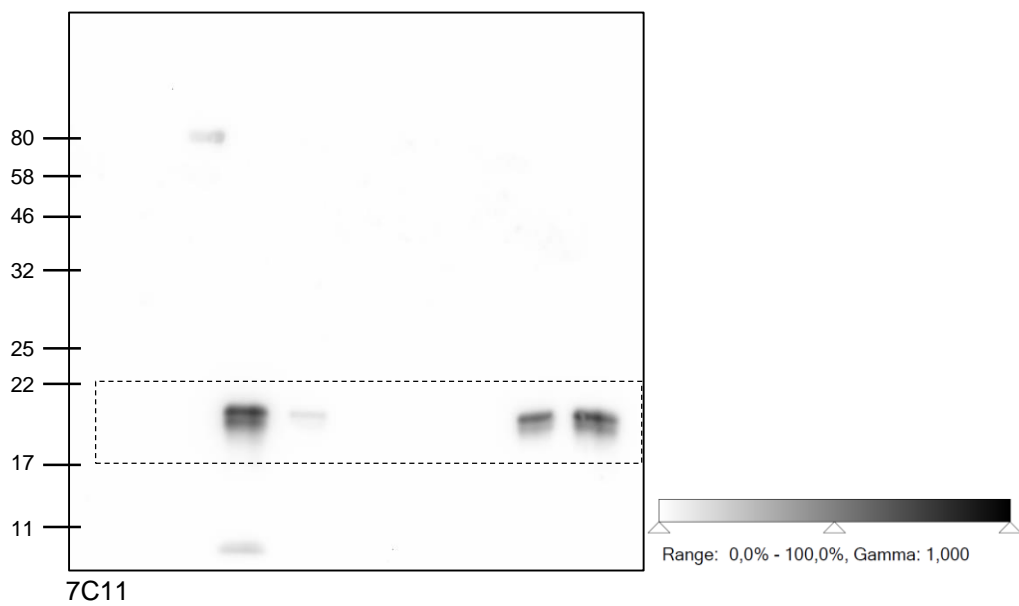
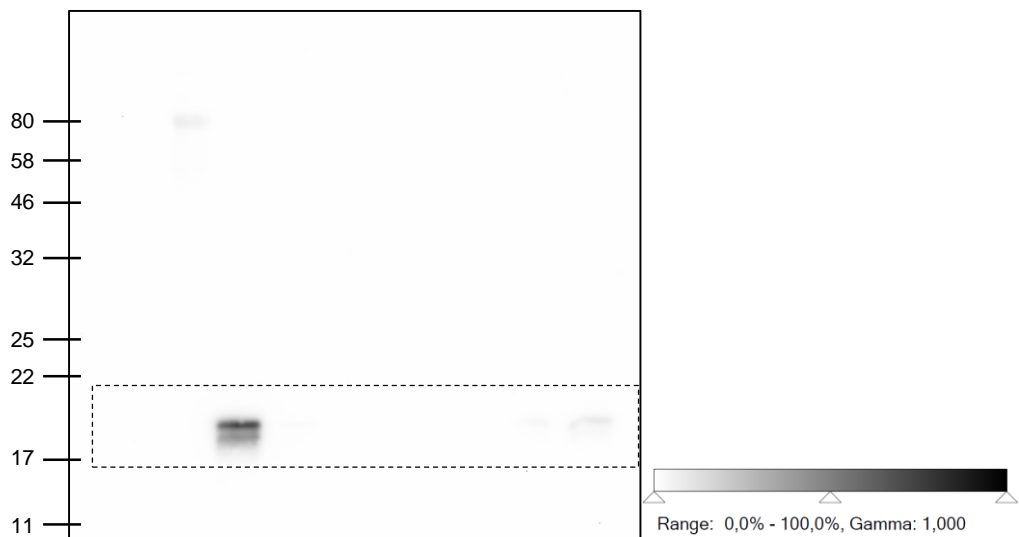


Figure 2D
1G11



7C11



17G6

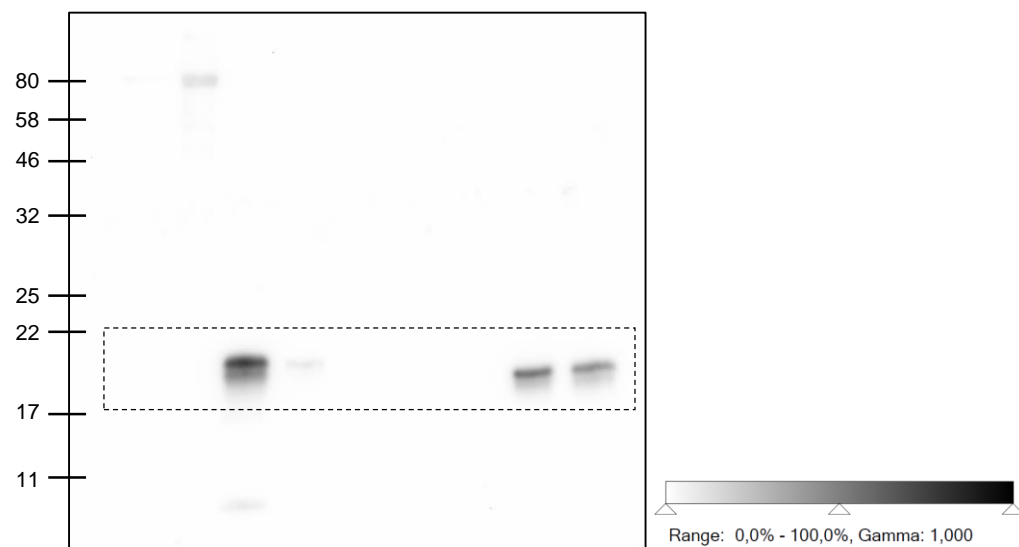
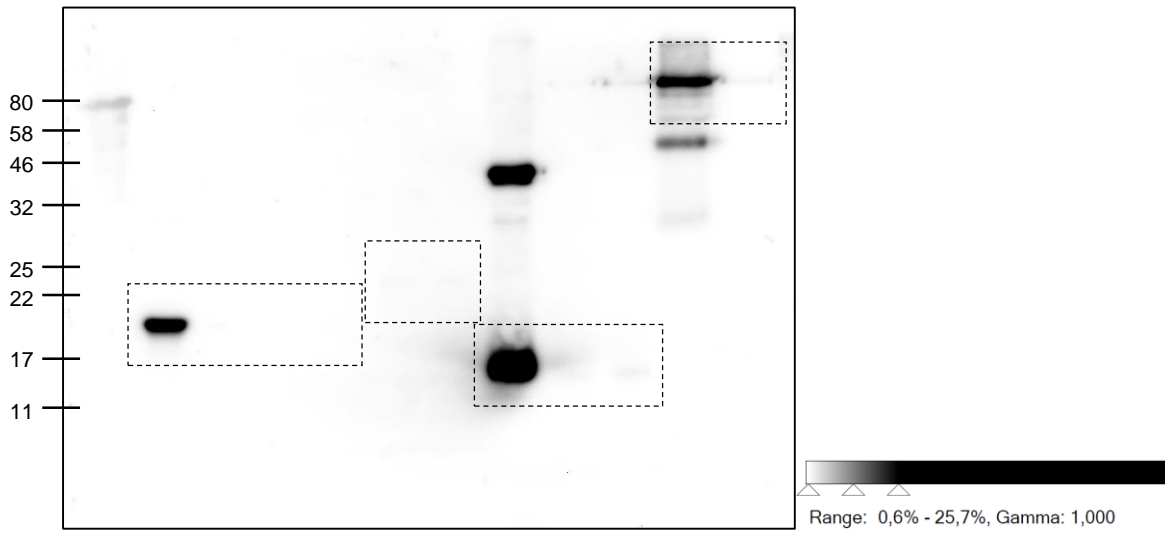
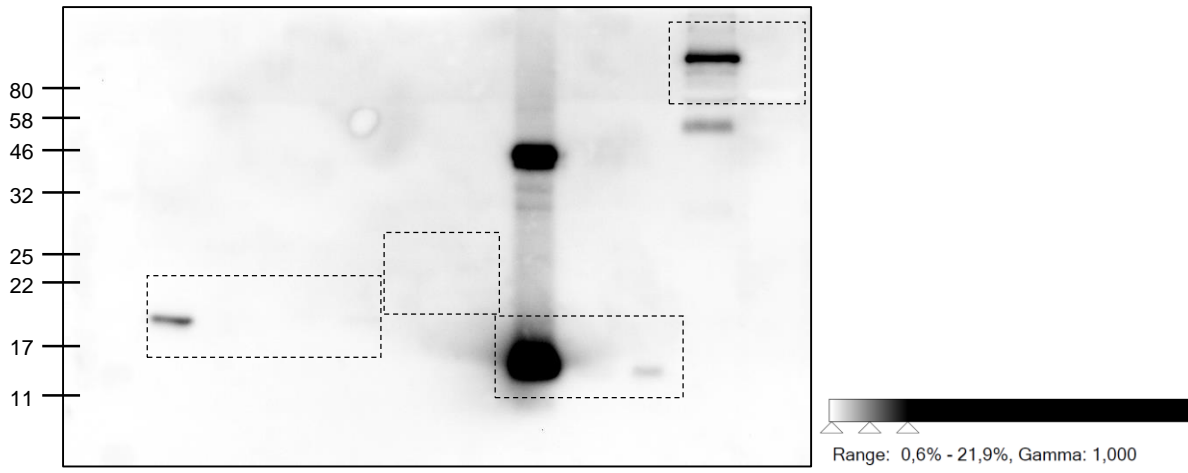


Figure 2E
1G11



17G6



7C11

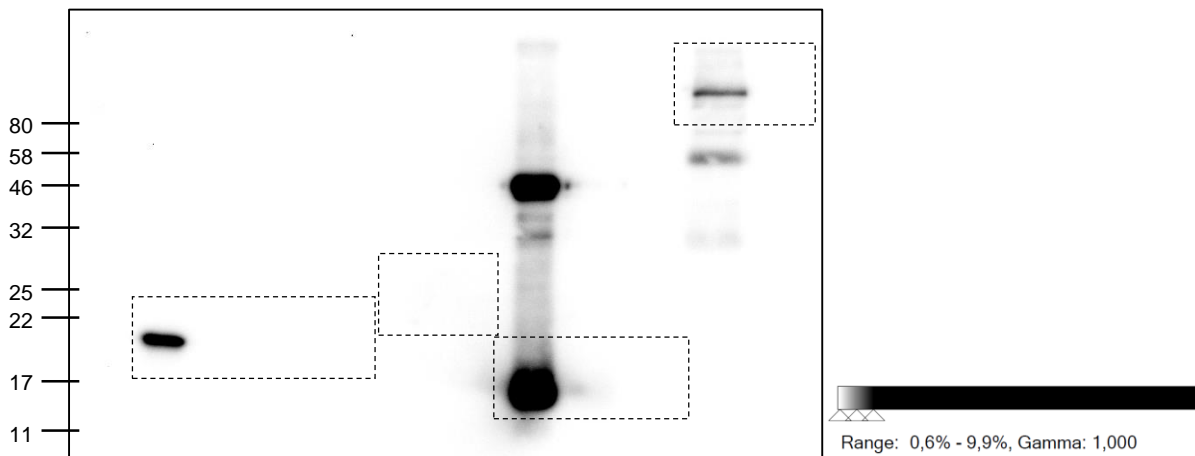
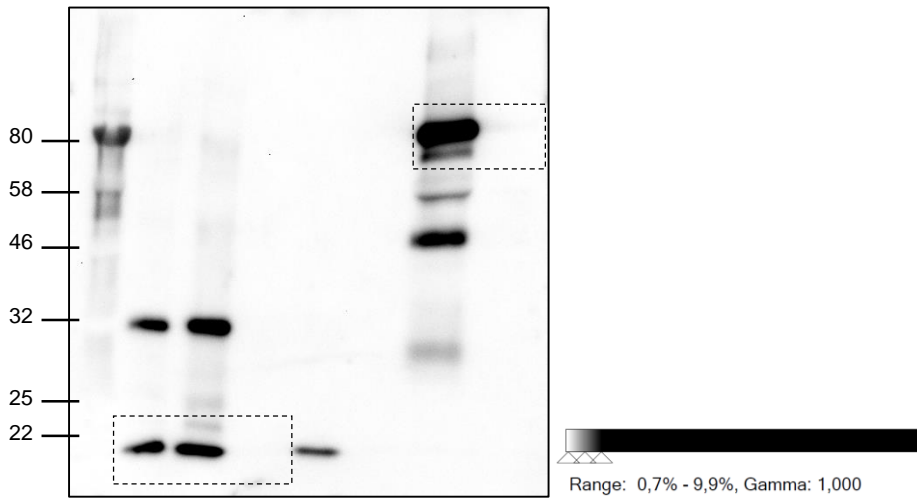
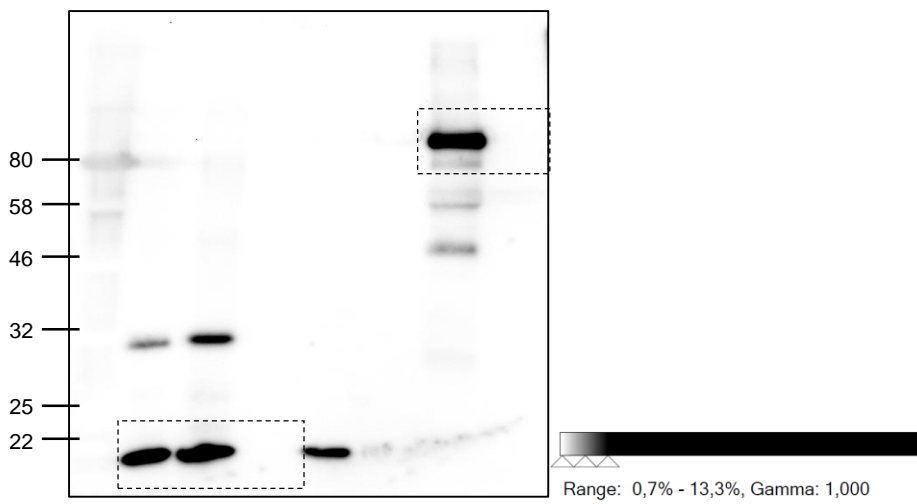


Figure 3A

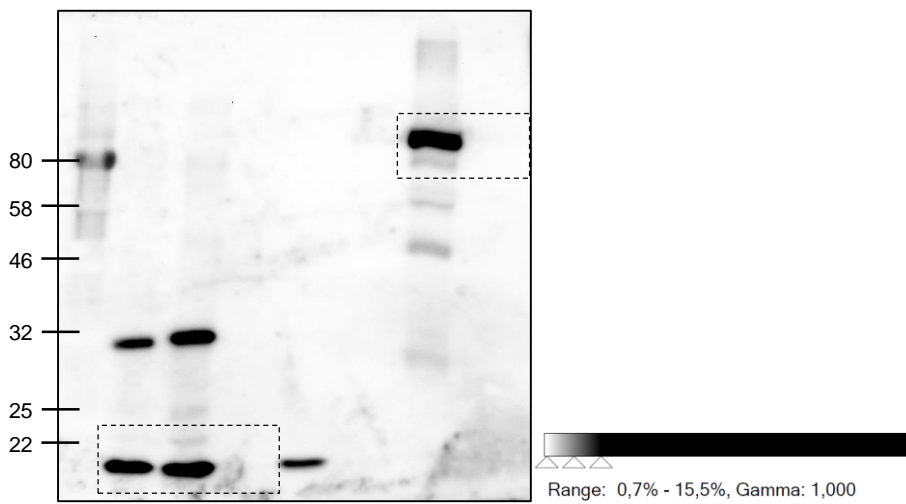
17G6_1 mM MgCl₂



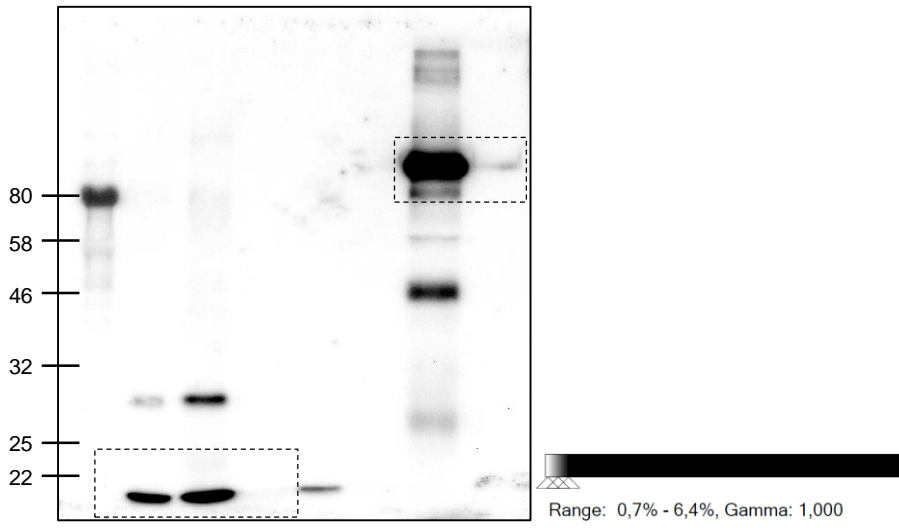
17G6_1 mM MnCl₂



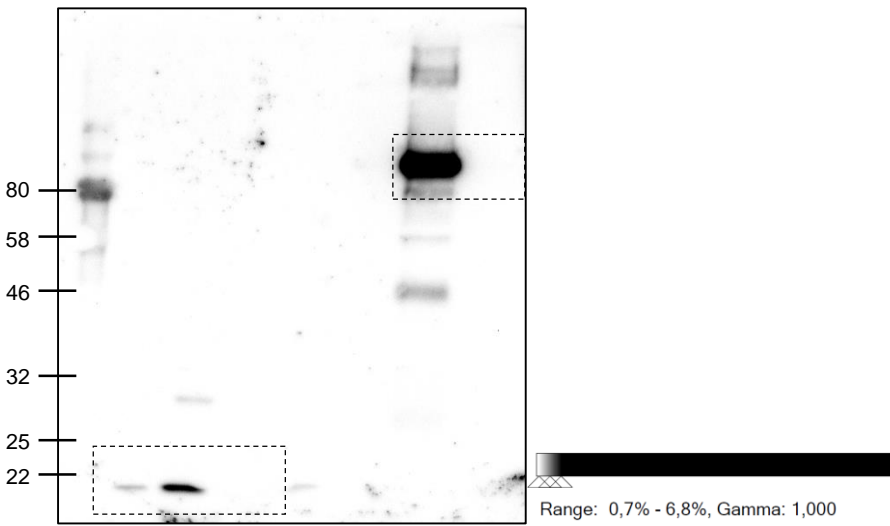
17G6_no additive



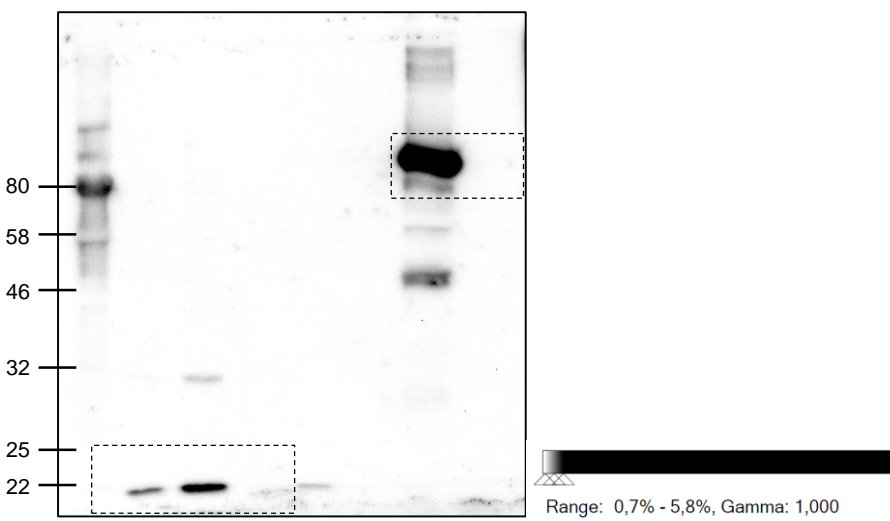
17G6_1 μ M adenosine



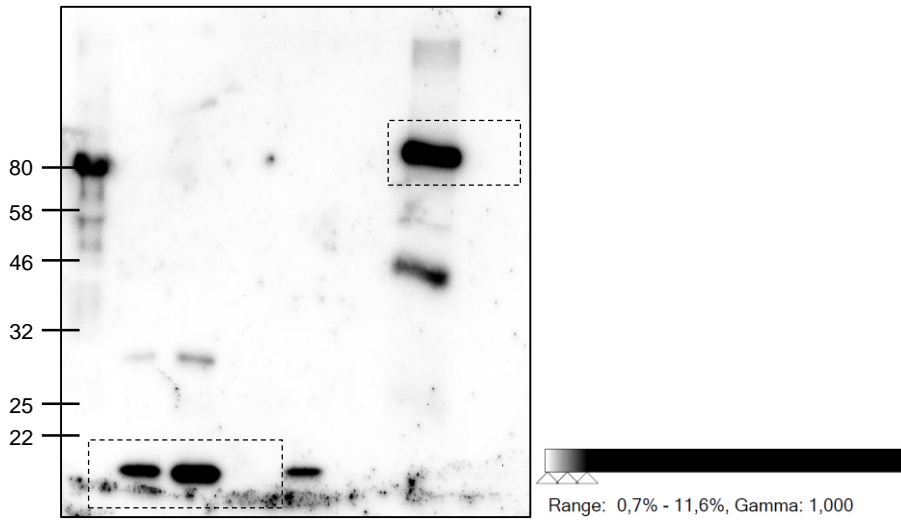
17G6_1 μ M ADP



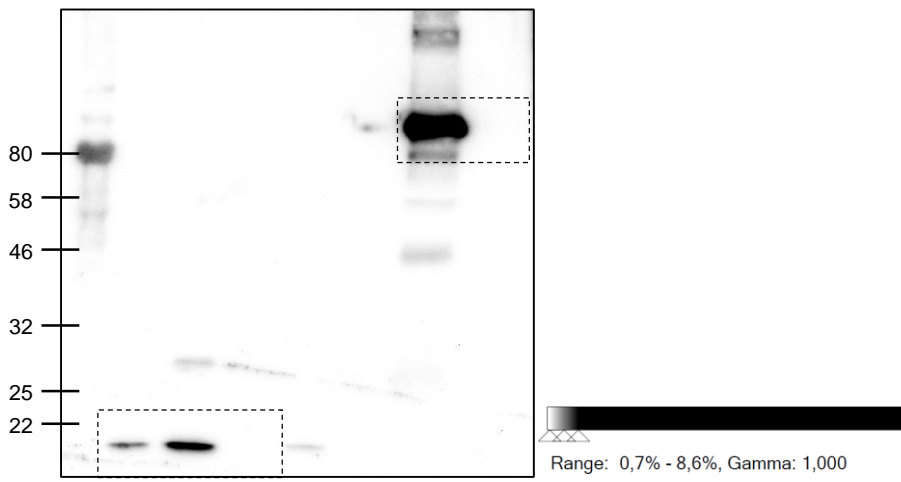
17G6_1 μ M AMP



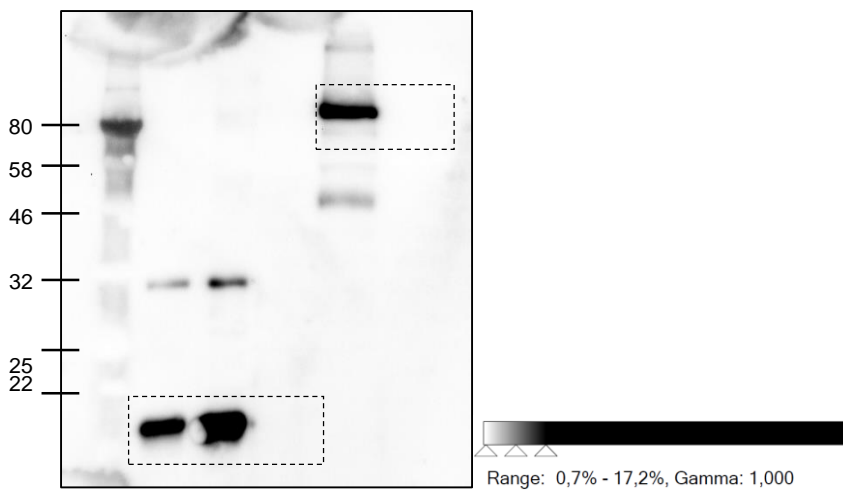
17G6_1 μ M ATP



17G6_1 μ M NAD⁺



17G6_1 μ M ADPR



17G6_Hydroxylamine treated (previously 17G6_1 uM ADPR)

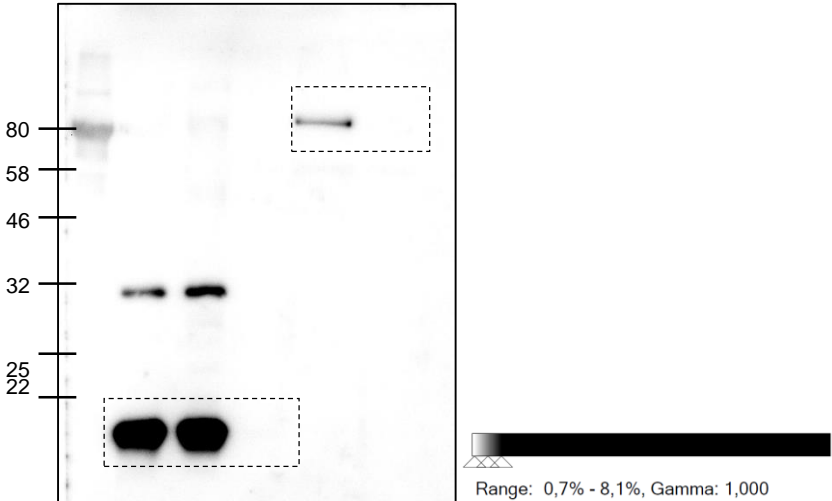
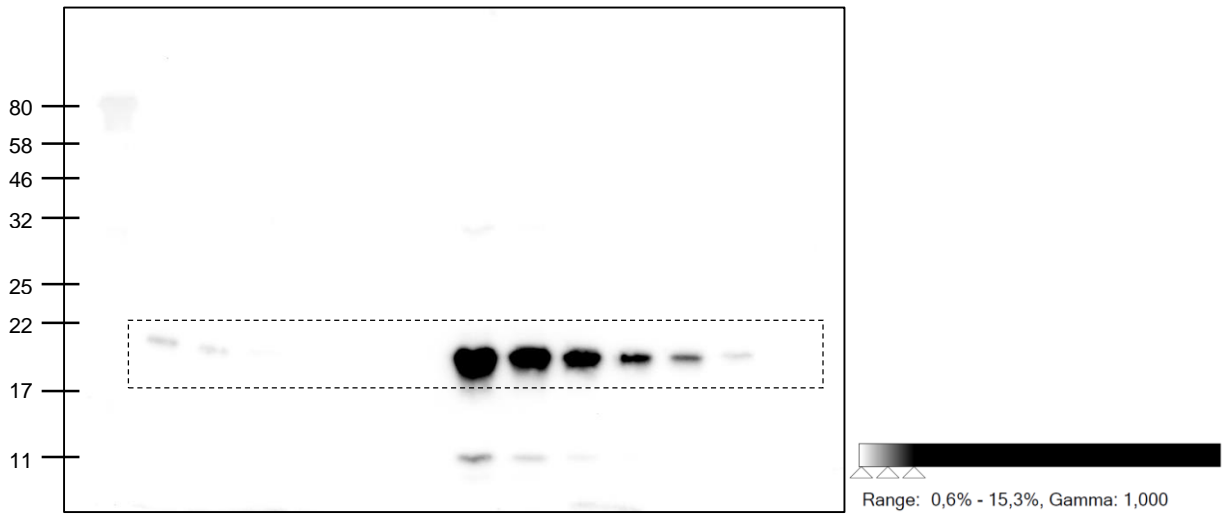
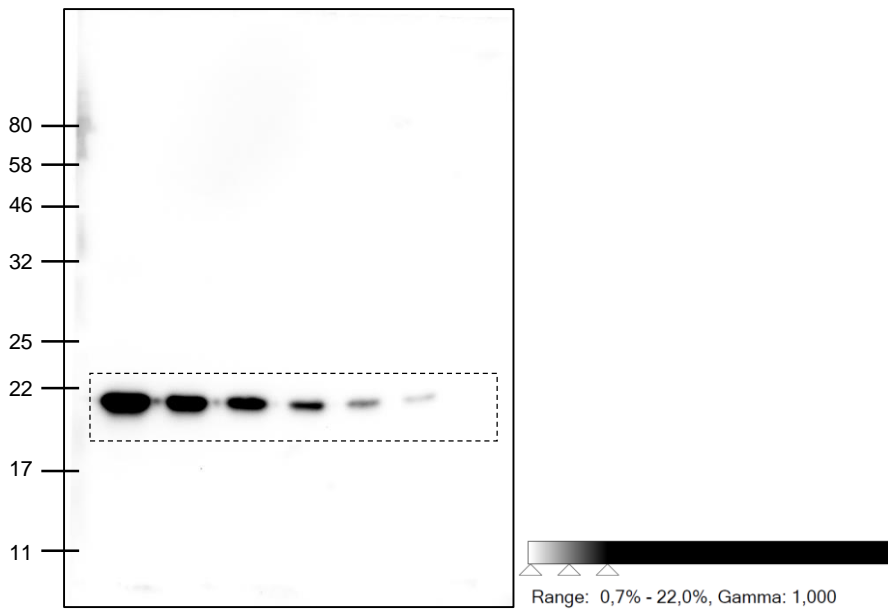


Figure 3B

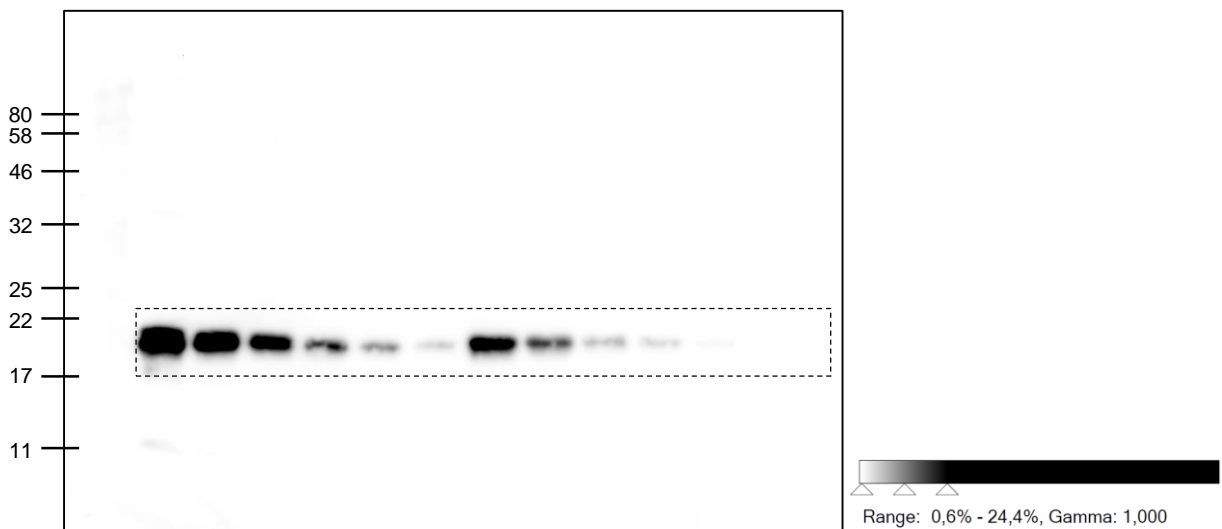
1G11 + MnCl₂_Cdc42



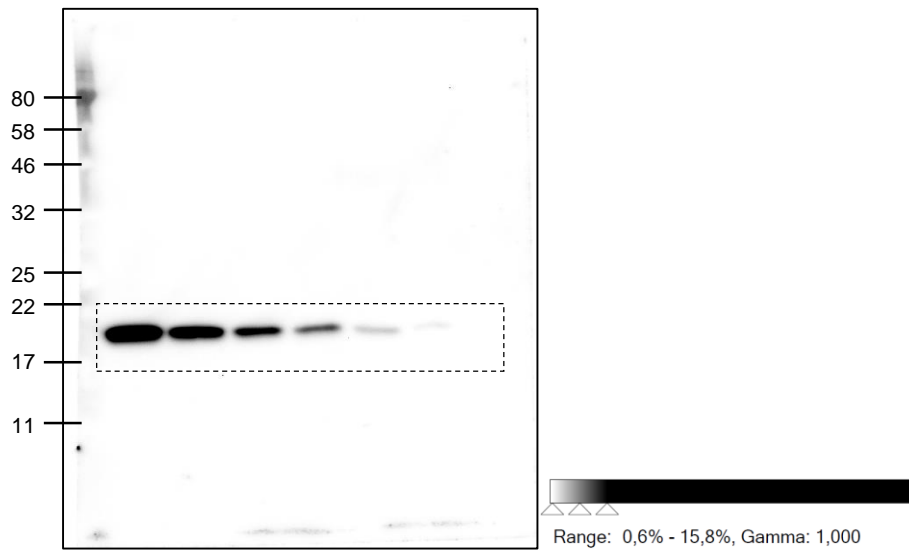
1G11 + MnCl₂_Rab1



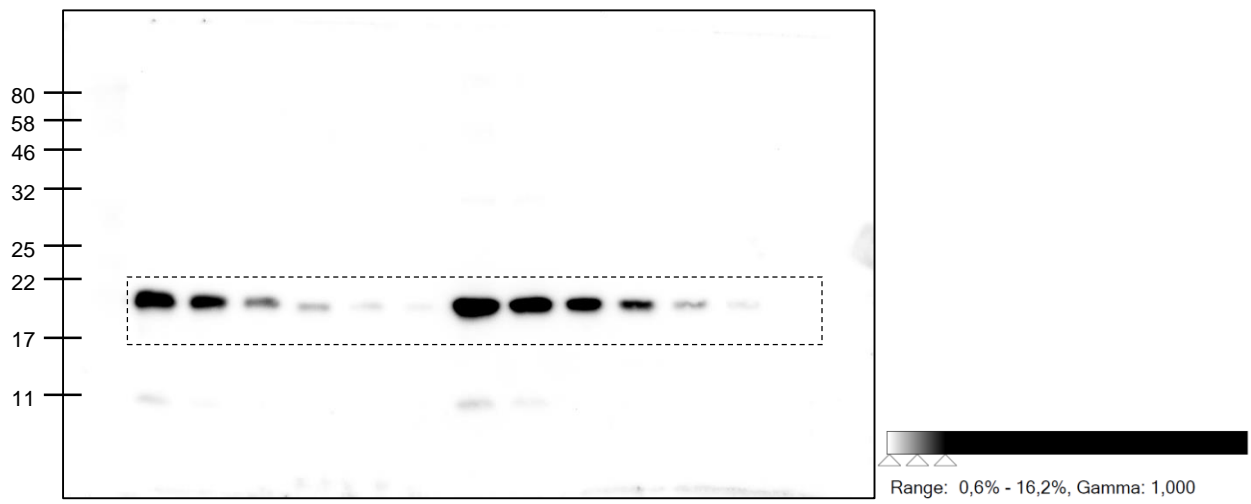
7C11 + MnCl₂_Cdc42



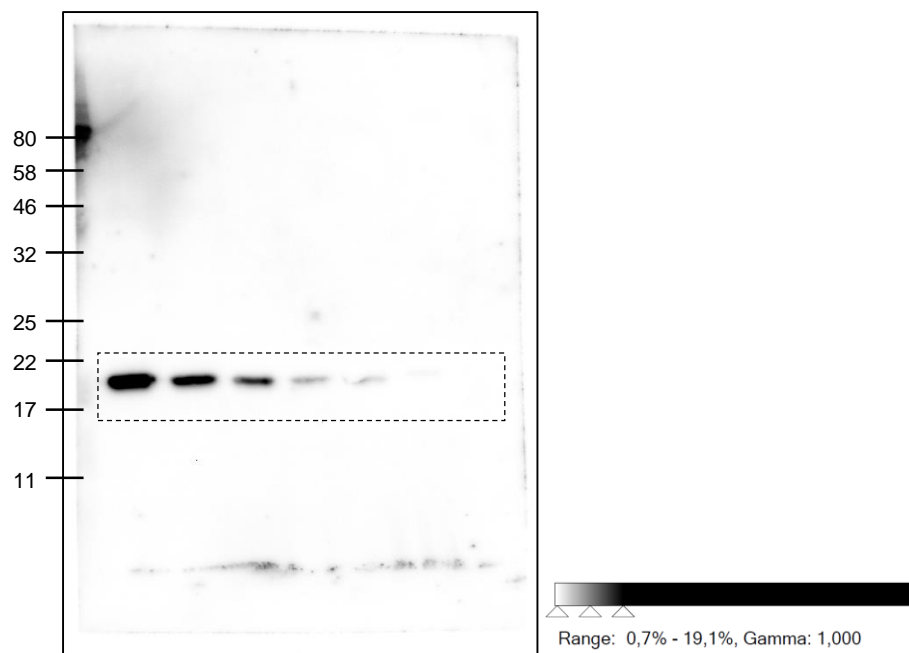
7C11 + MnCl₂_Rab1



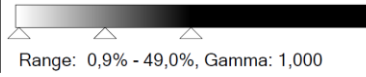
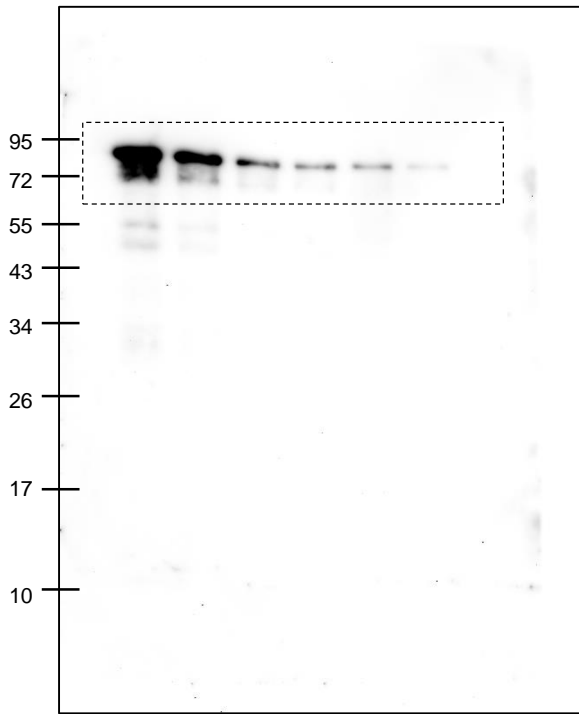
17G6 + MnCl₂_Cdc42



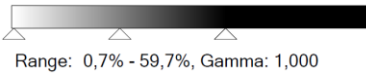
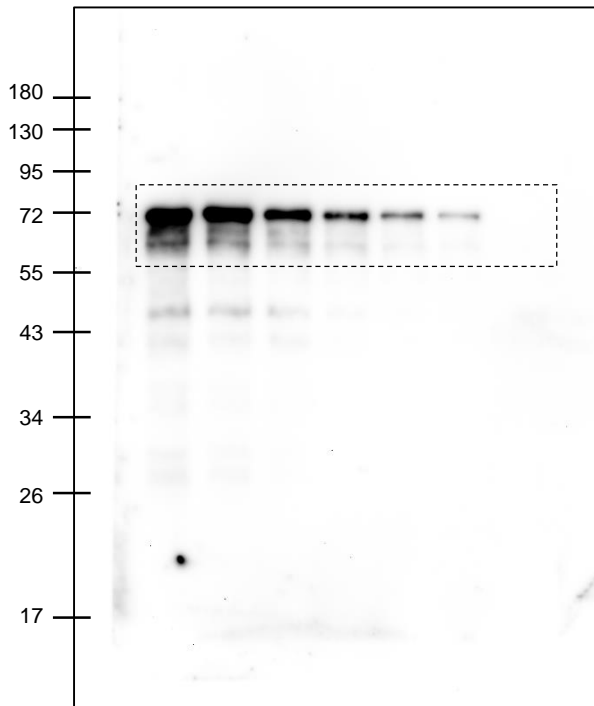
17G6 + MnCl₂_Rab1



7C11 + MnCl₂_BiP



17G6 + MnCl₂_BiP



1G11 + MnCl₂_BiP

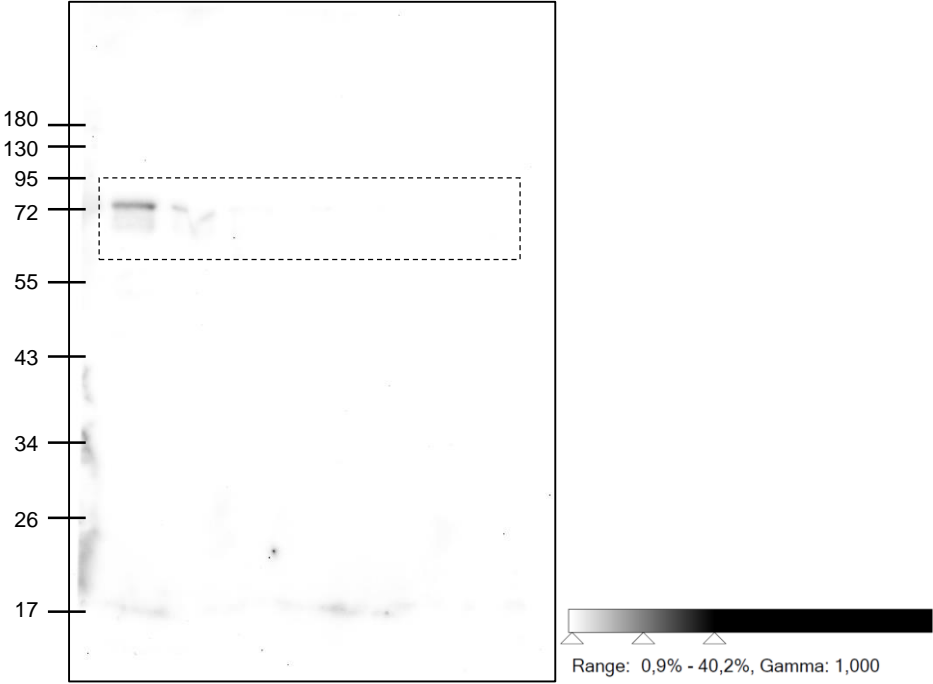
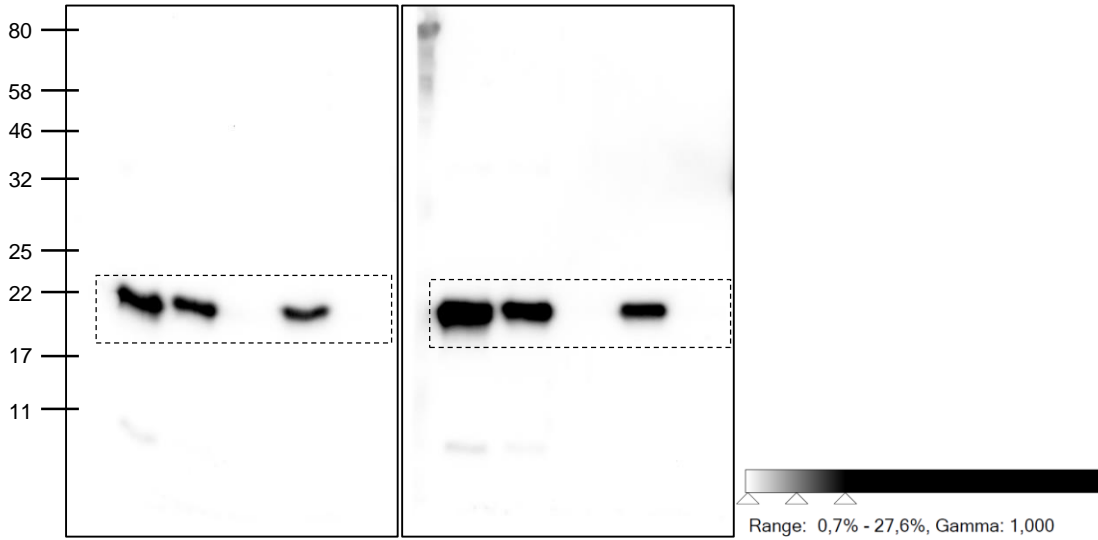
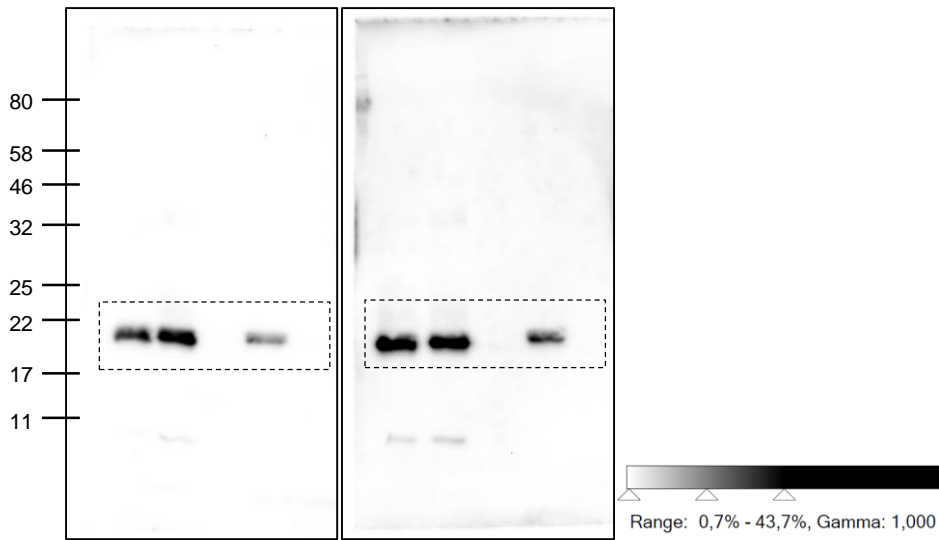


Figure 3C

7C11_MnCl₂ (left) and _without additive (right)



17G6_MnCl₂ (left) and _without additive (right)



1G11_MnCl₂ (left) and _without additive (right)

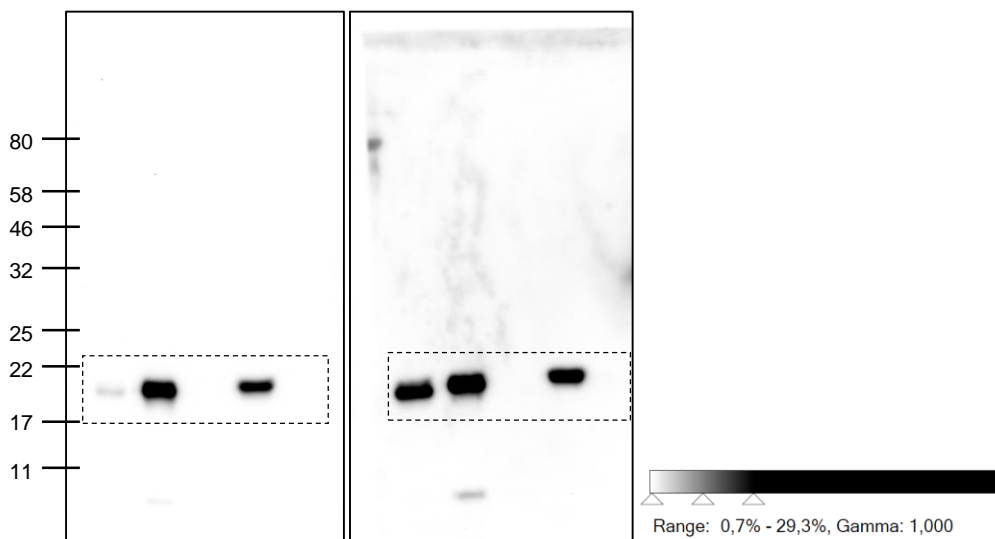
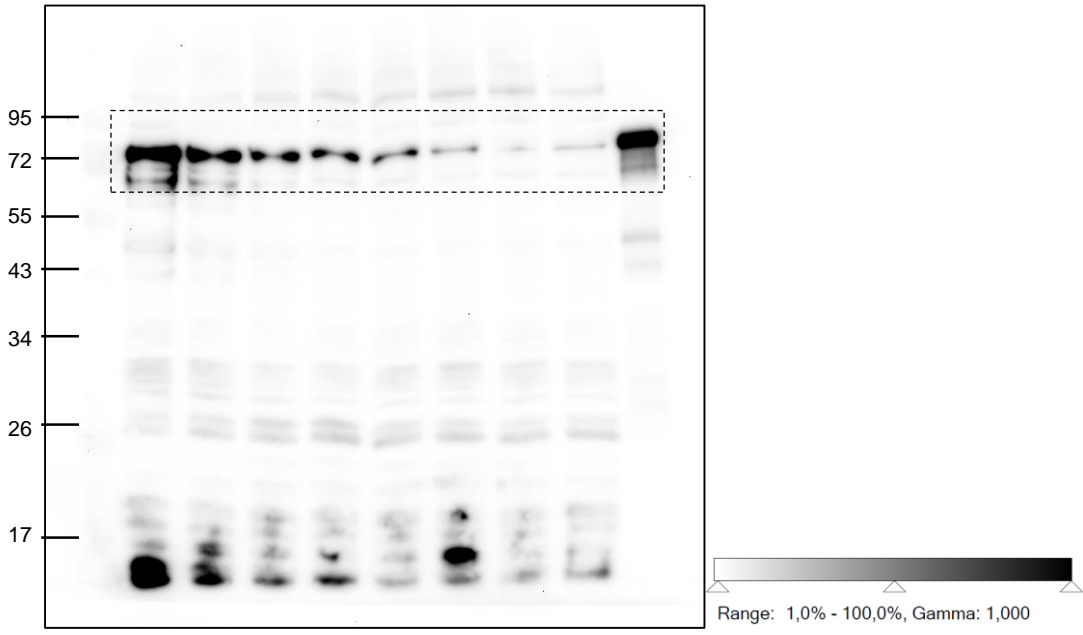


Figure 4A
17G6 + MnCl₂_ctrl



17G6 + MnCl₂_2 h TG

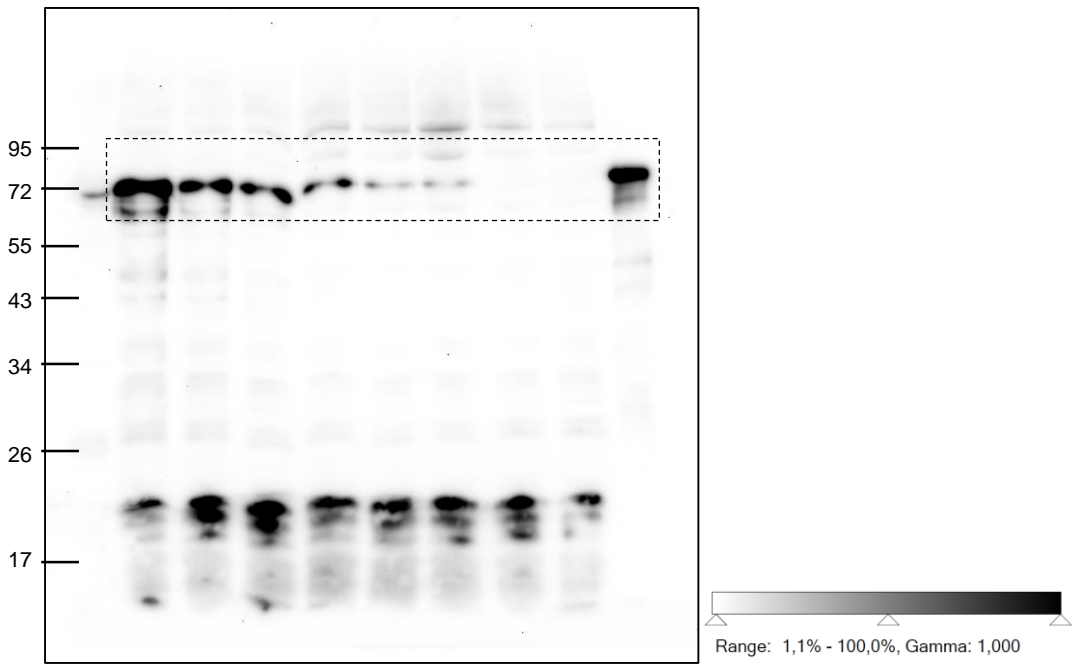
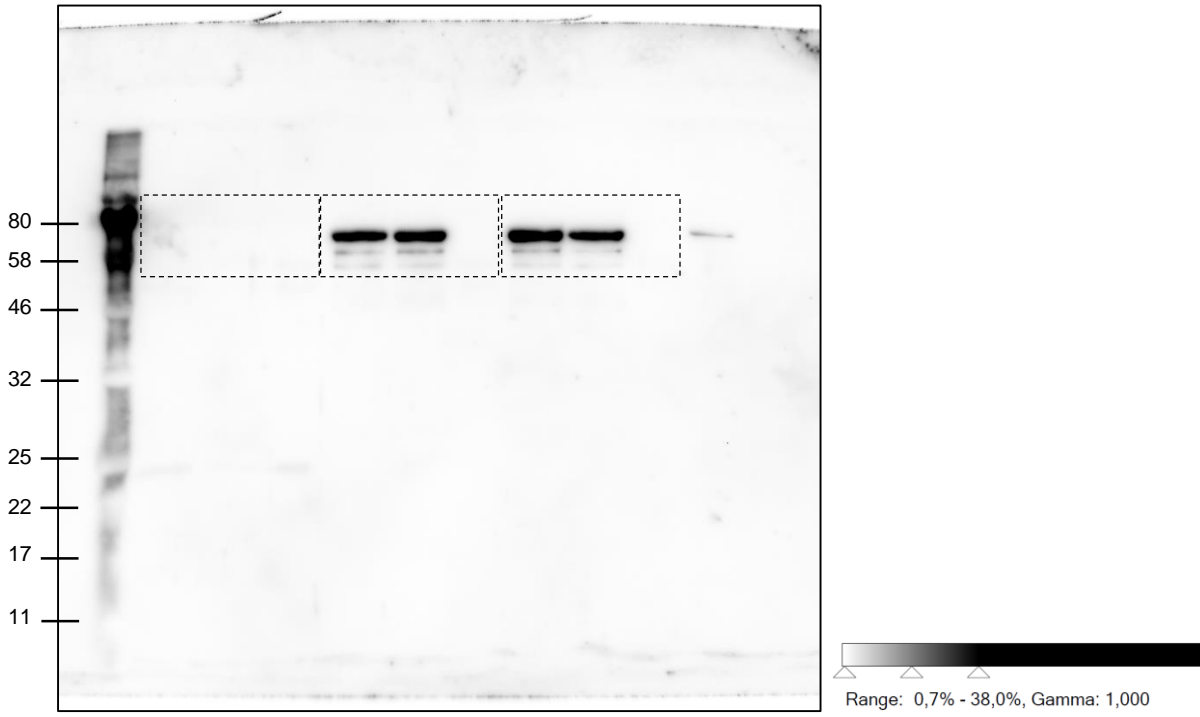


Figure 4B

aBiP_IP: beads only_ - (left), _BiP (middle) and _BiP-AMP (right)



aBiP_IP: 17G6_BiP (left) and _BiP-AMP (right)

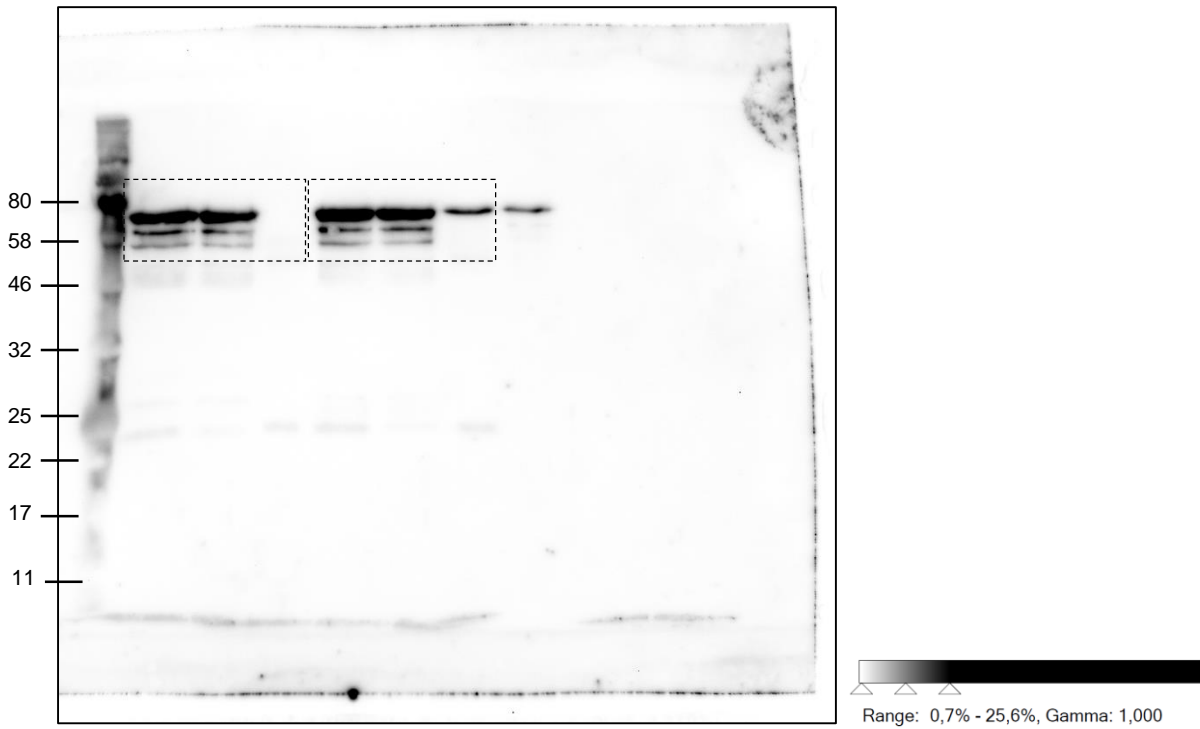
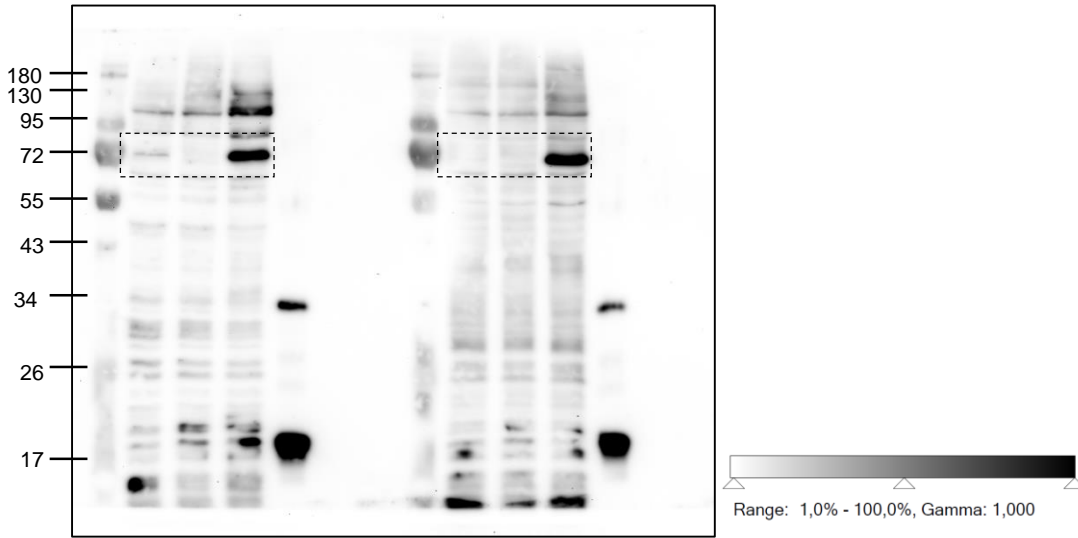
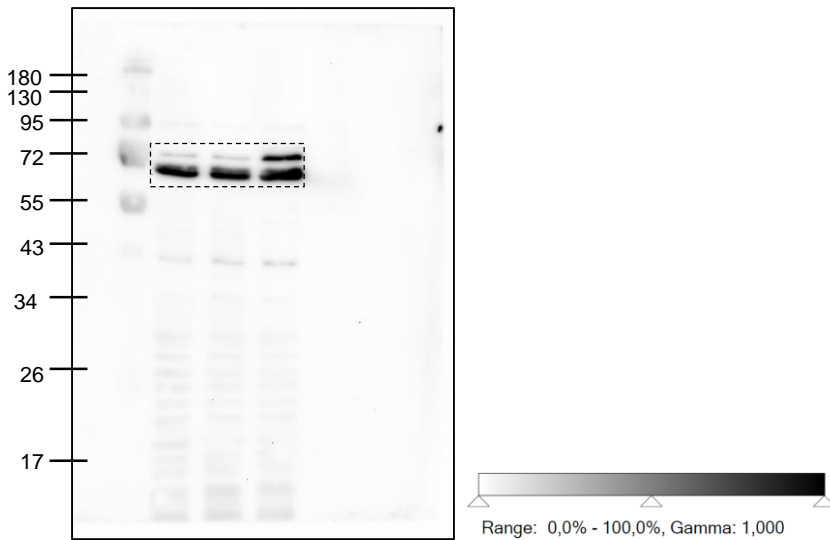


Figure 4C

17G6 + MnCl₂_HEK293 (left) and _CHO-K1 (right)



α -BiP_HEK293 (stripped, previously 17G6 + MnCl₂)



α -BiP_CHO-K1 (stripped, previously 17G6 + MnCl₂)

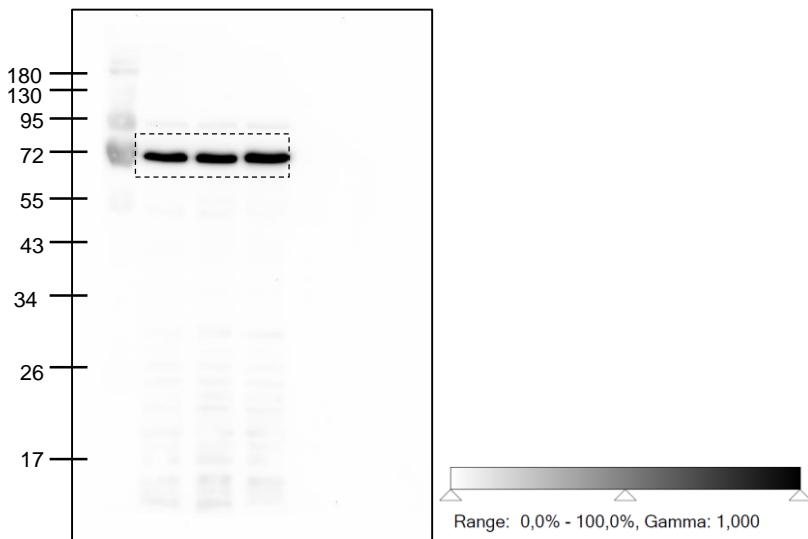


Figure 4D
 α -BiP_IP:17G6

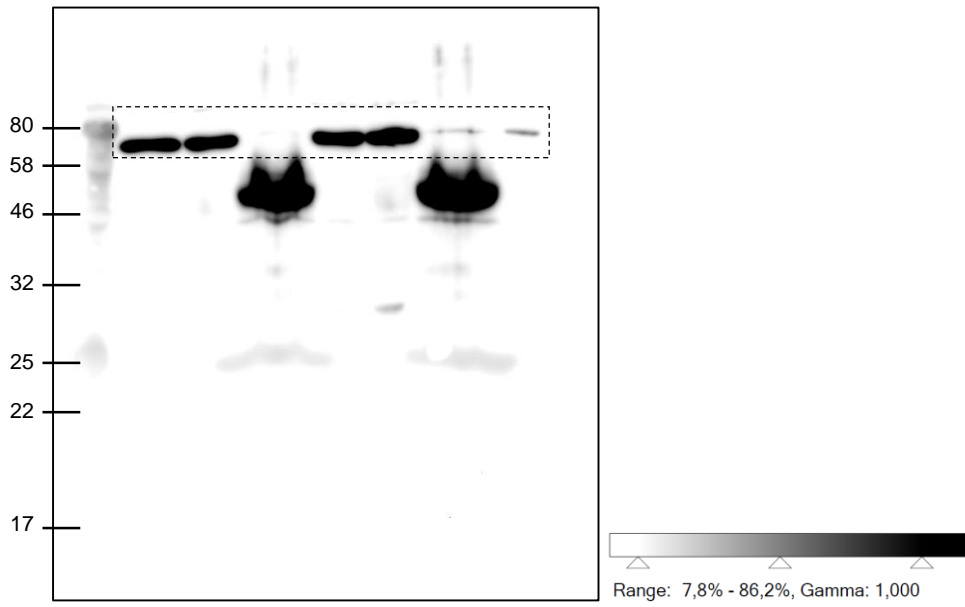


Figure 4E
aBiP_IP 17G6_input (left), _unbound (middle), _bound (right)

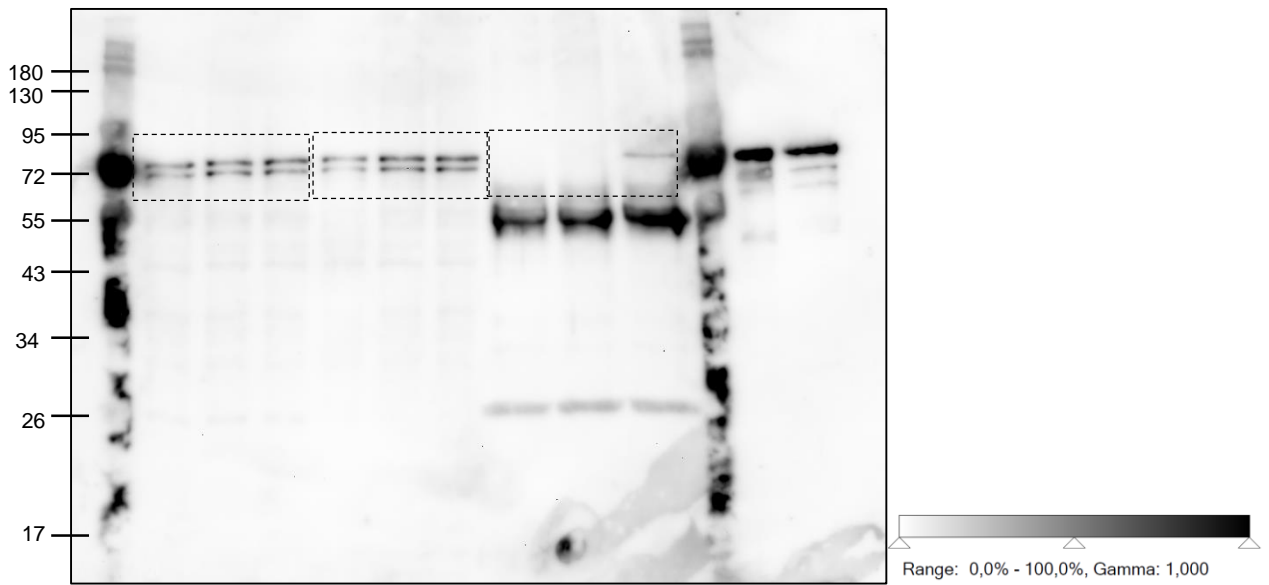
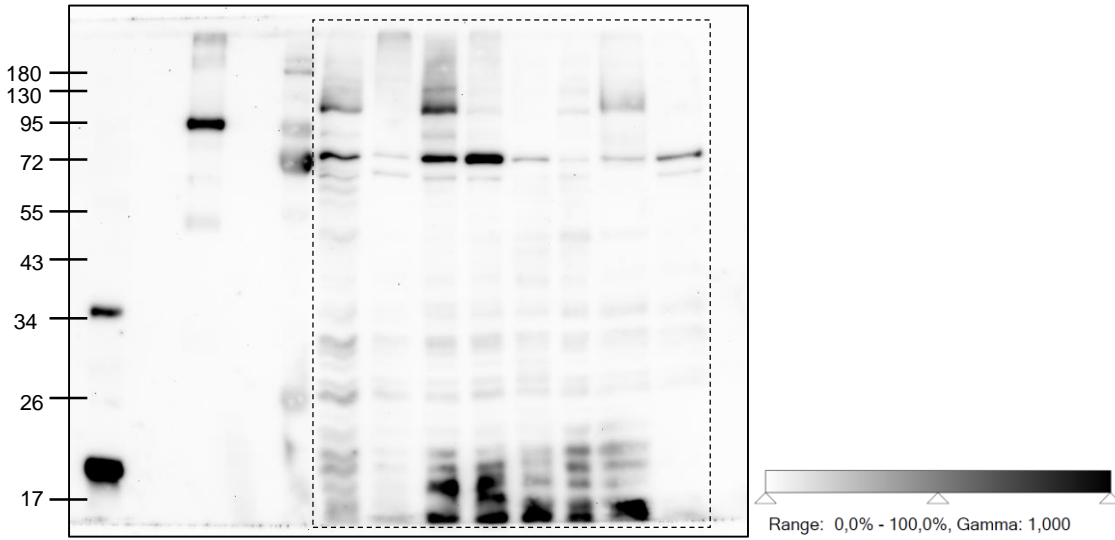
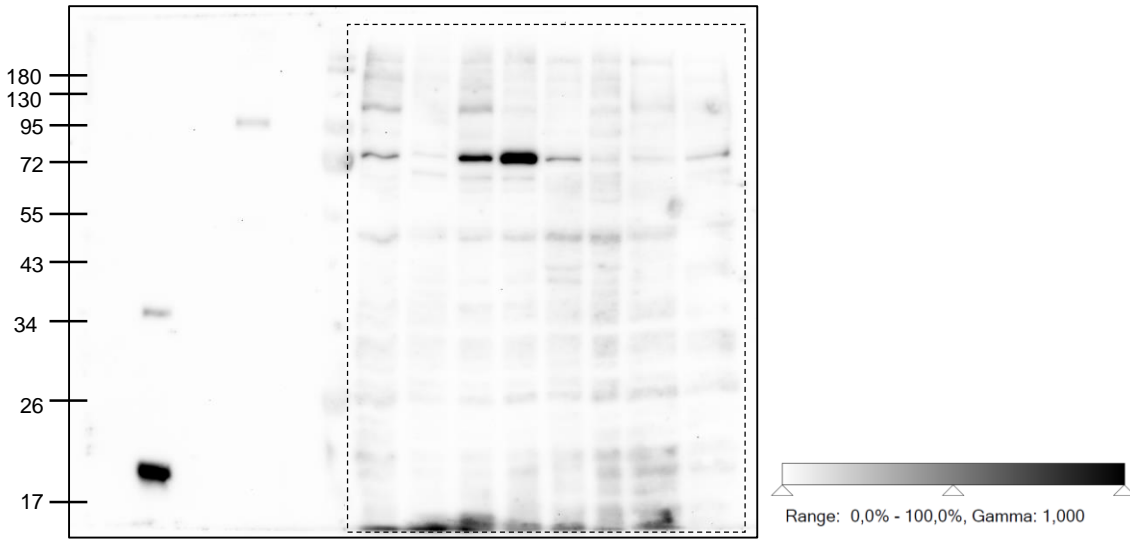


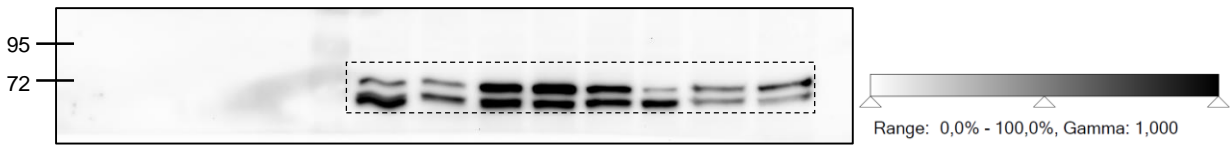
Figure 4F
17G6 + MnCl₂



17G6 + MnCl₂ (after hydroxylamine treatment)



α-BiP (stripped, previously 17G6 + MnCl₂)



α-GAPDH (stripped, previously 17G6 + MnCl₂)

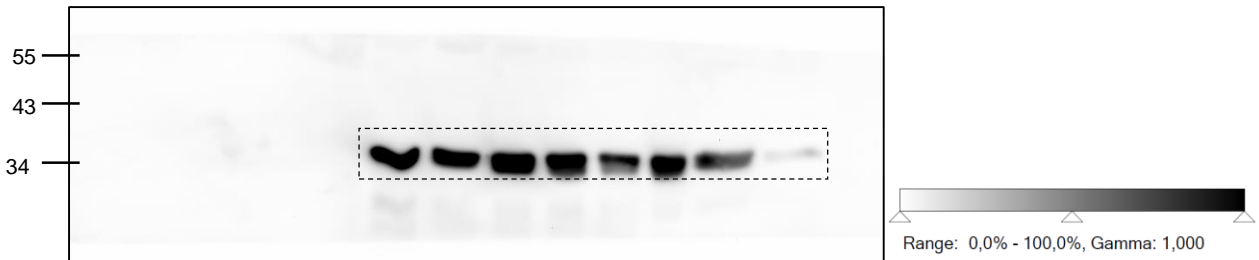
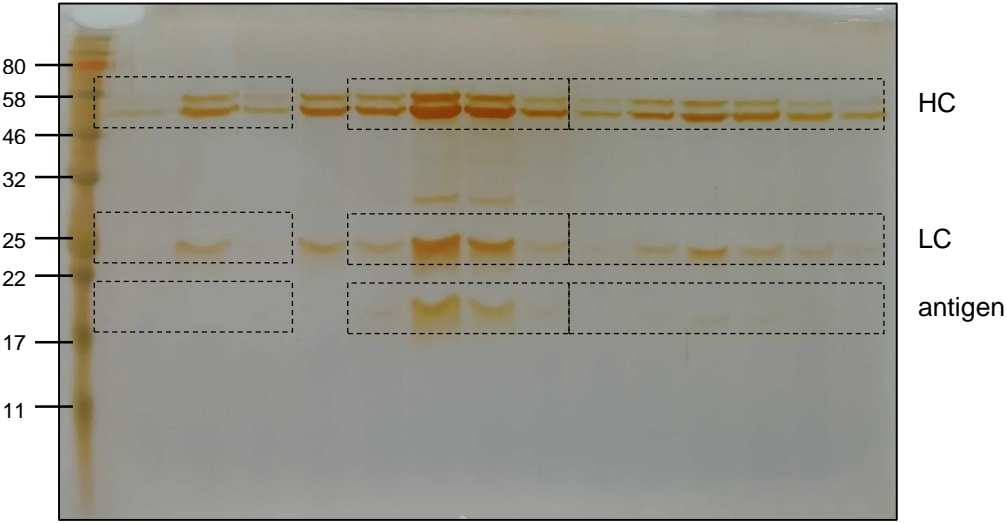


Figure S4

1G11_Cdc42-Thr-AMP (left), _Cdc42-Tyr-AMP (middle), _Rab1-AMP (right)



7C11_Cdc42-Thr-AMP (left), _Cdc42-Tyr-AMP (middle), _Rab1-AMP (right)

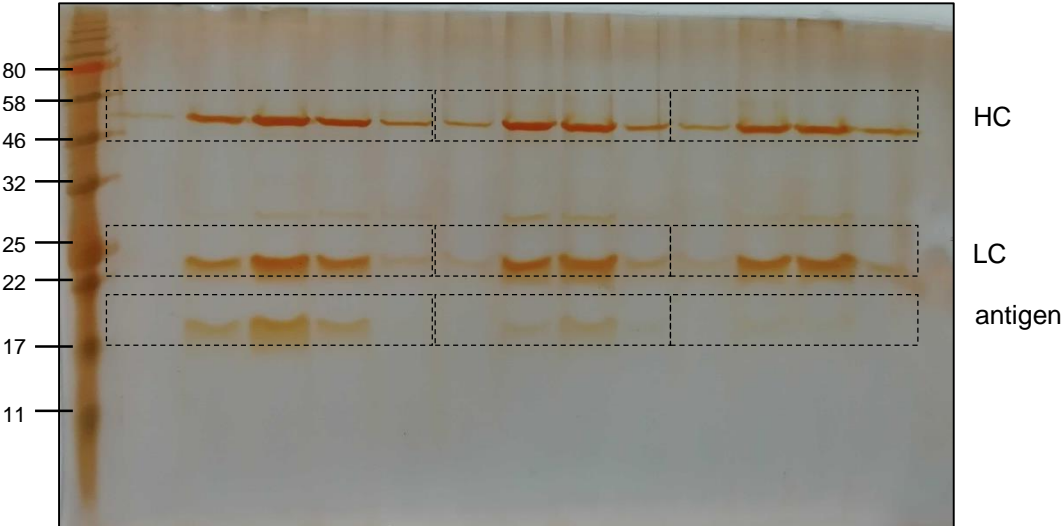
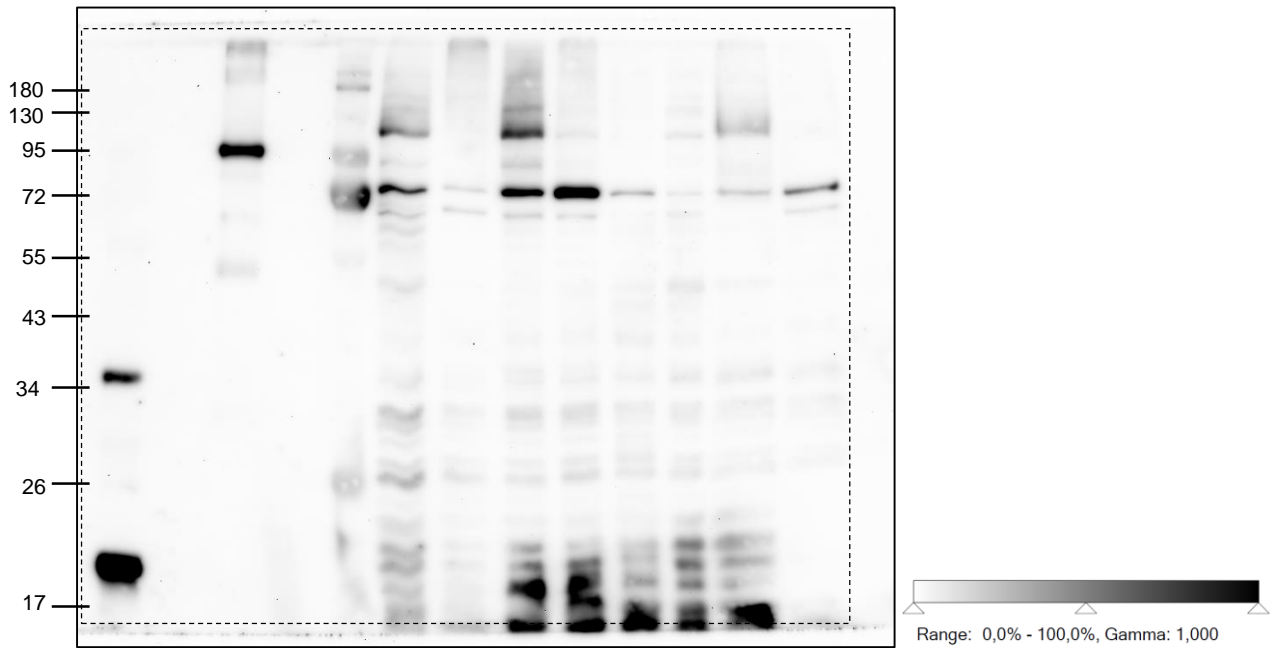
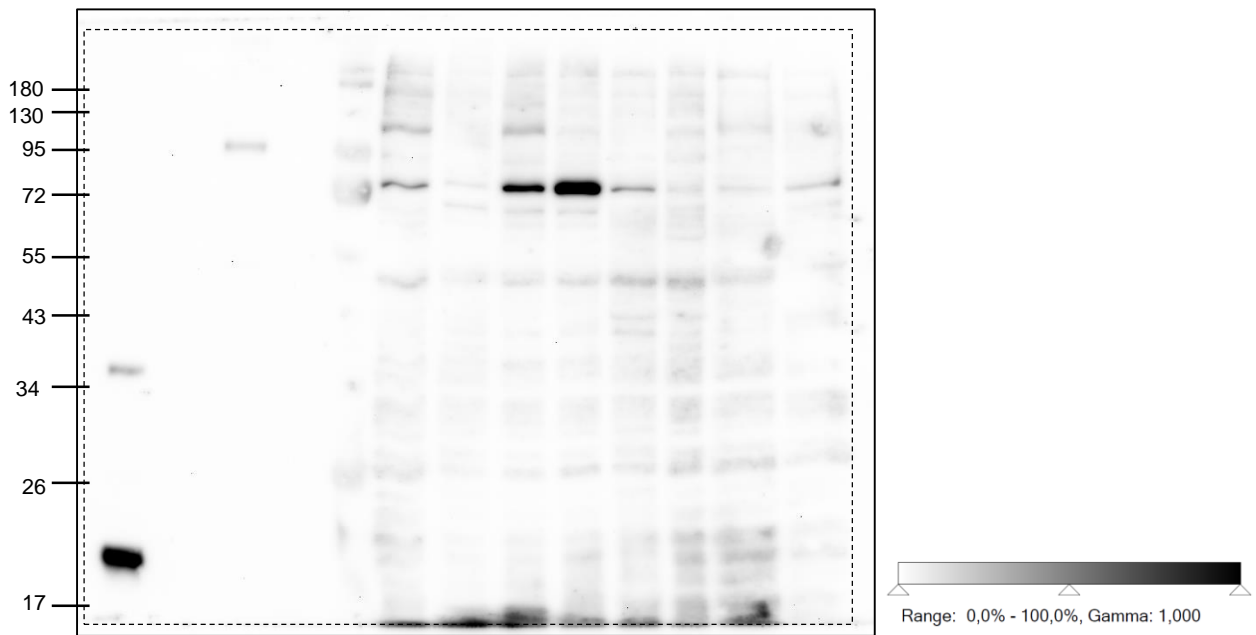


Figure S6
17G6 + MnCl₂

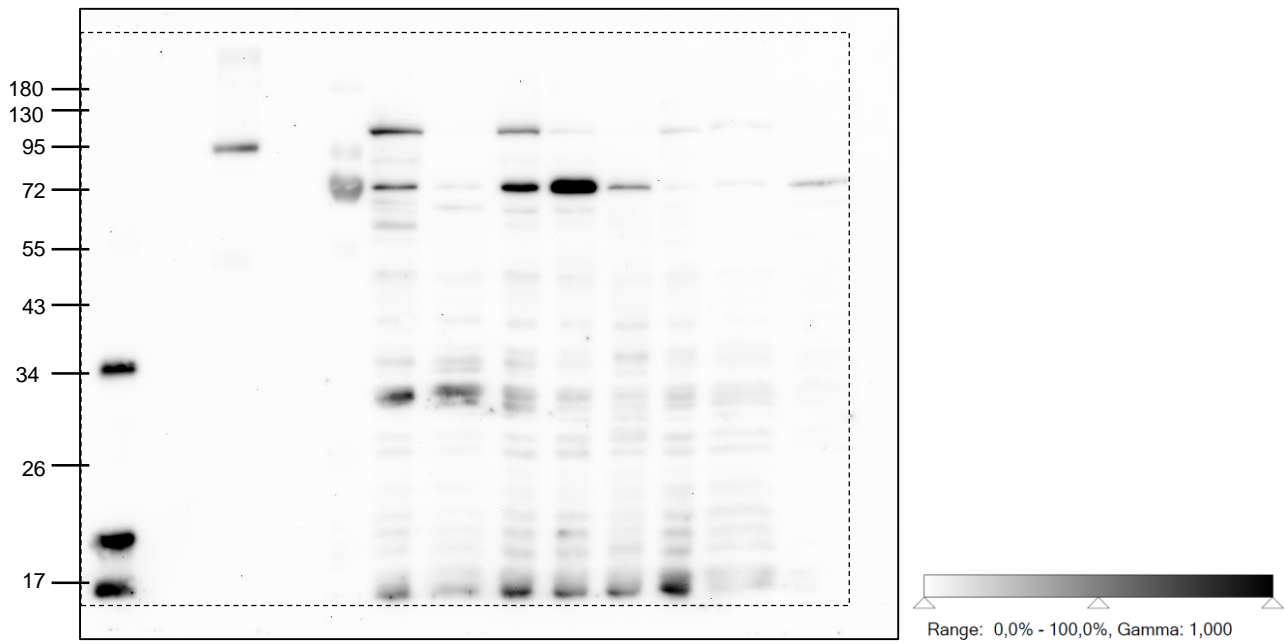


17G6 + MnCl₂ (after hydroxylamine treatment)

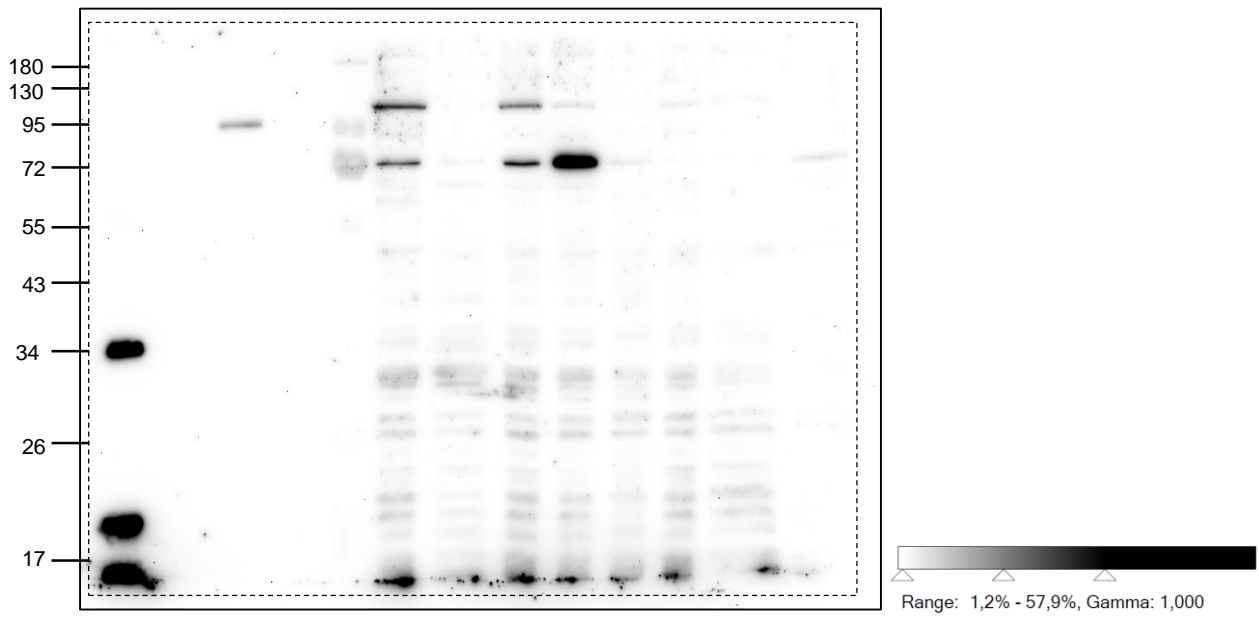


(Same as Figure 4F 17G6 + MnCl₂ before and after hydroxylamine treatment)

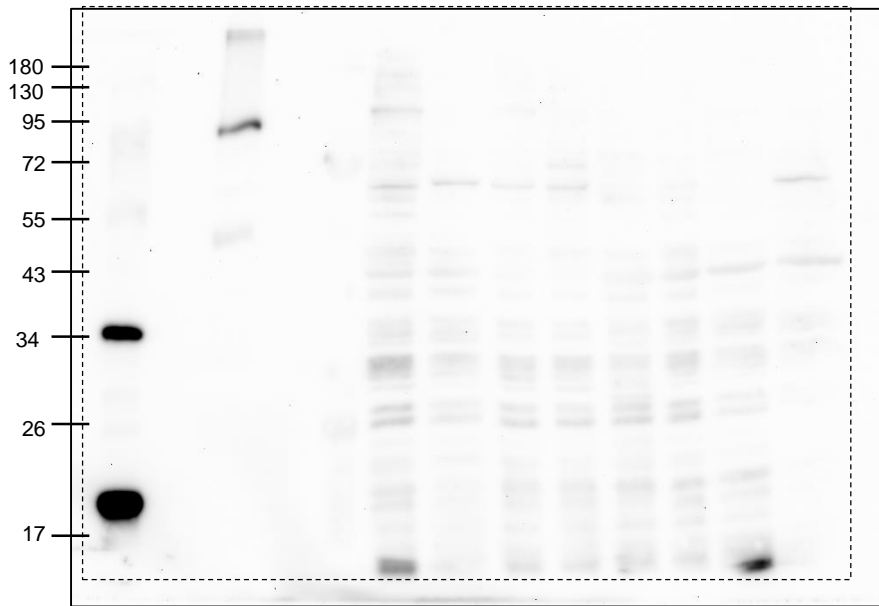
7C11 + MnCl₂



7C11 + MnCl₂ (after hydroxylamine treatment)

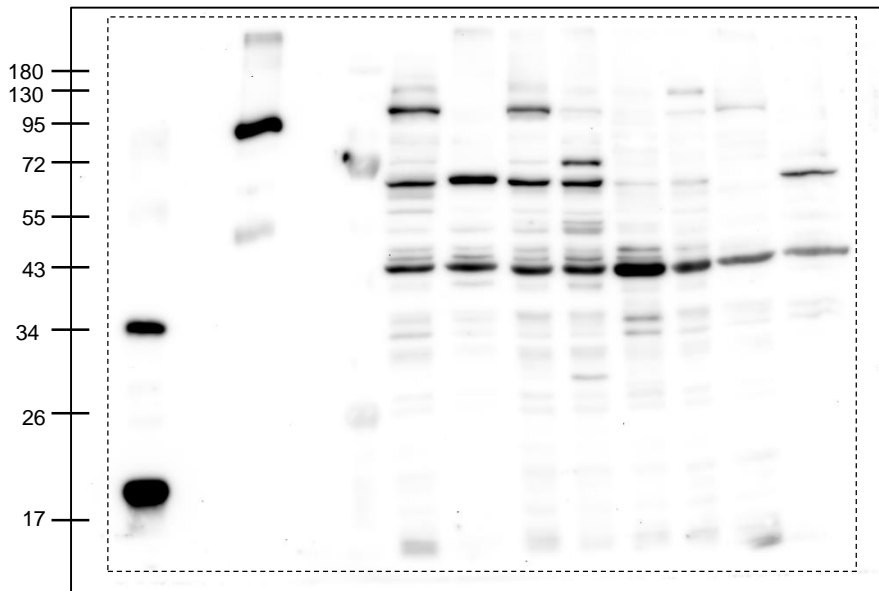


1G11 + MnCl₂



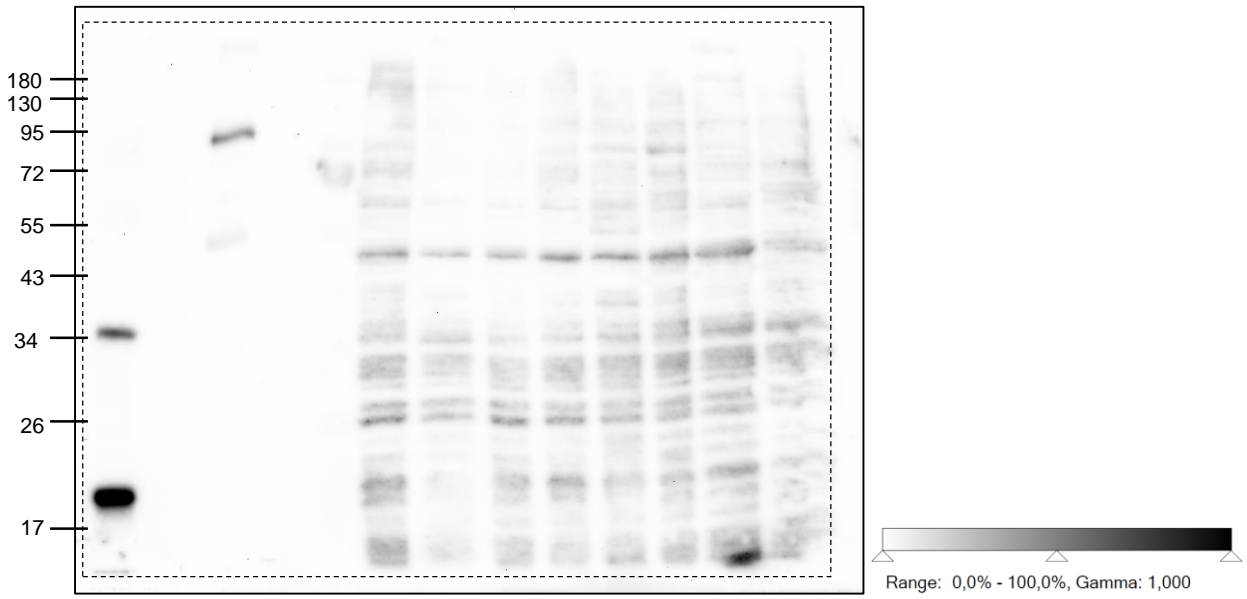
Range: 0,0% - 100,0%, Gamma: 1,000

1G11 reprobe without MnCl₂



Range: 1,0% - 100,0%, Gamma: 1,000

1G11 + MnCl₂ (after hydroxylamine treatment)



1G11 reprobe without MnCl₂ (after hydroxylamine treatment)

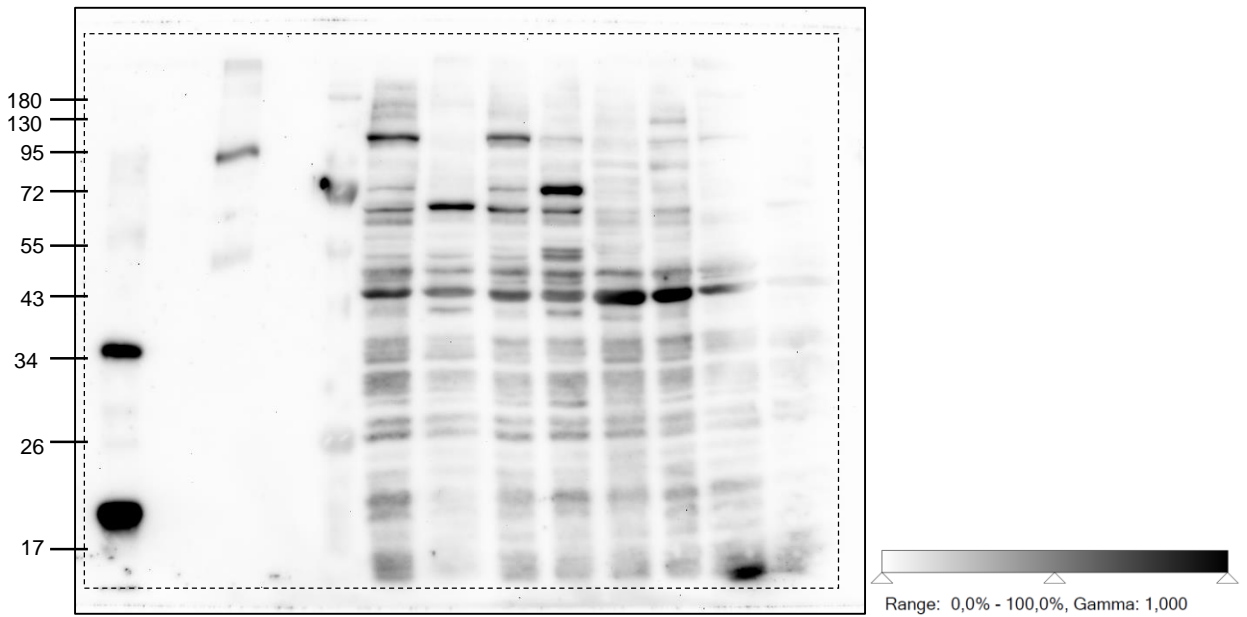
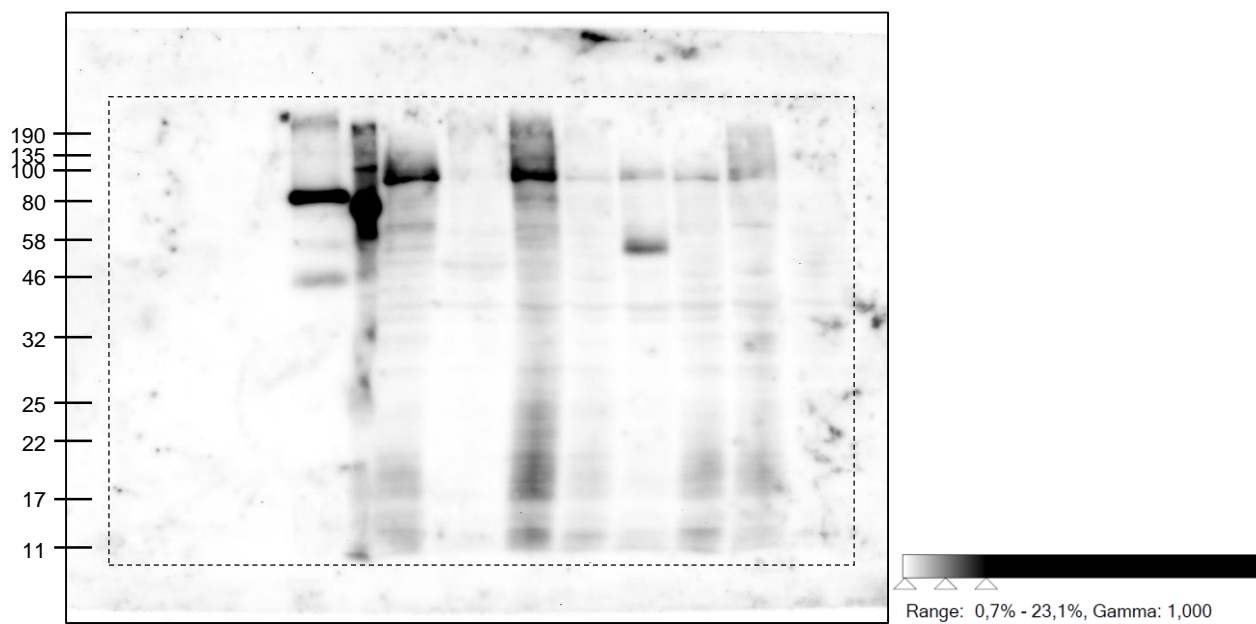
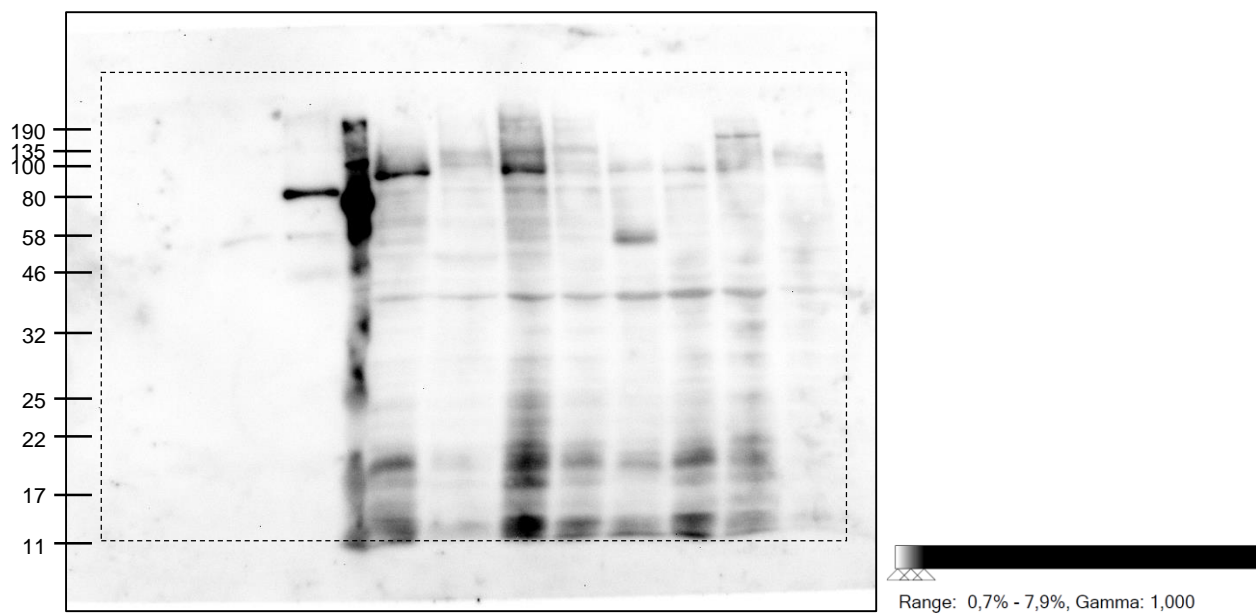


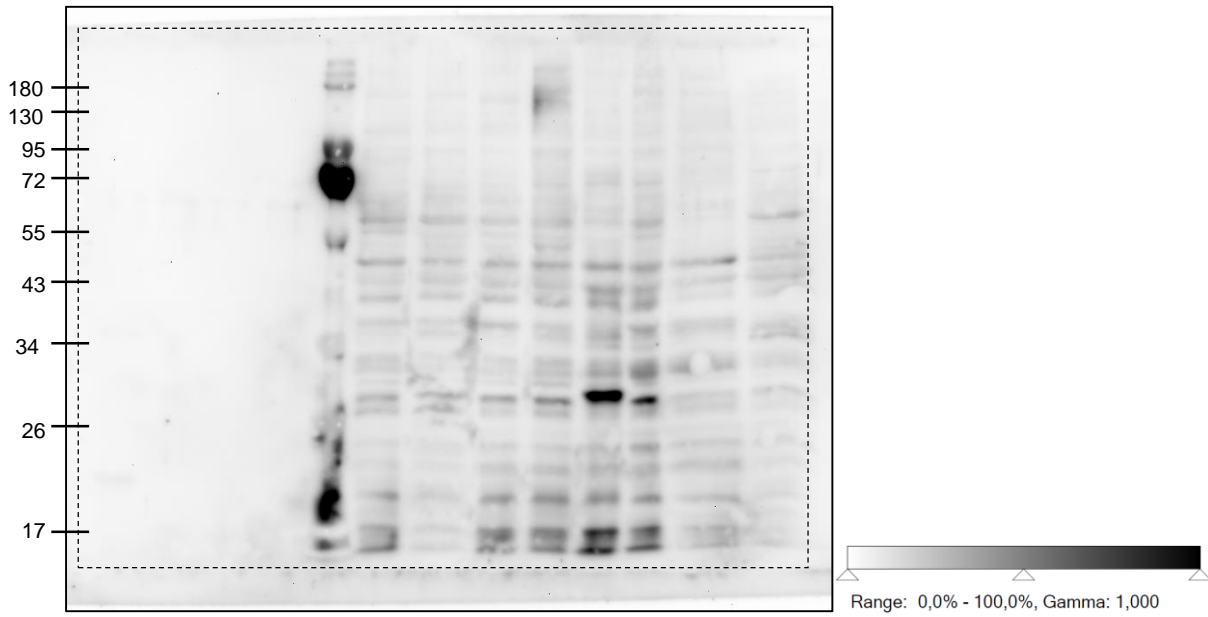
Figure S7
a-pan-ADPR (Merck)



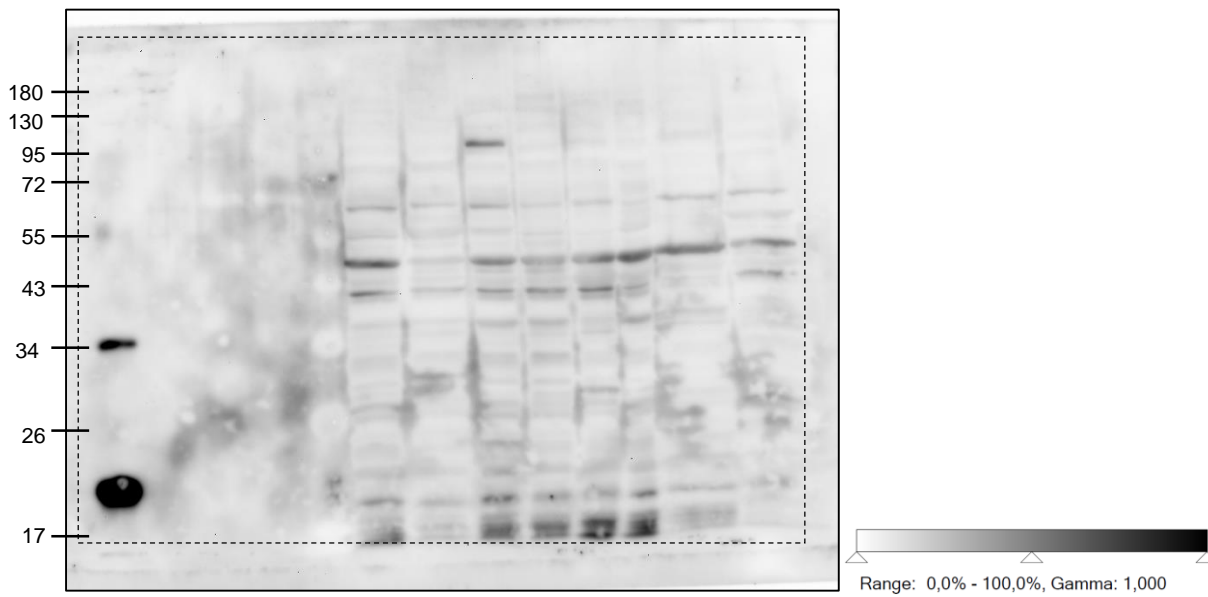
α -pan-ADPR (Merck) (after hydroxylamine treatment)



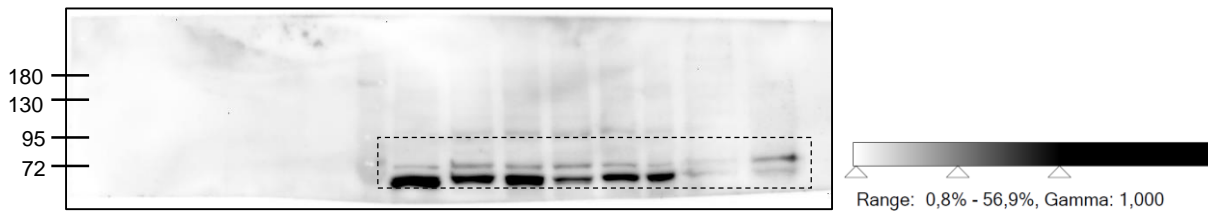
α -Tyr-AMP (Merck)



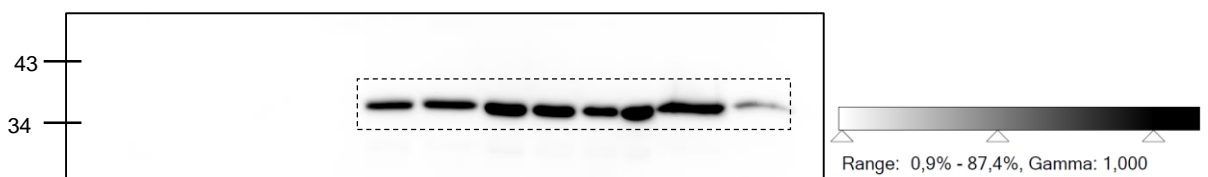
α -Thr-AMP (Merck)



α -BiP (stripped, previously α -Thr-AMP)



α -GAPDH (stripped, previously α -Thr-AMP)



Supplemental References

- Barthelmes, K., Ramcke, E., Kang, H.S., Sattler, M., Itzen, A., 2020. Conformational control of small GTPases by AMPylation. *Proc. Natl. Acad. Sci. U. S. A.* 117, 5772–5781.
- Ernst, S., Ecker, F., Kaspers, M.S., Ochtrup, P., Hedberg, C., Groll, M., Itzen, A., 2020. *Legionella* effector AnkX displaces the switch II region for Rab1b phosphocholination. *Sci. Adv.* 6, eaaz8041.
- Gibson, B.A., Conrad, L.B., Huang, D., Kraus, W.L., 2017. Generation and Characterization of Recombinant Antibody-like ADP-Ribose Binding Proteins. *Biochemistry* 56, 6305–6316.
- Goody, P.R., Heller, K., Oesterlin, L.K., Müller, M.P., Itzen, A., Goody, R.S., 2012. Reversible phosphocholination of Rab proteins by *Legionella pneumophila* effector proteins. *EMBO J.* 31, 1774–1784.
- Schoebel, S., Oesterlin, L.K., Blankenfeldt, W., Goody, R.S., Itzen, A., 2009. RabGDI Displacement by DrrA from *Legionella* Is a Consequence of Its Guanine Nucleotide Exchange Activity. *Mol. Cell* 36, 1060–1072.
- Vieweg, S., Mulholland, K., Brauning, B., Kacharia, N., Lai, Y.-C., Toth, R., Singh, P.K., Volpi, I., Sattler, M., Groll, M., Itzen, A., Muqit, M.M.K., 2020. PINK1-dependent phosphorylation of Serine111 within the SF3 motif of Rab GTPases impairs effector interactions and LRRK2 mediated phosphorylation at Threonine72. *Biochem. J.* <https://doi.org/10.1042/bcj20190664>
- Zhang, Z., Marshall, A.G., 1998. A universal algorithm for fast and automated charge state deconvolution of electrospray mass-to-charge ratio spectra. *J. Am. Soc. Mass Spectrom.* 9, 225–33.